Investigation of the Nearshore, Episodic Poleward Current in the Southern Benguela:

A Numerical Modelling Approach

Anél Viljoen

Submitted in fulfilment of the requirements for the degree of Masters of Science
in the Department of Oceanography, Faculty of Science
University of Cape Town

June 2006

Supervisors: F A Shillington, G B Brundrit

Declaration

I, the undersigned, hereby declare that the work contained in this dissertation is my own original work and has not previously in its entirety or in part been submitted at any university for a degree.

Signature: Signed by candidate

Date: 20 AUGUST 2006

Abstract

Fisheries are of great economic importance on the South African West Coast (the Southern Benguela). The St Helena Bay region is a key nursery habitat for these fisheries because of its retention, upwelling and stratified water column characteristics. However, these characteristics also result in other outcomes such as hypoxia and harmful algal blooms (HAB's) which impact on the habitat suitability character of the system. A nearshore, episodic poleward current has been observed in this region, and it is believed that this current plays an important role in the incidence of HAB's as well as hypoxia events. The drivers and dynamics of this nearshore, episodic poleward current have not been clearly understood, nor thoroughly investigated, due to the complexity of the scales and processes. However, the importance of this current in transporting harmful algae from the north into St Helena Bay and its role in habitat hypoxia has emphasized the need to understand its dynamics.

This study investigates the drivers and dynamics of the nearshore, episodic poleward current (on a synoptic scale) in the St Helena Bay region. The investigation was undertaken by means of numerical modelling. The Delft3D-FLOW numerical model was used to set up two model domains: A simplified, "block" model (the Reference Model), which formed the focus of the thesis, and a more complex model of the St Helena Bay region. A series of numerical experiments were undertaken with these models. The Reference Model had a straight coastline and an artificial bottom topography, which was chosen to be simple, yet complex enough to include the main topographical features that were necessary for the study of the poleward current. Idealized winds were used in this model. The St Helena Bay model had an irregular coastline and an alongshore varying bottom topography. Observational data was used during the set up of this model. The Reference Model experiments investigated in some detail the influence of three processes on the formation of the nearshore poleward current namely, stratification, bottom topography and wind variability.

In agreement with observations, the nearshore poleward current in the Reference Model experiments always appeared during wind relaxation following an upwelling event. In the absence of stratification, no nearshore poleward flow became visible; hence the process of stratification appeared to be an important factor during the formation of the nearshore poleward surface current. This poleward current appeared in the nearshore region where the geostrophic and baroclinic adjustment (due to the removal of the wind forcing) gave rise to a reversal in the surface slope as well as a (opposite) reversal in the isotherm slope. It appeared that a reversed (upward sloping) surface close to the coast, which led to a cross shore horizontal pressure gradient force acting in an offshore direction, was the driving force of the poleward current, and that it could therefore be viewed as being 'driven from the surface'.

Furthermore, the bottom topography had an important influence on the characteristics of the nearshore poleward current. A flatter inner shelf slope caused a narrower nearshore poleward current, and this current took longer to develop and longer to reach a steady state. The nearshore poleward current only disappeared once another equatorward wind event started.

The development of the poleward current in the St Helena Bay region seemed to be mostly based on similar basic mechanisms as was identified during the Reference Model experiments. The dominant conclusions from the Reference Model were also apparent in the St Helena Bay model, although some discrepancies were evident. These discrepancies could probably be attributed to the higher level of complexity of the St Helena Bay model (the irregular coastline, the presence of a cape, and an alongshore variation in bottom topography). The complex topography did, however, not make a substantial difference in the dynamics. Even if spatially varying winds are used in future models, there might be differences in the detail, but nevertheless the formation of a nearshore poleward current should be evident.

Acknowledgements

I sincerely thank my supervisors, Prof Geoff Brundrit and Dr Frank Shillington, for their advice, guidance and encouragement, as well as the many hours of discussion during the course of this research. I could not have asked for better supervision.

I further thank Dr Pedro Monteiro for his valuable inputs and continued interest in this research. Also thanks to Roy van Ballegooyen for his support and positivism when it was most needed, and to Dr Marten Gründlingh for his role in providing me with an environment where I could focus on the completion of this dissertation.

To my husband, Quintin, thank you for all your support, patience and encouragement during this period. Your belief in me kept me motivated.

Table of Contents

List of Figures

List of Tables

List of Acronyms

ADCP	Acoustic Doppler Current Profilers
BEP	Benguela Ecology Programme
CODE	Coastal Ocean Dynamics Experiment
GMT	Greenwich Mean Time
HAB	Harmful Algal Bloom
LOW	Low Oxygen Water
MCS	Mike Cotton Systems
MM5	Mesoscale Model 5
MSL	Mean Sea Level
QuickScat	Quick Scattermeter
ROMS	Regional Ocean Model System
SAN	South African Navy
SAWS	South African Weather Service
SST	Sea Surface Temperature

1. INTRODUCTION

1.1 The Benguela

The Benguela System is one of four major eastern boundary upwelling systems, and is unique among these regions in that it is bounded on both the equatorward and poleward ends by warm water regimes. In the past, numerous reviews have been written to describe the macroscale features of the Benguela System. In reviews conducted by Shannon (1985), Shannon & Nelson (1996), as well as Shillington (1998), a thorough description of the Benguela System is given, including its topographic features, overlying wind fields, oceanic boundaries and fronts, deep and shelf circulation and system variability.

The meteorology of the Benguela upwelling system is relatively complex. The upwelling system is strongly influenced by both the semi permanent high pressure system over the subtropical South Atlantic (the so-called South Atlantic Anticyclone, or SAA), and the continental heat low that develops over southern Africa during the summer months (Risien et al, 2004).

Wind driven upwelling is a strong feature of the ocean circulation along the entire West Coast of southern Africa. The prevailing winds in the region blow from a south to southeasterly direction, resulting in an offshore Ekman transport, which drives the upwelling of cold, nutrient-rich water onto the continental shelf (Peterson & Stramma, 1991). This upwelling shows significant spatial and temporal variability, all along the southwest coast of Africa, from Cape Agulhas to Cape Frio (Lutjeharms & Meeuwis, 1987).

Poleward of the Orange River (28.5° S), the dominant southeasterly wind regime is modulated by the passage of midlatitude cyclones south of the continent, and associated frontal systems. Other weather systems which occasionally modulate the upwelling favorable winds are: Cut off lows (spring and autumn), west coast troughs (summer), and coastal lows, as well as mesoscale systems that are trapped by the coastal mountains and the subsidence inversion and which propagate as a type of Kelvin wave around the southern African coast (Gill, 1977; Reason & Jury, 1990). Coastal lows tend to be forced by offshore flow trailing an eastward tracking anticyclone; this offshore flow, known locally as a berg wind, also has a significant impact on the upwelling region. In addition, local land-sea breezes (Hart & Currie, 1960) may be important in some locations, although usually the synoptic-scale wind masks their signature along the southern part of the west coast. The Benguela is particularly influenced by the diurnal pulsing of the local and regional winds while the entire region experiences seasonal variations of importance.

The location and characteristics of the main upwelling cells in the Benguela System have been documented and described by authors such as Nelson & Hutchings (1983) and Shannon (1985). Six such cells have been identified along the west coast of southern Africa. There is a distinct seasonal cycle in upwelling, with the strongest upwelling occurring during spring and summer (October – March) in the Southern Benguela. The upwelling cells are normally located near regions of cyclonic wind-stress curl, and are in most cases in regions where there is a change in orientation of coastline (Shannon & Nelson, 1996).

The southwest coastline of Africa is relatively straight incised with only a few major capes and embayments, most of which occur in southern region (e.g. False Bay, Cape Peninsula, Saldanha Bay and Cape Columbine). A broad (100 km) shelf occupies the area to the south of Africa, with a narrowing past the Cape Peninsula and Cape Columbine. Cape Columbine (33°S) is one of the major upwelling centres present in this System. St Helena Bay can be defined as the wide shelf area extending 200 km north of Cape Columbine. Figure 1.1 gives an illustration of the West Coast of South Africa, indicating the position of Cape Columbine and St Helena Bay.

Several studies have been undertaken to identify the typical circulation patterns in the Cape Columbine – St Helena Bay area. A strong equatorward surface jet in excess of 50 cm/s flows offshore of Cape Columbine (Nelson & Hutchings, 1983). This jet separates in two branches just north of Cape Columbine, one branch bending into St Helena Bay, the other flowing offshore (with a stronger intensity). A shelf edge poleward undercurrent has also been observed in a number of cross-sections (Nelson & Hutchings, 1983). Holden (1985) found that, whereas the flow is predominantly northward, a cyclonic vortex remains in St Helena Bay, leading to St Helena Bay acting as a retention zone. This retention feature in St Helena Bay is one of the reasons why this region is such an important nursery ground for pelagic fish (Hutchings, 1992).

A series of comparative studies of the climatology and geography of known preferred spawning areas (Bakun, 1993) have identified three major classes of physical processes that combine to yield a favourable reproductive habitat for coastal pelagic fish, namely (1) enrichment processes (upwelling, mixing, etc.), (2) concentration processes (frontal formulation, water column stability), and (3) processes favouring retention within appropriate habitat. All three of the above elements are present in St Helena Bay. However, also as a result of these productivity and retention effects, several problems arise in the St Helena Bay – Lamberts Bay areas, especially the occurrence of low oxygen water (LOW) (Monteiro *et al*, 2004), as well harmful algal blooms (HAB's) (Pitcher *et al*, 1998).

Seasonal LOW events impact on ecosystem properties such as habitat suitability for the different life

cycle stages of economically important marine resources. Major mortalities and shifts in the distribution of these marine resources have taken place due to the timing, spatial extent and persistence of such events. There are two scales of significance that play a role during LOW development (Monteiro *et al*, 2004): A seasonal scale as a result of upwelling, and an event scale related to large blooms of harmful algae (HAB's) which are being transported into the St Helena Bay region by a narrow poleward current.

HAB's also have a significant impact on the commercial and recreational fisheries in the coastal region. Mass faunal mortalities (resulting from algal toxins) and human illness (from contaminated shellfish) occur (Pitcher *et al*, 1998). Such blooms are usually characterised by the dominance of particular species of harmful or toxic alga (typically a group of phytoplankton known as dinoflagellates), which leads to a red discolouration of the water, hence the term "red tide". The development of HAB's is closely related to the prevailing winds of the southern Benguela, which govern most hydrodynamic processes on the continental shelf. HAB's occur in the inshore zone, mostly from January to May, during the latter part of the upwelling season. During this time, changes in the synoptic weather patterns result in diminished upwelling activity and increased thermal stratification. The development of HAB's is thus seasonal and associated with periods of wind relaxation.

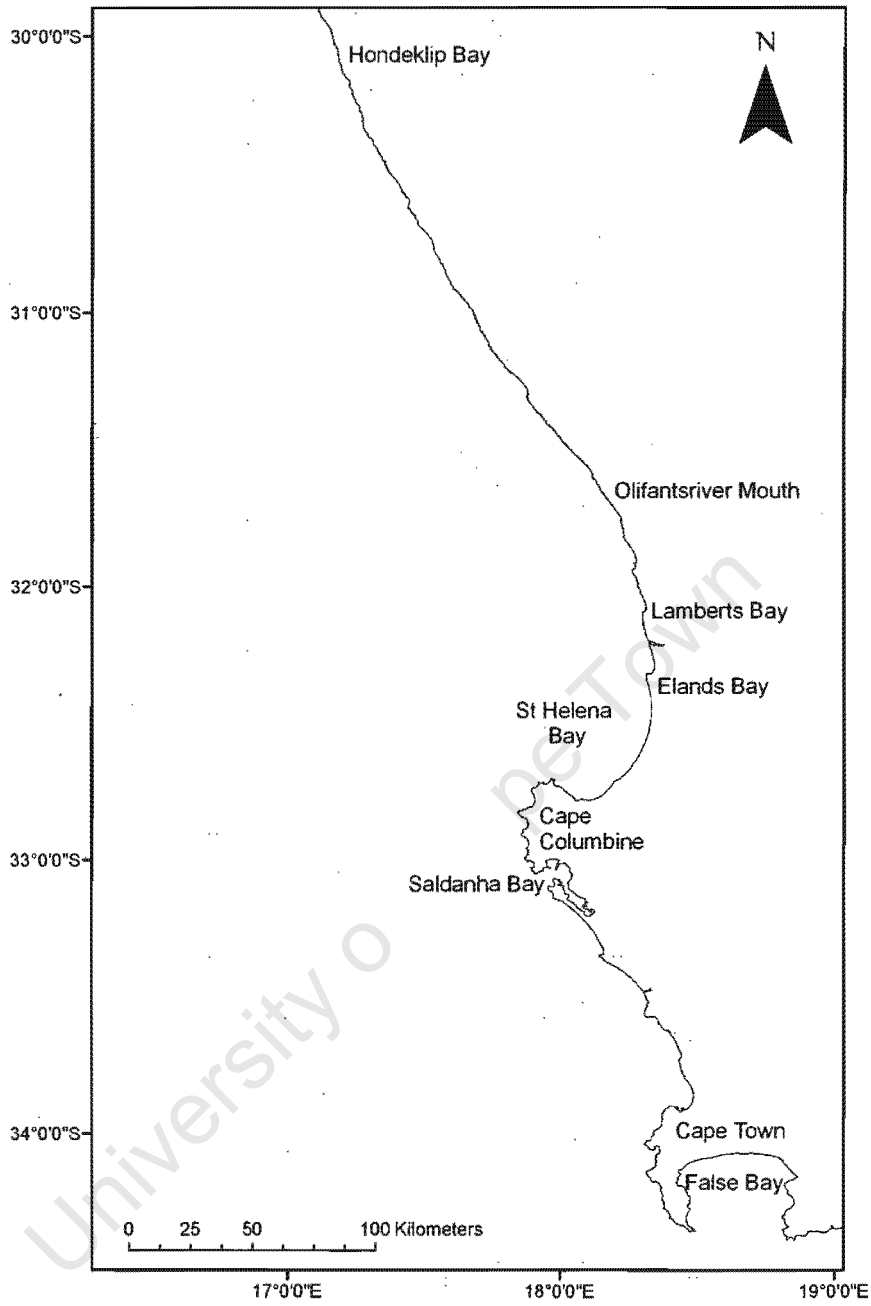

Figure 1-1 Illustration of the West Coast of South Africa.

Observations made during a study of the formation of HAB's (Pitcher & Boyd, 1996; Pitcher *et* al, 1998) in the Southern Benguela (conducted in the Lamberts Bay region), led to the development of a conceptual model of the formation of HAB's within the upwelling system of the southern Benguela. The across-shelf and alongshore phytoplankton distributions in the regions of upwelling fronts were investigated, where they found surface dinoflagellate accumulation. Dinoflagellates increase as seasonal stratification increases during the course of the upwelling season. The population develops subsurface in association with the thermocline. The inshore region is subjected to a narrow coastal

strip of upwelling and the dinoflagelllate population appears as a surface bloom in the region of the upwelling front, which is displaced from the coast during active upwelling. Following relaxation of upwelling, wind stress decreases and cross-shelf currents become weak and directed onshore. During this phase, the return of warm near-surface water corresponds to the onshore movement of the upwelling front. These conditions cause the dinoflagellate blooms to accumulate inshore. Their investigations found that a net poleward surface current propagates these blooms southward, into St Helena Bay. Probyn *et al* (2000) suggests that this poleward flow (often occurring as a "flood" event) could possibly be caused by coastal-trapped waves or wind stress on the surface friction layer. According to Lamberth & Nelson (1987) it is quite likely that barotropic shelf waves dominate this flow.

Holden (1985) found evidence of southward flow along the coast of St Helena Bay, by means of five radio drifters released in St Helena Bay in February 1979. According to Holden, historical data frequently showed some evidence of southward flow along the coast. Generally, this was confined to the region south of Lamberts Bay, but occasionally it occurred along the entire coast. In support of Holden's findings, Bailey & Chapman (1985) found that there was a strong northward-setting current offshore and a southerly counter-current inshore between Elands Bay and the southern end of St Helena Bay. Furthermore, CODE (Coastal Ocean Dynamics Experiment) drifters used to study 2-m currents in the St Helena Bay area indicated the presence of a strong time-dependent surface current flowing southward from St Helena Bay (Lamberth & Nelson, 1987). The barotropic nature of inshore flow over a strip some 25 km wide has also been observed on several current-profiling exercises (Nelson, 1985 and Nelson & Hutchings, 1987).

Thus far, the drivers and dynamics of this nearshore, episodic poleward current, as observed in the Southern Benguela (Holden, 1985), has not been clearly understood nor thoroughly investigated, due to the complexity of the scales and processes. However, the importance of this current in transporting harmful algae from the north into St Helena Bay and its role in habitat hypoxia has emphasized the need to move from a conceptual model to a more quantitative numerical model that would reveal the underlying dynamics. Understanding the origin and dynamics of this poleward current will lead to better knowledge about the oceanography of harmful algal blooms, which will in turn contribute to the improved prediction of HAB events. This will lead the way to improved skills at forecasting their occurrence and lowering human health risk.

The purpose of this thesis, therefore, was to investigate the origin and dynamics of the nearshore poleward current (on a synoptic scale) in the Southern Benguela, in the region of St Helena Bay (Figure 1-1). The two main questions that formed the focus of this study, were as follows:

- What is the nature of the narrow coastal poleward flow?
- What processes govern its characteristics?

These questions were explored by means of numerical modelling.

1.2 The need for modelling

The need to manage economically important fisheries in a variable environment led to an effort by the South African marine research institutes through the BEP (Benguela Ecology Programme) over the last 30 years to analyse and understand the system (Hutchings *et al*, 1998). This involved mainly physical investigations: hydrological samplings, current meter deployments, drifter deployments, SST measurements, ADCP current measurements, satellite data analysis and theoretical studies. However, the physical patterns observed in the Southern Benguela have proven to be very complex, and the various physical observations available only offer piecewise information, thus making it difficult to analyse the dynamics effectively.

The use of numerical modelling tools for studying the Benguela System is highly advantageous, because a numerical model provides a means by which these complex systems can be studied holistically. Several numerical models are now widely available and are becoming more and more useful to explore coastal processes. For this study, numerical modelling allowed the understanding of the timing, location, magnitude and duration of the nearshore poleward current. Another advantage to using a numerical model is its flexibility relating to the specific forcing mechanisms that can be included in a simulation; it was therefore possible to test and identify the oceanic response to different forcing mechanisms during the development of a nearshore poleward current.

At present, there is scope for more numerical modelling of the Benguela Upwelling system. Penven (2000) and Penven *et al* (2001) have undertaken modelling studies of the Southern Benguela upwelling system in order to understand the physical oceanic processes affecting pelagic fish recruitment in this region. Idealized experiments were set up in order to provide an understanding of the circulation in St Helena Bay. Thereafter, a realistic 3D model was implemented to reproduce the dynamics of the ocean around the Southwestern corner of Africa. The numerical model ROMS (Regional Ocean Model System) was used, covering an extensive area from 40°S to 28°S and from 10°E to 24°E, with a spatial resolution of 9-20 km. The model reproduced most of the characteristic, large-scale surface features of the circulation over the Benguela region, but mesoscale patterns that develop over the shelf off the west coast could not be resolved, mainly due to the coarse grid resolution.

No modelling investigations have previously been undertaken to specifically study the nearshore poleward current in the Southern Benguela. However, numerical modellers have conducted some studies that focus on similar nearshore currents as observed in other parts of the world.

A relevant study from a different part of the world is the modelling study undertaken by Gan & Allen (2002a and 2002b) on the continental shelf off northern California. A characteristic response observed during the CODE (Coastal Ocean Dynamics Experiment) is the time-dependant development of poleward currents over the inner shelf next to the coast, following the weakening, or relaxation, of equatorward upwelling favourable winds. An important observation was that the presence of poleward winds is not necessary for this response. Gan & Allen (2002a and 2002b) investigated the dynamics of the shelf flow response to upwelling wind relaxation events by setting up a numerical model and undertaking simulations, firstly under idealized conditions (Gan & Allen, 2002a), and thereafter by applying observed time varying winds (Gan & Allen, 2002b). After thorough investigation, they concluded that the poleward currents seem to be forced by a poleward pressure gradient force. Wind-forced flow interacts with alongshore variations in shelf topography to set up these poleward pressure gradients, and a relaxation of the wind then drives the current poleward.

Wang (1997) conducted a modelling study to investigate the effects of small-scale wind on coastal upwelling with application to Point Conception. An idealized wind forcing was applied to a three-dimensional, limited-area circulation model, and the study considered an upwelling spinup and wind relaxation event. During the relaxation event, a narrow poleward current penetrated well into what used to be the equatorward current regime. This poleward current also brought along warm water. According to Wang, this current was driven by the alongshore pressure gradients, which was suddenly unbalanced due to the relaxation of the wind.

For the purpose of this study, the Delft3D-FLOW numerical model (WL|Delft Hydraulics, 2003) was used. This model forms part of the Delft3D modelling suite developed by Delft Hydraulics in the Netherlands, and has been successfully used in numerous circulation studies. Examples of such studies can be found in CSIR (2002), CSIR (2003a), CSIR (2003b) and CSIR (2005).

The approach undertaken in this thesis is as follows. The focus of this study was the application of Delft3D-FLOW in setting up and utilizing a so-called *Reference Model*: a simplified, symmetric "block" model of alongshore length 500 km and cross shore length 300 km, representing a long, straight coastline. This model applied an artificial bottom topography that was chosen to be complex enough to include the main topographical features that were necessary for the study of the nearshore poleward current. The topography consisted of an inner shelf area (approximately 30 km wide), an

outer shelf area (approximately 170 km wide) and a deep ocean area.

The purpose of the Reference Model was to establish the main forcing mechanisms that influence the formation and strength of a typical nearshore poleward current by undertaking simple numerical experiments. These experiments illustrated the effect of winds, bottom topography and stratification on the current profile along the coastline, and was thus aimed at investigating the key questions presented in this thesis. A numerical model of St Helena Bay and the surrounding areas was then set up (once again using Delft3D-FLOW) in order to study the detail of the actual poleward current. The modelling period was January to mid February 2002, to include the months that HAB's occur most often. The St Helena Bay numerical model domain covered an area stretching from just south of Saldanha Bay to north of Olifants River mouth (an alongshore distance of approximately 280 km). In the cross shore direction the domain had an approximate distance of 120 km. The St Helena Bay model is much more complex than the Reference Model, as it contains a large cape (Cape Columbine) as well as several small embayments. This adds a level of difficulty to the modelling and the interpretation of the model results. The purpose of the St Helena Bay model was therefore merely to test whether the newfound knowledge concerning the dynamics of the poleward current that was obtained from the Reference Model, could be observed in the St Helena Bay model. Although acknowledged that a more complex topography and the presence of a cape might lead to some additional dynamics concerning the current profiles, the detailed investigation of such an influence was beyond the scope of this thesis.

It should be noted that the period of study falls within the protracted 1998–2001 La Niña episode. Typically, high-pressure anomalies develop over the midlatitude South Atlantic and South Indian Oceans during La Niñas with low-pressure anomalies over southern Africa (Reason et al, 2000), and hence stronger south easterlies tend to occur over the Benguela region. The 1999–2000 austral summer conditions over the Benguela region were compared with other La Niña events in the 1949–2000 period (Roy et al, 2001) and it was concluded that this particular summer was broadly similar to other events.

All modelling only considered the hydrodynamic forcing mechanisms; no bio-geochemical processes were included.

1.3 Layout of the thesis

The layout of this thesis is as follows. Chapter 2 (Methodology) gives a description of the methodology that was followed during the modelling investigations, including a description of the

Delft3D-FLOW numerical model. The specific processes that were included in the Reference Model and St Helena Bay Model (for instance winds and Coriolis effects), as well as the observational data that were available for application in the St Helena Bay model simulation, are also described.

In Chapter 3 (Modelling Investigations), details of the set-up of the Reference Model as well as a description of the three numerical experiments that were undertaken with this model are given. As mentioned earlier, these three experiments were developed to test the influence of stratification, bottom topography and winds on the formation of a nearshore poleward current. Also, a description of the set-up of the more complex St Helena Bay numerical model is given, as well as a description of the three studies that were undertaken with this model. The difference between these studies is the response to different wind scenarios that were applied in the model. The first study applied winds that were measured at the St Helena Bay weather station at Cape St Martin (the position of this station is indicated in Figure 2-1), while the second study also applied the St Helena Bay weather station winds, but this time the winds were smoothed (the diurnal component was removed). The third study applied winds from the same source, but the measured wind speeds were reduced by 30 %. Details surrounding these wind time series are also given in this chapter.

To ensure that the input values (winds, bottom topography) to the Reference Model are realistic and useful for its intended application, Chapter 4 (Results from the Reference Model) starts off by giving an analytical validation of these input values. Model results (current speed and surface slope) are compared to analytical calculations to see if there is a satisfactory agreement between these values. Thereafter, the results from the three Reference Model numerical experiments are presented individually. In Chapter 5 (Results from the St Helena Bay numerical model), the results from the three St Helena Bay numerical model studies are presented. All the results are presented by means of descriptive figures, which include vertical and horizontal velocity and temperature fields, time series plots of currents at specific locations, as well as absolute surface slopes.

The discussion that follows in Chapter 6 focuses on the learning points from the Reference Model numerical experiments, specifically addressing the two key questions presented in this thesis. Thereafter, the focus shifts to a discussion of the results from the St Helena Bay numerical model as well as the differences that could be identified between the two models regarding the formation of the nearshore poleward current. The importance of having high resolution wind and boundary condition data is stressed. Furthermore, the limitations of the Delft3D-FLOW model that could be identified during the carrying out of this thesis are also discussed.

2. MODELLING METHODOLOGY

This thesis mainly used numerical modelling as a tool to understand the oceanic response to a particular wind forcing as well as the response during the presence/absence of stratification. Also, the influence of the bottom topography on the formation of a poleward current is investigated. Two models were set up in order to study the nearshore poleward current, namely the Reference Model (a simplified process model) and the St Helena Bay Model (a more complex simulation model). This chapter describes the numerical modelling tool, Delft3D-FLOW, which was used during the above-mentioned modelling investigations.

Several physical processes were tested during the modelling experiments in order to determine the relative importance (if any) of each process during the formation of the nearshore poleward current. This chapter therefore also describes the physical processes that were included (not necessarily simultaneously) during the model investigations.

A description of the data sources that were used during the setup of the St Helena Bay numerical model is also given in this chapter. The Reference Model only used artificial data, as it was a simple, idealized model used to illustrate and investigate certain characteristics of the current. The St Helena Bay model was a much more complex model in which measured data sets were used.

Lastly, a list of conventions used during the modelling investigations, are given.

2.1 Description of the numerical model Delft3D-FLOW

The modelling of the hydrodynamics of the Reference Model as well as the St Helena Bay numerical model was undertaken using Delft3D-FLOW (WL|Delft Hydraulics, 2003). This hydrodynamic model is designed to simulate multi-dimensional hydrodynamic flows and transport phenomena, including sediments, in shallow seas, coastal areas, estuaries, rivers and lakes. Delft3D-FLOW solves the Navier-Stokes equations for an incompressible fluid, under the shallow water and the Boussinesq assumptions. The equations and their numerical implementation are described in detail in the Delft3D-FLOW user manual (WL|Delft Hydraulics, 2003) as well as in Lesser *et al* (2004).

In the horizontal direction, Cartesian rectangular co-ordinates are used in the Reference Model, due to the simplicity of the grid and its straight coastline. For the St Helena Bay model, however, orthogonal curvilinear co-ordinates are used. The boundaries of a coastal sea are in general curved and are not

smoothly represented on a rectangular grid. Curvilinear co-ordinates allows the grid to be "fitted to the coast", and also allows local grid refinement in areas with large horizontal gradients.

In the vertical, a so-called sigma (σ) co-ordinate system is used. The flow domain of a 3D shallow water model consists in the horizontal plane of a limited area composed of open and closed (land) boundaries, and in the vertical of a number of layers. In a σ co-ordinate system the number of layers is the same at every location in the horizontal plane, i.e. the layer interfaces are chosen following planes of constant σ. For each layer a set of coupled conservation equations is solved.

At the open boundaries, water levels are specified. No river flow, precipitation or evaporation is included in any of the numerical experiments undertaken during this study.

The vertical velocity in the adapting σ co-ordinate system is computed from the continuity equation. The vertical velocity is defined at the iso σ-surfaces and it is the vertical velocity relative to the moving σ-plane. It may be interpreted as the velocity associated with up- or downwelling motions.

Under the shallow water assumption, the vertical momentum equation is reduced to a hydrostatic pressure equation. Vertical accelerations due to buoyancy effects and due to sudden variations in the bottom topography are not taken into account. The pressure forcing which is adopted depends upon whether or not the situation can be adequately described with constant density or whether it requires a non-uniform density. In the case of a non-uniform density, the local density is related to the values of temperature and salinity by the equation of state.

Details of the turbulence closure model are also given in WL|Delft Hydraulics (2003) as well as in Lesser *et al* (2004).

2.2 Processes included in the numerical models

2.2.1 Processes available in the Delft3D-FLOW model

The Delft3D-FLOW model can be used to model tide and wind driven flows, as well as stratified and density driven flows. Its standard features include (among others):

- Tidal forcing;
- The effect of the earth's rotation (Coriolis force);
- Density driven flows (pressure gradients terms in the momentum equations);

- Space and time varying wind and atmospheric pressure;
- Various options to model the heat exchange through the free water surface;
- Wave induced stresses and mass fluxes;
- Influence of waves on the bed shear stress.

The magnitude of the wind shear stress is determined by the following widely used quadratic expression:

$$\tau = \rho_a . C_d . |U_{10}| . U_{10}$$

where:

ρ_a	=	air density (kg/m^3)
U_{10}	=	wind speed (m/s) 10 m above the free surface
C_d	=	wind drag coefficient, dependent on U_{10} (see Chapter 2.2.2).

2.2.2 Processes included in the Reference Model

Four main hydrodynamic forcing mechanisms were included in the Reference Model experiments, namely,

- Winds;
- Coriolis force;
- Stratification and
- Heat Flux (only included when stratification was included).

The equatorward wind is important in setting up horizontal pressure gradients, leading to the development of alongshore equatorward currents. The Coriolis force was incorporated into the model by specifying a latitude, in this case -32.75°. From this latitude, the Coriolis parameter is calculated by the Delft3D-FLOW model ($f = 2\Omega \sin\phi$, where Ω is the angular velocity of the Earth about its axis and ϕ is the latitude).

The wind drag coefficient, C_d, reflects increasing roughness of the water surface with increasing wind speed (see Smith and Banke, 1975). The following equation was used to calculate the wind drag coefficient C_d as a function of the wind speed:

$$C_d(U_{10}) = C_d^A + (C_d^B - C_d^A)\frac{U_{10} - U_{10}^A}{U_{10}^B - U_{10}^A}$$

with the following user-specified values:

$$C_d^A = 0.0011 \text{ and } C_d^B = 0.0065$$
$$U_{10}^A = 0 \text{ and } U_{10}^B = 100.$$

Stratification is also one of the important processes included during the Reference Model experiments. Experiments were undertaken under vertically mixed and stratified conditions, to determine the influence of the vertical temperature structure on the formation of the nearshore poleward current.

Heat fluxes were included as part of the model experiments (except when stratification was not modelled). Strong stratification is maintained by atmospheric heat fluxes into the surface waters and the inflow of cold bottom waters from upwelling on the adjacent open shelf. These processes are important in controlling the thermocline dynamics and vertical mixing of the water column.

Tidal forcing and wave driven currents were not modelled in the Reference Model experiments. The effect of waves is only evident very close inshore, while the nearshore poleward current appears in a wider (nearshore) band. Salinity was also not explicitly modelled (a constant salinity of 35 ppt was specified).

2.2.3 Processes included in the St Helena Bay numerical model

The same forcing mechanisms that were included in the Reference Model experiments were included in the St Helena Bay numerical model simulations. Experiments were always undertaken under vertically stratified conditions.

Note:

River flow

Two major river systems run into the ocean within the region surrounding Cape Columbine / St Helena Bay, namely the Great Berg Estuary and the Olifants Estuary (Shillington, 1998). Compared to the large-scale marine processes that are being modelled and investigated, the freshwater run-off from these rivers is insignificant. Therefore, the assumption was made that the river run-off inside the model domain could be ignored for the purpose of this study.

2.3 Observations for the St Helena Bay numerical model

The forcing mechanisms (e.g. wind speed and direction) that were included in the idealized Reference Model were synthetic and experimental, and no real data was used. For the St Helena Bay model, however, actual observational data was used. This section discusses the sources of data used to set up the St Helena Bay numerical model.

2.3.1 Bathymetry

A detailed bathymetry of the St Helena Bay model domain was compiled by combining the following (digitised) data sets:

- S A Navy hydrographic chart of Olifantsrivier to Cape Columbine (SAN 117);
- S A Navy hydrographic chart of Cape Columbine to Table Bay (SAN 118);
- S A Navy hydrographic chart of St Helena Bay – Eastern part (SAN 1008);
- S A Navy hydrographic chart of St Helena Bay – Western part (SAN 1009).

2.3.2 Temperature

A time series of temperature data was collected by the CSIR at 2 m depth intervals by deploying a thermistor chain in 25 m depth in St Helena Bay. Figure 2-1 indicates the position of the thermistor chain. The data was collected for the period July 2001 to June 2002, at hourly intervals, and was used for model calibration purposes.

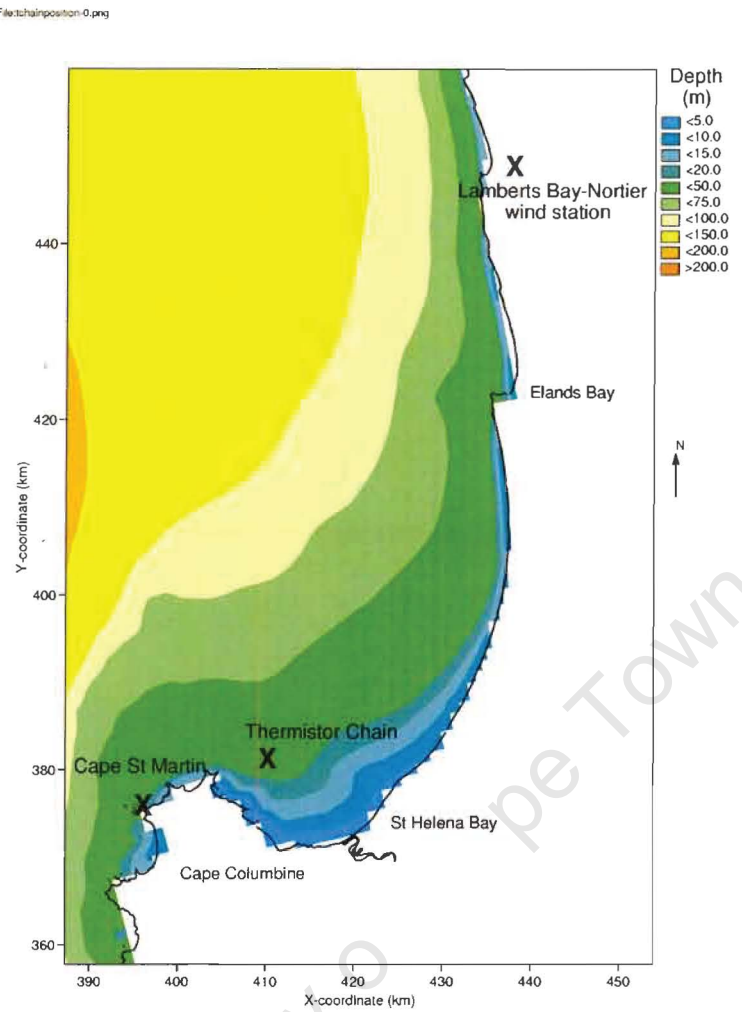

Figure 2-1 Positions of the thermistor chain in St Helena Bay, the St Helena Bay weather station at Cape St Martin and the Lamberts Bay – Nortier wind station.

Figure 2-2 indicates temperature time series, measured by the thermistor chain, for the period January to mid February 2002, at depths of 0 m (surface), 10 m, 16 m and 25 m (bottom). This time series shows an upwelling event (around 24 – 26 of January) during which southwesterly winds persist and cold bottom water is entrained into the surface layers, leading to a weakening of stratification and a cooling of surface water. Following the period of upwelling, the wind reduces, leading to a relaxation event and a subsequent warming of the surface water. During this time, the water becomes strongly stratified again. In early February, a strong southwesterly wind blows, leading to another upwelling event and a significant weakening in stratification.

Temperature data obtained from Hondeklip Bay (Figure 1-1) was originally used at the model's northern and southern open boundaries (Monteiro, 1997). This data set was chosen because it was the best continuous data set available at the time when the St Helena Bay model was set up. The

boundary conditions applied in any numerical model are normally a problem, usually due to the lack of good quality data. Chapter 3 discusses in more detail the way the open boundaries of this model were treated.

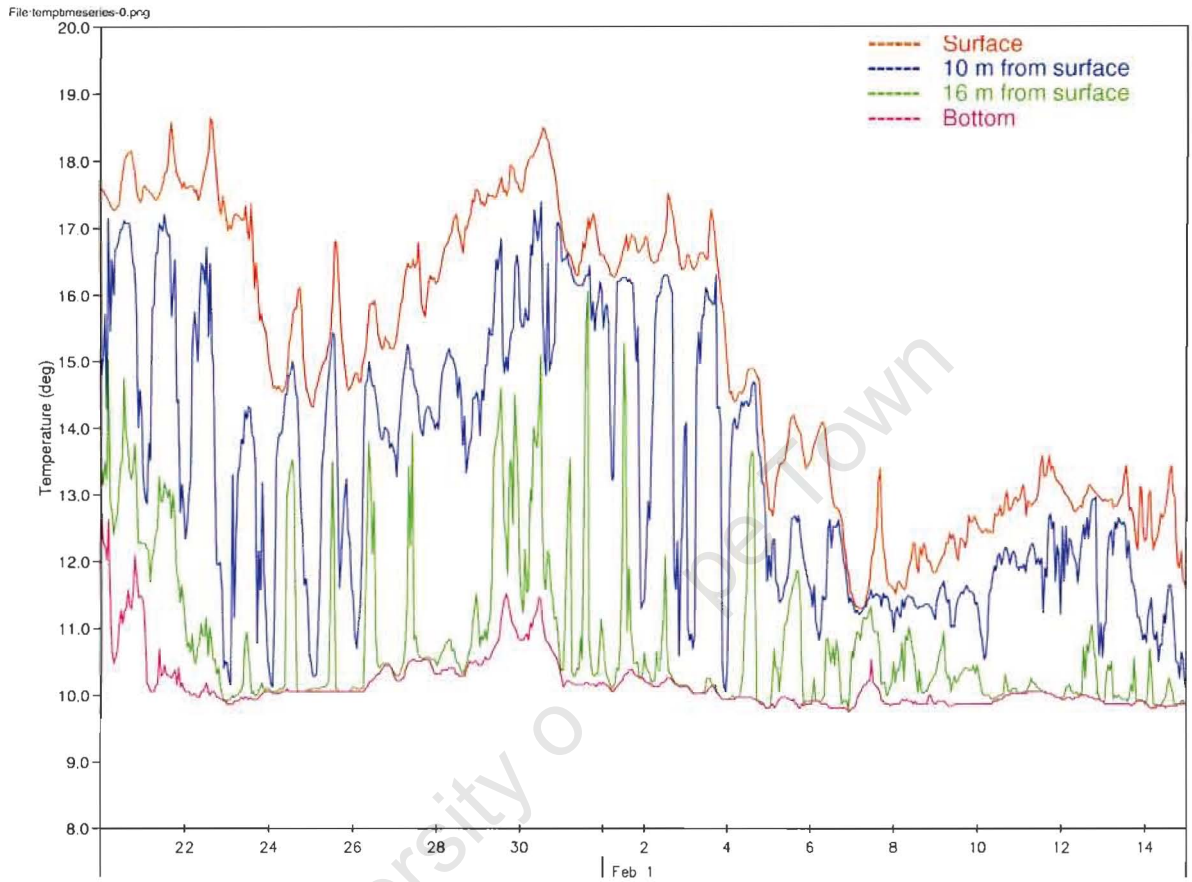

Figure 2-2 Temperature time series in St Helena Bay at four different depths, for January to mid February 2002.

2.3.3 Winds

Cape Columbine is a headland consisting of low smooth hills rising to about 250 m. The leewards coast bends away into the wide St Helena Bay, an area that is usually protected from summer winds (Jury, 1984 and Jury, 1985). In comparing wind shear and differential upwelling in the lee of Cape Columbine using mesoscale aerial survey case studies, Jury (1984) found evidence of spatially varying winds in the St Helena Bay area. However, due to the uncertainties surrounding the exact nature of the wind curvature as well as that of the wind speed reduction in the wake of Cape Columbine, a spatially uniform wind was applied in each of the case studies.

For the purpose of the present study, it was decided to focus on two wind scenarios, one representative of the western part of St Helena Bay (the "high wind scenario"), and one representative of the eastern part of St Helena Bay (the "low wind scenario"). Wind measurements in the vicinity of St Helena Bay were available at two locations, namely the St Helena Bay weather station at Cape St Martin (north of Cape Columbine), and the Lamberts Bay – Nortier station at Lamberts Bay. Figure 2-1 indicates the positions of these stations.

The St Helena Bay weather station is situated within an abalone farm (close to the coast) at 32.43S 17.55E and uses a MCS (Mike Cotton Systems) wind station, which is set up 20 m above MSL. The wind sensor measures the wind speed and direction on an hourly basis. Due to the exposed nature of the wind station, the winds measured at this location were considered representative of the western part of St Helena Bay.

The Lamberts Bay – Nortier wind station is set up in an unobstructed area (32.03S 18.33E) approximately 6 km inland at a height of 10m. The height of the ground, however, is 92.8 m above MSL, implying that the wind sensor is actually situated 102.8 m above MSL. The wind sensor is a RM Young automatic wind sensor, and it samples the wind three times in 10 seconds. Thereafter the zonal and meridional components of the wind are used to calculate the hourly wind speeds and directions, by using a fairly complex algorithm, which was developed in-house at the SAWS.

The location of the Lamberts Bay – Nortier station (relatively far inland) leads to several uncertainties concerning the influence that the surrounding terrain might have on the wind speed and direction. Also, the difference in air temperature between the coast and a site inland can also influence the wind measurements. Caution therefore had to be taken concerning the Lamberts Bay – Nortier station winds and it could not be considered as representative of the eastern part of St Helena Bay. However, to obtain a reasonable idea of the difference in wind speed and direction between the western and eastern parts of St Helena Bay, a comparison had to be made between the winds measured at the above two locations.

Before a sensible comparison between the measurements at the two locations could be made, in fact, before any numerical case study could be undertaken, the wind data extracted from the St Helena Bay weather station firstly had to be adjusted. Delft3D requires wind speed and direction equivalent to 10 m above the ground, and the measured winds at the St Helena Bay weather station therefore had to be reduced from a 20 m height to a 10 m height. (Note that the winds measured at the Lamberts Bay – Nortier station were already measured at 10 m above the ground and thus did not have to be reduced). The following equation was used (American Petroleum Institute, 1991):

$$V(z_R) = V(z_M)/(\frac{z_M}{z_R})^{0.125}$$

where

$V(z_R)$	=	wind speed (m/s) at reference level (10 m above MSL)
$V(z_M)$	=	wind speed at measured level
z_M	=	height above sea level at measured level
z_R	=	height above sea level at reference level (10 m)

The adjusted wind speeds at 10 m above MSL were approximately 8% less than those measured at 20 m at the St Helena Bay weather station.

For the purpose of making a simple comparison between the St Helena Bay weather station winds (adjusted to 10 m) and the Lamberts Bay – Nortier station winds, the measured wind speeds and directions at both locations were smoothed to remove diurnal effects. This was done by separating the winds into north-south and east-west components, and then computing a running 25-hour mean twice on each component, thus removing the diurnal component of the winds. Although more sophisticated filters are available, this filtering method was considered sufficiently accurate for the purpose of this application. The smoothed St Helena Bay weather station winds are applied later in St Helena Bay numerical case studies (described in Chapter 3).

Figure 2-3(a) shows the measured winds (adjusted to 10 m above MSL) as well as the smoothed winds at the St Helena Bay weather station for the period January to mid February 2002. During this period the predominant wind direction was southwesterly, with average speeds ranging between 2 m/s and 8 m/s. A strong upwelling event was evident from 19 – 24 January, with wind speeds that reached 12 m/s. An even stronger upwelling event occurred from 1 - 7 February, with wind speeds ranging between 10 m/s and 13 m/s.

The smoothed winds exclude the diurnal component of the wind, and do therefore not contain the diurnal peaks as seen in the measured winds. The smoothed wind speeds are generally lower (on average ranging between 1 m/s and 6 m/s), with a maximum wind speed of 8 m/s during the early February upwelling event.

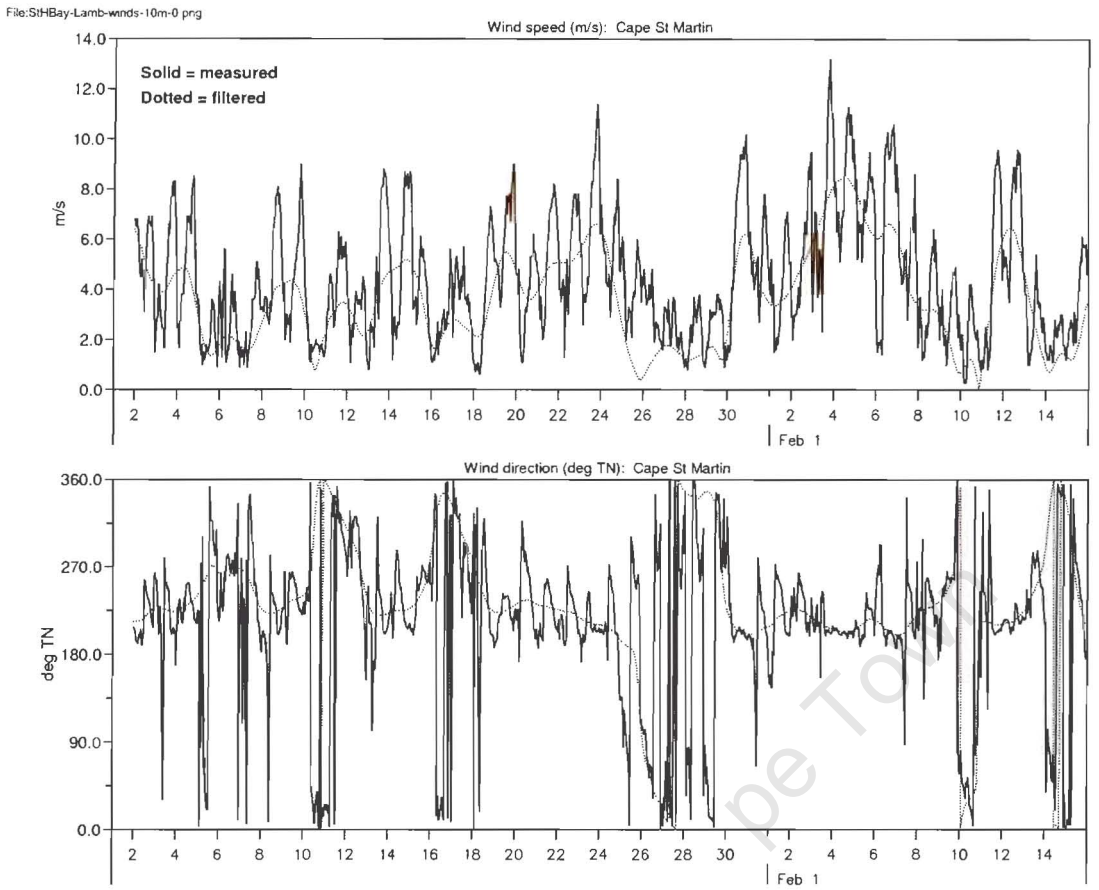

Figure 2-3(a) Measured wind speed and direction (solid line) at the St Helena Bay weather station at Cape St Martin for January to mid February 2002, and the smoothed wind speed and direction (dotted line) for the same period. Note the long periods of upwelling favourable southwesterly winds, followed by periods of relaxation.

Figure 2-3(b) shows a comparison between the smoothed wind speeds and directions at the St Helena Bay weather station and the Lamberts Bay – Nortier station for January to mid February 2002. Immediately apparent is the low winds speeds at Lamberts Bay – Nortier in comparison with the wind speeds at the St Helena Bay weather station, especially during upwelling events, when the Lamberts Bay wind speeds are on average 30 % lower than the St Helena Bay weather station winds. During wind relaxation events, the Lamberts Bay winds are marginally stronger than the St Helena Bay weather station winds (this might be due to the inland Lamberts Bay – Nortier wind station being away from the coast). At both the locations, the wind direction remained largely southwesterly, with instances of northerly winds (normally associated with periods of relaxation).

Furthermore, during 24 – 28 January as well as during 9 – 11 February, it can be seen that there is a discrepancy at the two stations concerning the way the wind changes to the north. In the case of the St Helena Bay weather station winds, the wind changes to the north through westward motion. On the

other hand, the wind at the Lamberts Bay – Nortier station changes to the north through eastward motion. This is most likely a response to the synoptic coastal wind system in the area.

Note:

In the above figures, 0° TN and 360° TN are the same direction. Wind oscillations around this point leads to the "up and down jumps" in the plots of wind direction.

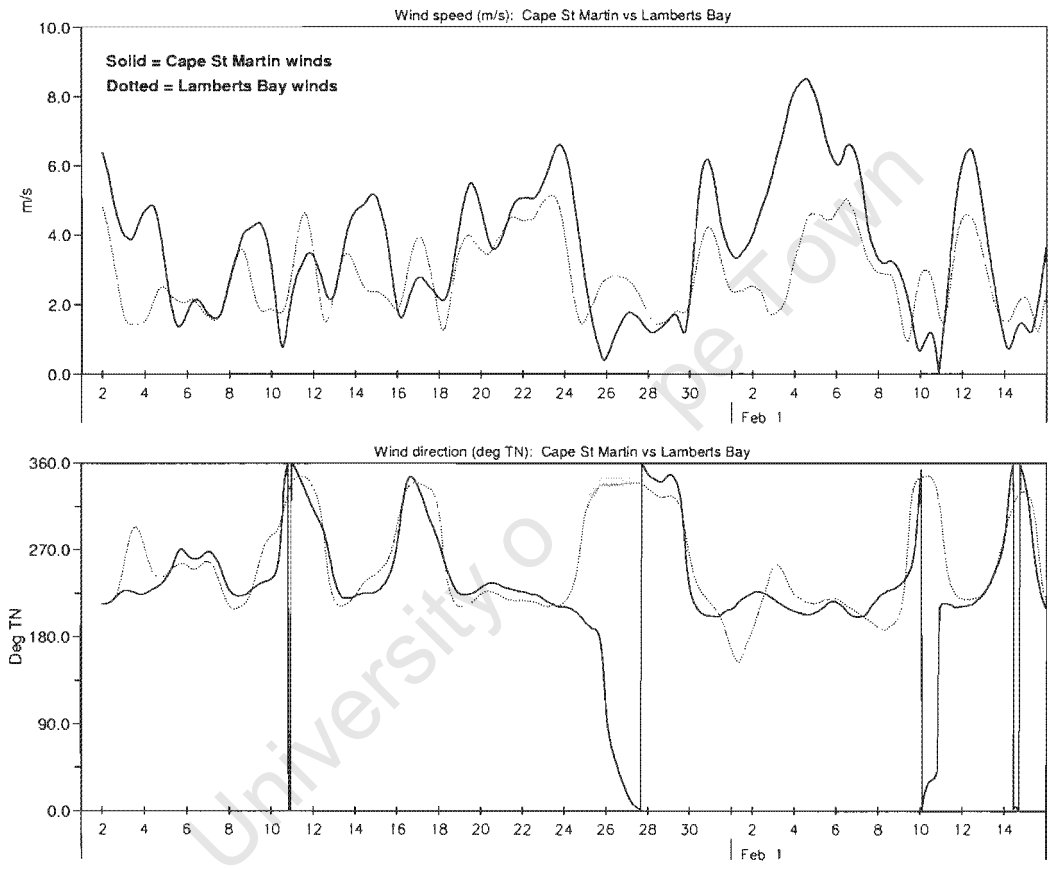

Figure 2-3(b) Comparison between the smoothed wind speed and direction at the St Helena Bay weather station at Cape St Martin (solid line) and at the Lamberts Bay – Nortier station (dotted line) for January to mid February 2002. Note the lower wind speeds at the Lamberts Bay – Nortier station during times of upwelling. The wind directions at the stations remained reasonably similar throughout the period.

After comparing the winds measured at the two locations in order to obtain a wind time series that could be representative of the eastern part of St Helena Bay, the decision was made to reduce the St Helena Bay weather station measured wind speeds by 30 %, and to keep the measured wind directions at this location unchanged. This reduced wind time series was considered a sufficient approximation of the wind in the eastern part of St Helena Bay.

2.3.4 Atmospheric data

Four data sets were necessary in order to include heat fluxes in the St Helena Bay model, namely: air temperature, humidity, cloudiness and net solar radiation.

Air temperature, humidity and cloudiness data were obtained from the South African Weather Services (SAWS). Cape Columbine is a first order station and thus has non-automatic instrumentation. The instruments that can be found at the station are: Wet and Dry Bulb thermometers, Maximum and Minimum thermometers, a digital barometer and a pressure plate anemometer mounted at 5 m above the ground. The relative humidity is calculated from the pressure and the Wet and Dry Bulb temperatures. The cloud information for Cape Columbine is reported three times a day by a volunteer observer and it is not a measured climate variable. All weather observers receive training in cloud identification and are equipped with a comprehensive cloud atlas in order to try to minimise subjectivity in these records.

The net solar radiation was measured at the St Helena Bay weather station at Cape St Martin (Figure 2-1). A MCS 155-1 radiation sensor was used to measure the radiation, with a scan period of once per minute. The data that was applied in the St Helena Bay numerical model was hourly averages for radiation.

2.4 List of conventions

Throughout this thesis, the following conventions are used:

- Time is in South African Standard Time (GMT + 2 hours);
- Current direction is the direction *to which* the current is flowing;
- Wind and wave directions are the direction *from which* the wind or wave is travelling;
- All directions are relative to True North;
- All depths and tidal levels are referenced to Mean Sea Level (MSL).

3. MODELLING INVESTIGATIONS

This chapter describes the details of the model setup (e.g. grids, bathymetry, and boundary conditions) for the Reference Model and for the St Helena Bay Model, respectively. Full descriptions of the studies that were undertaken using each model, are also given.

3.1 The Reference Model

3.1.1 Details of model setup

Hydrodynamic Grid

The Reference Model is a simplified, symmetric "block" model of alongshore length 500 km and cross shore length 300 km, representing a long, straight coastline. The alongshore length was chosen to be this extensive as to ensure that the model boundaries do not influence the behaviour inside the model domain in a significant way. The hydrodynamic grid has 67 x 56 lines and 3752 active cells. It is irregularly spaced, orthogonal and rectilinear. Figure 3-1 shows a full view of the grid (coastline to the right of the grid), as well as a close up view at the coast.

The grid has the highest resolution close to the coast, where the size of a typical grid cell is approximately 1.3 km in a cross shore direction and approximately 10 km in an alongshore direction. The grid decreases in resolution further away from the coast, where the largest grid cells have dimensions of approximately 18 km x 10 km. These cell sizes was chosen to ensure a high resolution in the coastal zone, so that the poleward current could be properly analysed, and a lower resolution further away from the region of interest.

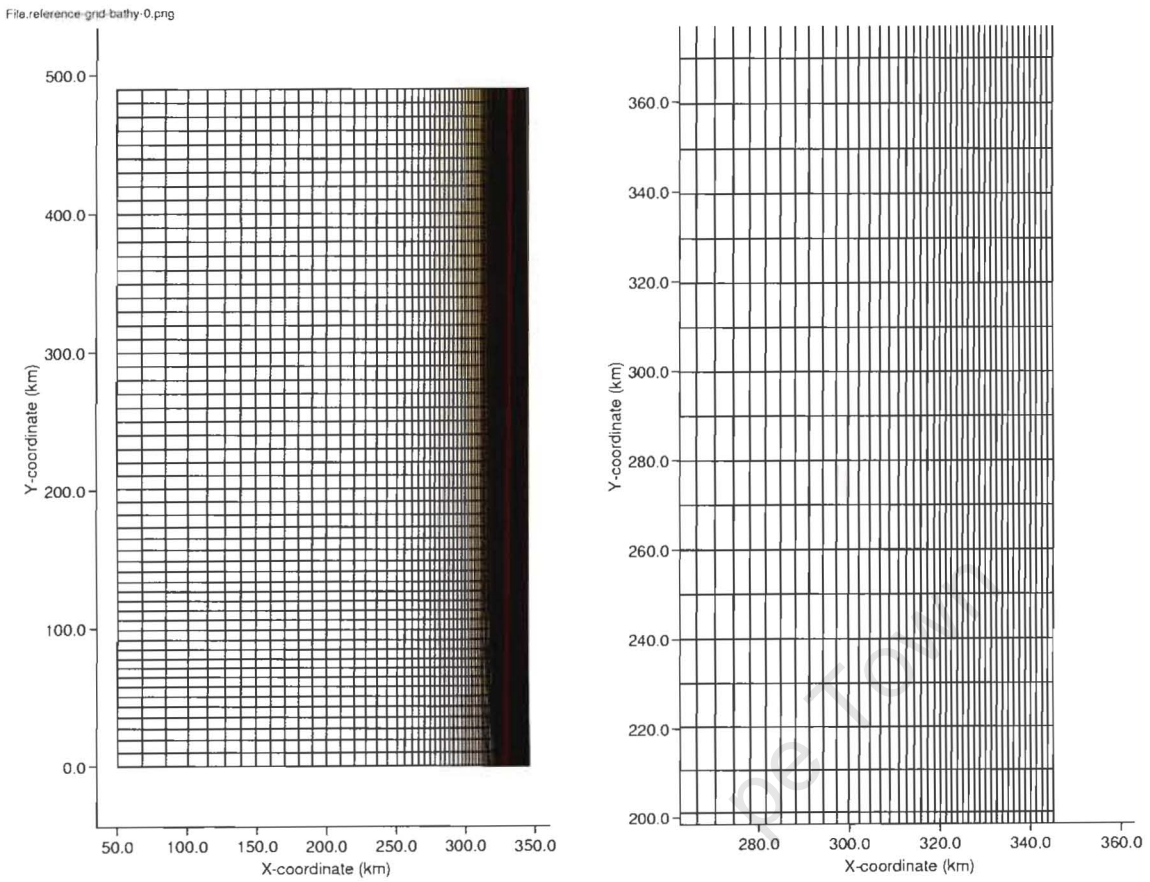

Figure 3-1 Reference Model hydrodynamic grid: Full domain (left) and a close up view of the coast (right). The coastline is on the right hand side of the model grid, where the high resolution in the grid cells is apparent.

In the vertical, ten layers were used with the thickness of the vertical layers (from surface to bottom) being 2.5 %, 2.5 %, 5 %, 7 %, 10 %, 14 %, 14 %, 15 %, 15 % and 15 % of the local water depth. Throughout the water column, the layers were kept as smooth as possible, with some concentration in the top layers. The thinner top layers were chosen in order to resolve the surface region accurately and the layer thicknesses gradually increased with depth. Table 3-1 illustrates the relative thickness of each of the ten layers. The percentage of the total water depth that each layer represents, as well as the cumulative percentage of the water column, is given. As an example, the 4th column in this table illustrates how deep it is from the water surface down to the bottom of each layer, for a total water depth of 100 m.

Table 3-1 Reference Model: Relative layer thickness.

Layer	% of total depth	Cumulative %	Distance from water surface to bottom of layer in 100m of water
1	2.5%	2.5%	2.5m
2	2.5%	5%	5m
3	5%	10%	10m
4	7%	17%	17m
5	10%	27%	27m
6	14%	41%	41m
7	14%	55%	55m
8	15%	70%	70m
9	15%	85%	85m
10	15%	100%	100m

Bottom topography

An artificial bottom topography was created for the purpose of the Reference Model investigations. This topography was chosen to be simple, yet complex enough to include the main topographical features that were necessary for the study of the nearshore poleward current. This topography was chosen to be a simple representation of the true bottom topography found in the area of interest on the West Coast. The topography consists of an inner shelf area (close to the coast), an outer shelf area, and a deep ocean area, with no variation in the alongshore direction. As will be described in Chapter 3.1.2, different slopes for the inner shelf area were applied during the Reference Model investigations in order to test the influence that the bottom topography has on the formation of a nearshore poleward current. The different slopes were obtained by specifying different minimum depths for the bottom topography (namely 20 m, 50 m and 100 m). The outer shelf and deeper ocean topography, however, remained the same for all the experiments.

The large scale features of the bottom topography are as follows: The 100 m depth contour is approximately 30 km offshore (with the bottom depth linearly decreasing from the coast down to the 100 m depth contour). The 200 m depth contour is approximately 200 km offshore (with the bottom

depth linearly decreasing form the 100 m to the 200 m depth contour). From the 200 m contour the bottom depth decrease linearly to a maximum depth of 320 m, approximately 300 km offshore. Figure 3-2(a) shows a vertical cross-section of the bottom topography over the full cross-sectional width of the model, for the three different bottom topography's that were applied during the Reference Model experiments (only the slope of the inner shelf region is different in each case).

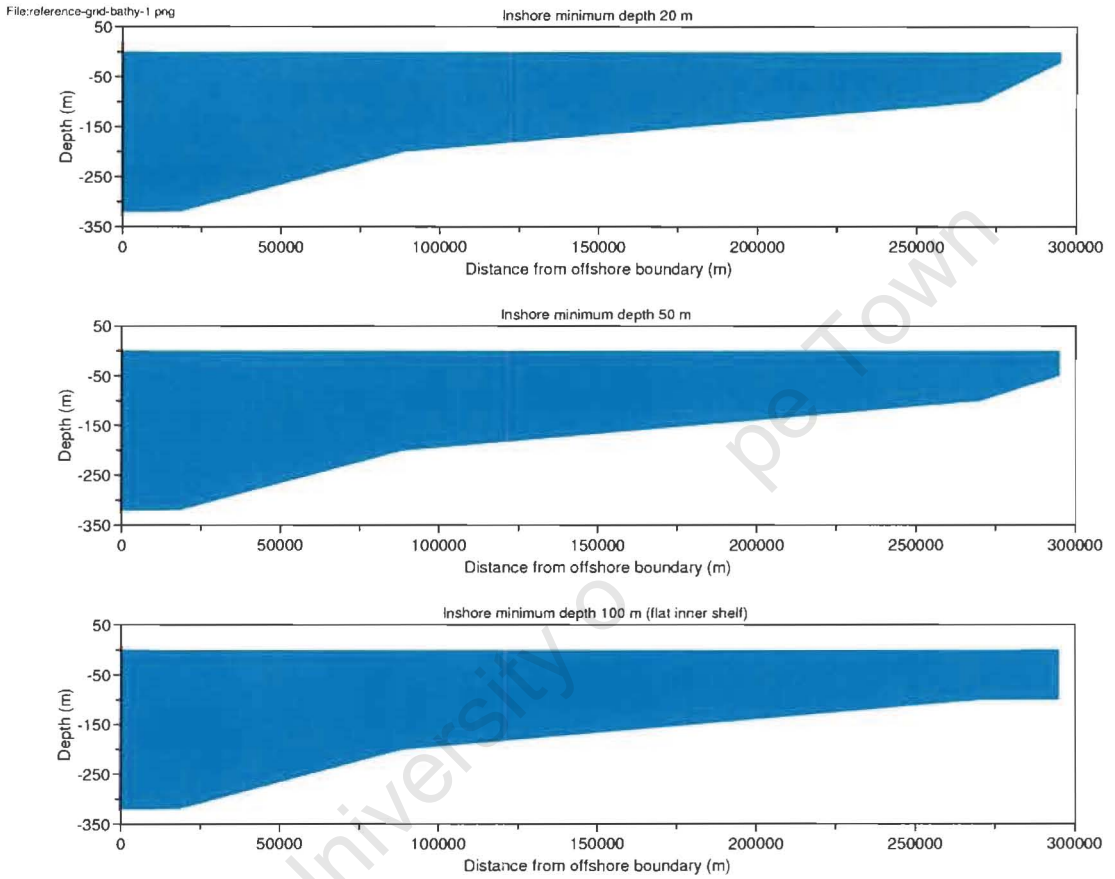

Figure 3-2(a) Reference Model: Vertical cross-section of the bottom topography over the full cross-sectional width. The difference between the three topographies is the slope of the inner shelf region. The coastline is on the right hand side.

Figure 3-2(b) shows a close-up view of the bottom topography in the inner shelf region. This figure clearly shows the three different inner shelf slopes that were used during numerical experiments undertaken with the Reference Model.

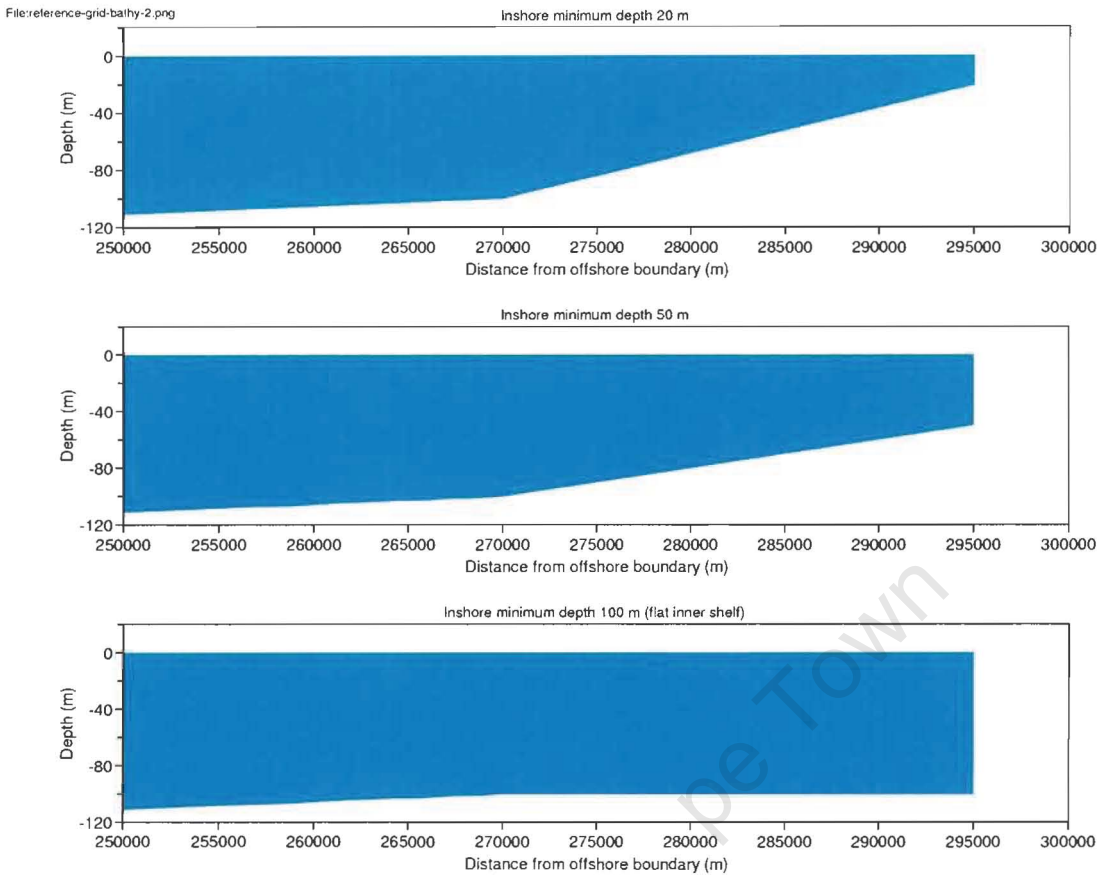

Figure 3-2(b) Reference Model: Vertical cross-section of the bottom topography showing a close-up view of the inner shelf region. Minimum depth 20 m (top), minimum depth 50 m (middle) and minimum depth 100 m (bottom). The coastline is on the right hand side in each case.

Winds

In the Reference Model experiments, synthetic, upwelling favourable winds were applied for a few days at a time, followed by calm periods, in order to simulate typical upwelling-relaxation events to investigate the formation of the poleward current. These winds were southerly and constant over whole model domain.

In two of the three numerical experiments undertaken with the Reference Model, a single wind event was applied. During this event, the wind starts off at 0 m/s and ramps up gradually over a period of one day, until it reaches its maximum of 10 m/s (southerly). The wind stays at this maximum for five days, and then linearly reduces back to 0 m/s over a period of 10 hours. For the rest of the modelling period, calm conditions prevail. This wind event can be seen in Figure 3-3 (the first peak, from day two to day eight).

One numerical experiment, however, applied a different wind time series, namely three wind events over a period of one month. This was done in order to simulate the more realistic conditions of several windy periods followed by calm periods. Figure 3-3 illustrates the change in wind speed over time for this synthetic wind time series (the direction remains southerly). The first wind event is similar to the event discussed previously, but four days after the first event, the wind speed increases again over a period of one day, and it remains at its maximum of 10 m/s for three days. The wind speed then dies down again for three days, after which it increases to 10 m/s again and blows for four days. Thereafter the wind dies down and remains at 0 m/s for the rest of the time.

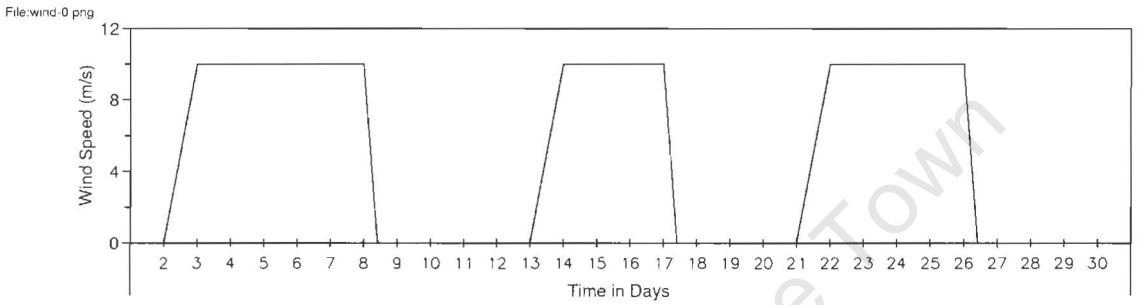

Figure 3-3 Reference Model Wind Time Series: Graph showing a time series of the wind speed that was applied during the numerical experiments. Two of the three numerical experiments applied only the first wind event, while the third experiment applied all three of the wind events. The direction of the wind was southerly.

Heat fluxes

The so-called *Proctor Model* formulation (WL|Delft Hydraulics, 2003) was used to model the heat fluxes in the Reference Model. A mean value for daytime and night time humidity, air temperature and cloudiness is specified, and these values are used by the model to simulate the heat fluxes at the water surface. These mean values were typical values obtained from the observations at the St Helena Bay weather station at Cape St Martin for the period January to mid February 2002, which was measured by the CSIR (described in Chapter 2.3.4). The heat flux models incorporated into Delft3D are discussed in more detail in Appendix B, which gives an extract from the Delft3D-FLOW manual. Table 3-2 shows the values for the heat flux parameters that were specified in the model.

Table 3-2 Reference Model: Heat flux parameters.

	Day-time (12:00)	***Night-time (00:00)***
Relative Humidity (%)	80	95
Air temperature (°C)	23	19
Cloudiness (%)	10	10

Boundary Conditions – water levels

The open boundaries in the sea are located along the three offshore edges of the model, which are the Southern, Northern and Western boundaries (Figure 3-1). In hydrodynamic models such as Delft3D-FLOW, the open boundary conditions may be specified as water levels, currents, discharges or Riemann invariants, and may vary along the boundaries in both time and space. The specification of correct open boundary conditions was identified from the start as one of the most challenging issues for applying the Delft3D-FLOW model to Southern African conditions, which are characterised by open coastlines, weak tidal currents, strong wind-driven currents and a lack of field data. This is in contrast to Europe, where tidal currents are often dominant and the boundary conditions may be specified as tidal levels obtained from well-calibrated regional models.

To enable the commonly encountered hydrodynamic conditions in Southern Africa to be simulated, a hydrodynamic boundary module, TILT, was developed (Luger & Stelling, 2000). The conditions include wind-driven current forcing, large-scale ocean circulation (e.g. the Agulhas Current) and a combination of wind and large-scale ocean circulation.

This module assumes a relatively open coastline where the model domain has three open boundaries, i.e. two cross shore boundaries orientated approximately normal to the coastline and an alongshore boundary orientated approximately parallel to the coastline. Water levels have been selected as the boundary type for all three open boundaries. This is because water levels offer the most simple and flexible specification by allowing the hydrodynamic model to determine the details of the two- or three-dimensional flows through the boundaries. The tide can also be added by simple superposition.

The theory behind the development of the module as well as the assumptions that have been made during the solving of the momentum equations are described in Luger & Stelling (2000) and is presented in Appendix A. By applying the model, the change (or the 'tilt) in the water level at the boundaries of the model due to the presence of an alongshore wind is calculated (assuming an infinite coastline beyond the model boundaries). This allows the water levels at the boundary to be dynamic and time varying.

Boundary conditions - temperature

Apart form specifying water levels at the model boundaries, temperature must also be specified. (Note that a constant salinity of 35 ppt was specified in the model.) The approach was to specify an initial vertical temperature profile throughout the model domain as well as at the boundaries. Figure 3-4 shows the temperature profile that was chosen as an initial condition. This profile is synthetic, but was chosen in such a way as to be representative of a typical temperature profile.

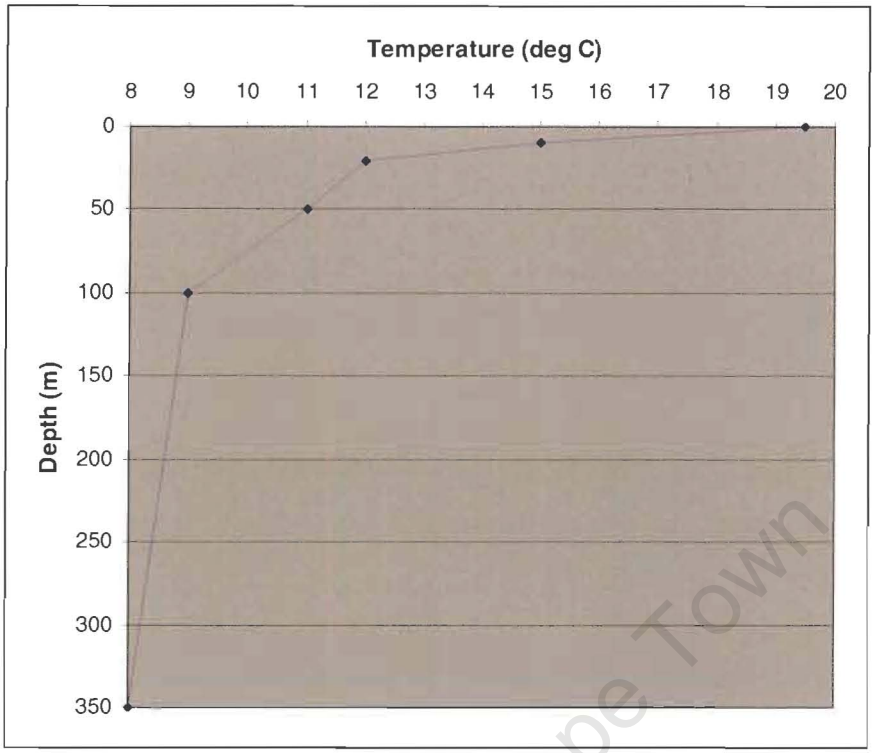

Figure 3-4 Reference Model Temperature Profile: Graph showing the vertical temperature profile that was initially applied throughout the Reference Model domain, as well as at the boundaries.

During a numerical study, the model is allowed to run free, but the boundary conditions are non-dynamic and will remain static ('clamped') throughout the study. The problem of having static temperature profiles at the boundaries is that after a short period of time there are growing discrepancies between the temperature at the boundaries and the temperature inside the model domain, because the inside of the model domain is allowed to change under the forcing conditions. As a consequence, artificial pressure gradients are set up across the boundaries, and an artificial current field is created. Such an artificial current may be so significant that it may influence the results inside the model domain. For this reason, the model domain is usually chosen to be large enough to keep the model boundaries as far away of the area of interest as possible. There are, however, limitations to the size of the model domain (for numerical stability reasons), and in some instances it is not possible to have the boundaries far enough away.

For the purpose of this thesis, a Fortran programme was developed to enable the model to apply a so-called 'zero gradient' across the model boundaries. The approach was as follows: Each Reference Model numerical experiment was run once, applying the static boundary conditions given in

Figure 3-4 at the model boundaries and applying TILT at the boundaries to calculate the water levels. Inside the model domain, approximately 140 km from the model boundaries, so-called 'observation points' were placed, which tracked the change in temperature throughout the water column while the model was running. The locations were chosen to be far enough away from the boundaries as to not be influenced by poor boundary conditions. After a numerical experiment has run once, the developed Fortran programme was used to extract the dynamic temperature time series from the 'observation points' inside the model domain. This extracted temperature time series was then specified at the model boundaries, and the experiment was repeated. This process ensured that the temperature field at the boundaries agreed with the temperature field inside the model domain, close to the boundaries. This minimized the possible artificial behaviour that could be created at the model boundaries due to ill-specified boundary conditions. Tests indicated that this had to be an iterative process, and that each study had to be repeated three times before a steady state was reached.

Other modelling parameters

Other modelling parameters that have been used in the Reference Model are shown in Table 3-3. The time step and horizontal eddy viscosity are calibration parameters. The values for gravity, water density, salinity and air density are widely used. The bed friction formulation is detailed in Nicholson *et al* (1990).

Table 3-3 Reference Model: Hydrodynamic model parameters.

Parameter	***Value***
Timestep	1 minute
Gravity	9.81 m/s^2
Water density	1024 kg/m^3
Air density	1.2 kg/m^3
Salinity	35 ppt
Bed friction formulation	Chezy
Roughness	55
Horizontal eddy viscosity	1 m^2/s

3.1.2 Description of Reference Model numerical experiments

The purpose of the Reference Model was to establish the main forcing mechanisms that influence the formation and strength of a typical nearshore poleward current by undertaking simple, idealized test experiments. These experiments illustrated the effect of bottom topography, winds and stratification on the current profile along the coastline.

From literature (Pitcher & Boyd, 1996; Pitcher *et* al, 1998; Probyn *et al*, 2000) it was found that whenever a poleward current formed, it always happened during the wind relaxation phase following a period of upwelling favourable winds. A period of wind-driven upwelling, followed by a period of wind relaxation, was thus included in each numerical experiment. A description of each numerical experiment follows.

Numerical Experiment 1

The aim of this experiment was to determine whether the presence of stratification is necessary for the formation of the poleward current.

Two studies were undertaken. These studies were identical, except that the one included the process of stratification, and the other did not. Heat fluxes were included where stratification was included. The bottom topography that was used during these studies is the "minimum depth 20 m" topography (Figure 3-2(b) top plot). This was the topography that contained the steepest inner shelf. The "single wind event" scenario was applied (thus only the first wind event indicated in Figure 3-3), and the studies were run for a period of twenty-five days. The wind event occurred during the first eight days of each study.

Numerical Experiment 2

The aim of this experiment was to determine the importance of the inner shelf slope (thus the topography) is during the formation of the poleward current.

Three studies were undertaken. All the studies included stratification and once again the "single wind event" scenario was applied. Heat fluxes were also included. The model period in each case was once again twenty-five days. The only difference between the three studies was the slope of the inner shelf. The slope was changed simply by changing the minimum depth at the coast (20 m – steep slope, 50 m – medium slope and 100 m – flat inner shelf). The three inner slopes that were applied can be seen in Figure 3-2(b).

Numerical Experiment 3

The aim of this experiment was to determine the ocean response to multiple wind events.

A study was undertaken by applying the full wind time series as shown in Figure 3-3. The study included stratification and heat fluxes. The "minimum depth 20 m" slope was applied during this study. The study period was thirty days.

3.2 The St Helena Bay numerical model

3.2.1 Details of model setup

Hydrodynamic grid

To enable an accurate study of the circulation patterns in the St Helena Bay area, it was necessary to include in the model a sufficiently large model domain. As stated previously, a large domain will ensure that the internal processes in the St Helena Bay model are not influenced in a significant way by the specified boundary conditions. The hydrodynamic grid is irregularly spaced, orthogonal and curvilinear, and is shown in Figure 3-5. As far as possible, the curvilinear grid is designed to follow the shoreline of the ocean, thus promoting a smooth flow pattern in these areas. It has a cross shore length scale of approximately 120 km, and an alongshore length scale of approximately 280 km, stretching from south of Saldanha Bay to north of Olifants River mouth.

The hydrodynamic grid has 80 x 57 lines and is designed so that the grid size at the offshore boundary is as large as 9 km x 12 km, but is refined to a small size of approximately 1.8 km x 1 km in the vicinity of St Helena Bay and along the coast, where a fine resolution in the results is required. The model grid has 3078 active cells. In the vertical, ten layers were used with the thickness of the vertical layers (from surface to bottom) being 2.5 %, 2.5 %, 5 %, 7 %, 10 %, 14 %, 14 %, 15 %, 15 % and 15 % of the local water depth (similar to the layers in the Reference Model). Throughout the water column, the layers were kept as smooth as possible, with some concentration around the top layers in order to resolve this area accurately. Table 3-1 gave a visualization of the relative layer thickness.

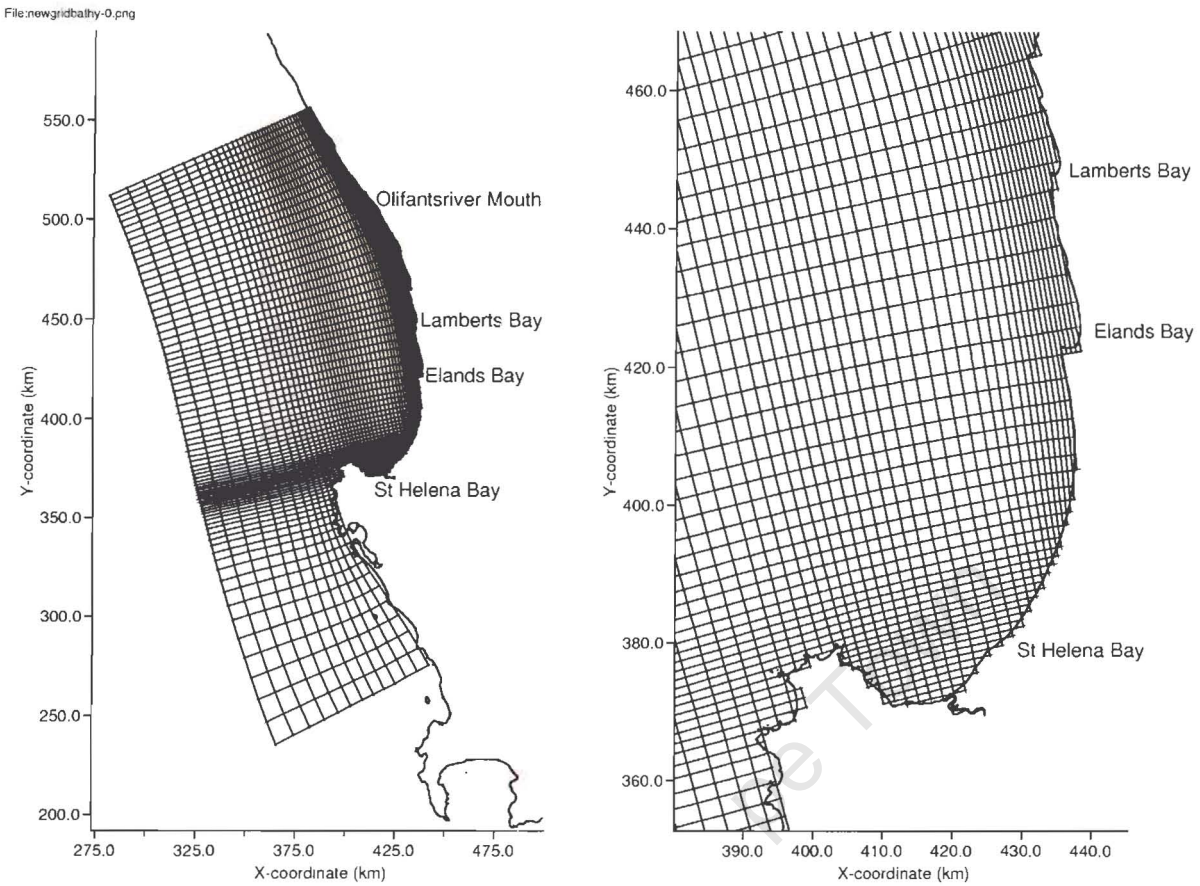

Figure 3-5 Hydrodynamic model grid: Full domain (left) and close up view of the St Helena Bay area (right).

Bottom topography

The x-y coordinate system used in the model is based on the Lo 19 coordinate system. Depth contours as well as spot depths were obtained by digitising the appropriate SA Navy Charts (Chapter 2.3.1). A linear transformation was applied to these digitised depths to provide model coordinates (x_{model}, y_{model}) that are positive and increase from South to North and from West to East. The transformation used is:

$$x_{model} = 500\,000 - y_{lo19}$$
$$y_{model} = 4\,000\,000 - x_{lo19}.$$

These depths were mapped onto the computational grid by using triangular interpolation as well as grid cell averaging (these are functions that form part of the Delft3D software). Towards the north of the model, for the top 20 km, a 'flat' area (fixed topography) was created in order to simplify the topography close to the boundary. This was done to ensure a smooth flow pattern close to the boundary. This artificial topography did not have an influence on the flow patterns in the area of interest. The resulting bathymetry for the model is shown in Figure 3-6.

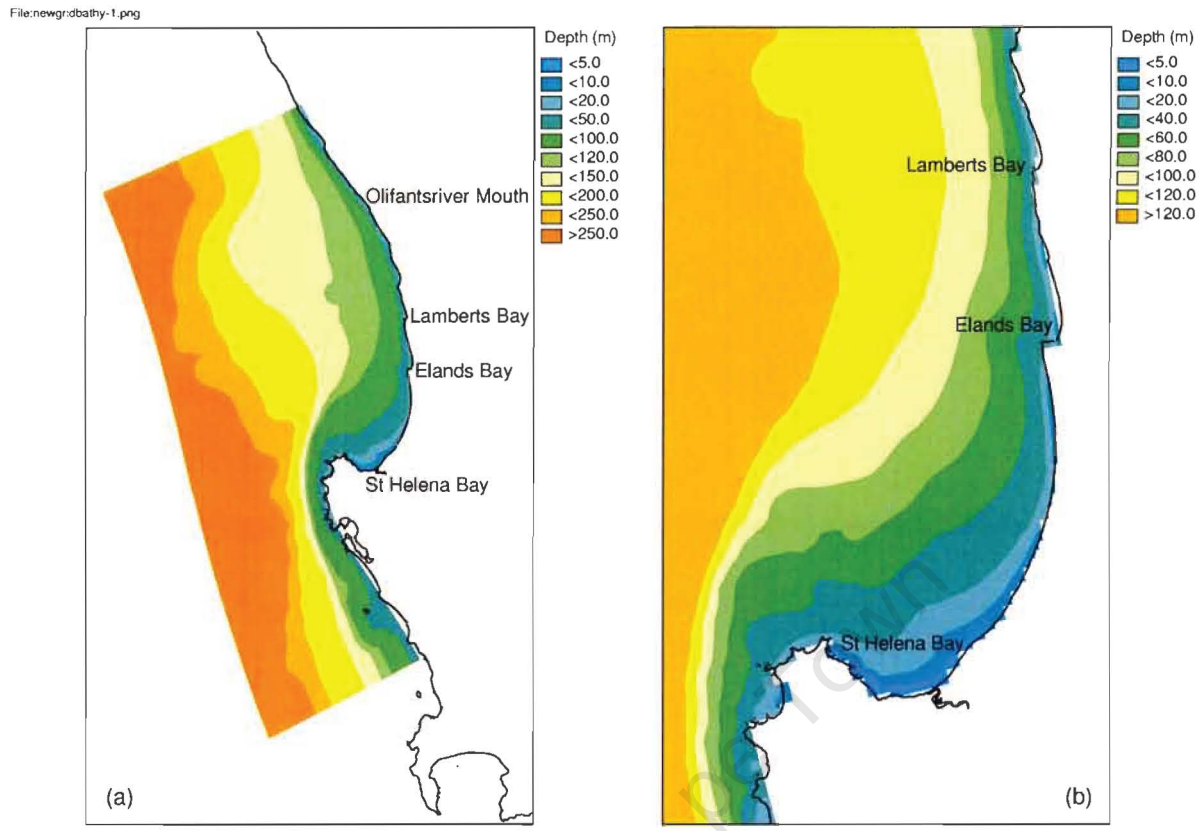

Figure 3-6 Hydrodynamic model bathymetry: Full domain (left) and close up view of the St Helena Bay area (right).

Heat fluxes

Because of the fact that measured values for the radiation were available, a different heat flux model was used for the purpose of this study, namely *Heat flux model 2* (WL|Delft Hydraulics, 2003). In this model, the combined net short wave solar and long wave atmospheric radiation is prescribed. The terms related to heat losses due to evaporation, back radiation and convection are computed by the model. Evaporation and convection depend on the air temperature, the water temperature near the free surface, relative humidity and wind speed. The heat flux models incorporated into Delft3D are discussed in more detail in Appendix B, which gives an extract from the Delft3d-manual.

Boundary conditions – water levels

The open boundaries in the sea are located along the three offshore edges of the model, which are the Southern, Western and Eastern boundaries (Figure 3-6(a)). No tide was included in the model studies.

The open boundary conditions were specified as water level boundaries (as with the Reference Model), and the TILT hydrodynamic boundary module (Luger & Stelling, 2000) was once again used (see previous discussion in Chapter 3.1.1).

Boundary conditions - temperature

The approach for the St Helena Bay model was to specify an initial vertical temperature profile throughout the model domain as well as at the boundaries. (Note that a constant salinity of 35 ppt was specified in the model.) Figure 3-7 shows the temperature profile that was chosen as an initial condition. As mentioned in Chapter 2.3.2, this profile was obtained from Hondeklip Bay data (Monteiro, 1997).

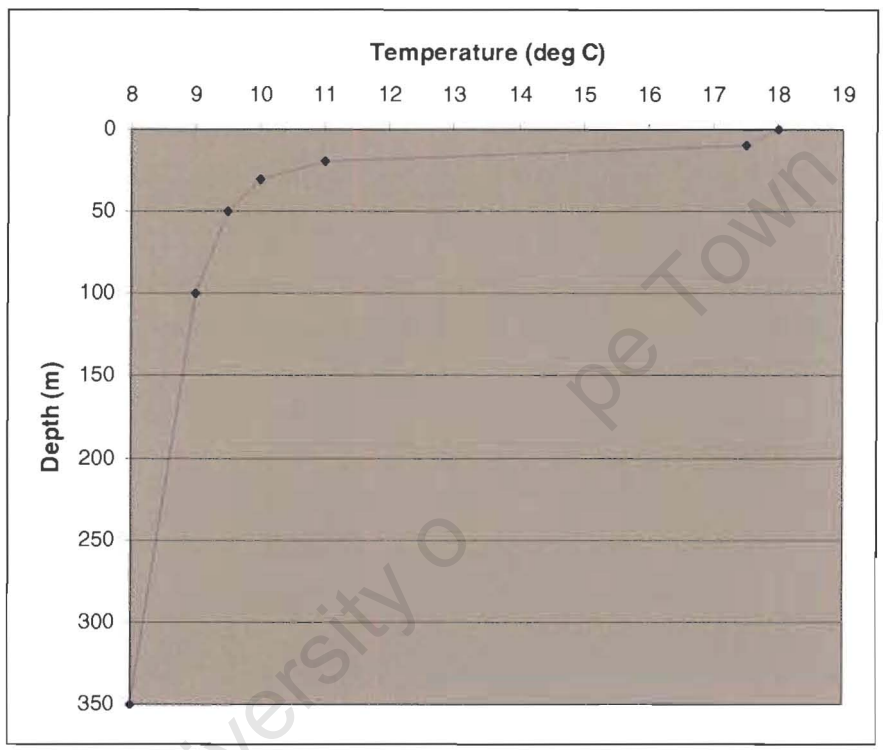

Figure 3-7 St Helena Bay Model Temperature Profile: Graph showing the vertical temperature profile that was initially applied throughout the St Helena Bay model domain, as well as at the boundaries.

Once again, the static boundary conditions were a problem, and no adequate temperature data was available to enable the use of dynamic boundary conditions. The software that was developed during the Reference Model experiments (as discussed in Chapter 3.1.1) in order to apply a 'zero gradient' across the model boundaries, was therefore used in the St Helena Bay model as well. The same process was followed as for the Reference Model, but in the case of the St Helena Bay model the locations of the "observations points" were approximately 60 km from the model boundaries. All of the St Helena Bay numerical case studies were thus also run three times to enable the achievement of a steady state condition. This minimized the artificial behaviour that could possibly be created in the model due to ill-specified boundary conditions.

All model runs used a "cold start" with the flow velocity being zero everywhere. The initial sea level was set to a constant 0 m above MSL. The relevant model parameters used in the model was the same as the parameters that were used during the Reference Model experiments (Table 3-2). As will be seen later on in the results, the model took approximately 1 week to spin up.

3.2.2 Description of St Helena Bay numerical model studies

The model setup as described earlier was used to undertake three case studies, each comprising the period from January to mid February 2002. This period was long enough to include the major upwelling events and to include the period of the year that HAB's occur most often (Pitcher *et al*, 1998). During the Reference Model numerical experiments, a straight coastline and uniform bottom topography were used. In the case of the St Helena Bay model, however, the coastline is irregular and there is an alongshore variation in bottom topography. This makes the St Helena Bay model much more complex.

In order to investigate whether the mechanisms behind the formation of the poleward current are the same in the case of St Helena Bay than what were identified by the Reference Model, three studies were undertaken. The difference between these studies is the response to different wind scenarios. A description of each of these studies is presented below:

Case 1

In this study, the measured St Helena Bay weather station winds (adjusted to 10 m above MSL) were used. This was the time series that contained the strongest upwelling favourable winds (Figure 2-3(a)).

Case 2

In this study, the measured St Helena Bay weather station winds (adjusted to 10 m above MSL) were used, but this time the wind speeds were reduced by 30 %. This was done to employ a so-called "low wind scenario" (as described in Chapter 2.3.3) that best agreed with the conditions in the eastern part of St Helena Bay and the Lamberts Bay region.

Case 3

In this study, the smoothed St Helena Bay weather station winds (adjusted to 10 m above MSL), which exclude diurnal sea breezes, were used (Figure 2-3(a)). The winds were still upwelling favourable, but generally weaker.

The results from the above studies are presented in Chapter 4.

4. RESULTS FROM THE REFERENCE MODEL

4.1 Reference Model Analytical Validation

In order to test whether the Reference Model is structured in an appropriate way to enable valid investigations by means of several numerical experiments, it was necessary to test the model results against the theory. One study was undertaken by solving the barotropic equations of motion. Stratification was thus not included in the model study, and the bottom topography that was applied during these studies, is the "minimum depth 20 m" topography (Figure 3-2(b) top plot). This was the topography that had the steepest inner shelf. The wind event occurred during the first five days of the study, after which the wind ceased. The comments that follow will focus on the steady state achieved after the wind has been blowing for some time.

In this analytical validation the hydrodynamic equations (WL|Delft Hydraulics, 2003) can be considerably simplified in the following ways:

- Cartesian rectangular co-ordinates can be used due to the simple grid and the straight coastline;
- Stratification is not included, therefore a single constant density layer is assumed;
- Internal turbulence is negligible in comparison with bottom friction.

By applying the above simplifications, the momentum equations and the continuity equation that are solved in Delft3D-FLOW during this study are as follows:

Conservation of momentum in x-direction:

$$\frac{\partial u}{\partial t} + u\frac{\partial u}{\partial x} + v\frac{\partial u}{\partial y} + g\frac{\partial \eta}{\partial x} - f.v + \frac{g.u|U|}{c^2(d+\eta)} - \frac{F_x}{\rho(d+\eta)} = 0 \quad (1)$$

Conservation of momentum in y-direction:

$$\frac{\partial v}{\partial t} + u\frac{\partial v}{\partial x} + v\frac{\partial v}{\partial y} + g\frac{\partial \eta}{\partial y} + f.u + \frac{g.v|U|}{c^2(d+\eta)} - \frac{F_y}{\rho(d+\eta)} = 0 \quad (2)$$

Conservation of mass, continuity equation:

$$\frac{\partial \eta}{\partial t} + \frac{\partial [(d+\eta)u]}{\partial x} + \frac{\partial [(d+\eta)v]}{\partial y} = 0 \tag{3}$$

where:

u, v	=	velocity in the x- and y-directions, respectively
d	=	still water level
t	=	time
x, y	=	horizontal Cartesian rectangular co-ordinates
η	=	water level elevation
U	=	magnitude of total current velocity
$F_{x,y}$	=	x- and y- components of the wind forcing
f	=	Coriolis parameter $2\Omega \sin\phi$, where Ω is the earth's angular velocity and ϕ is the geographic latitude
g	=	acceleration due to gravity
ρ	=	water density
c	=	Chézy coefficient

Furthermore, in the Reference Model experiment the assumption is that the alongshore variations are much smaller than the cross shore variations, therefore

$$\frac{\partial}{\partial y} << \frac{\partial}{\partial x}.$$

Also, the cross shore velocities are assumed to be very small in comparison to the alongshore velocities, so that

$$v >> u.$$

In the numerical study undertaken for the purpose of model validation (in fact, in all the numerical experiments undertaken with the Reference Model), the wind stress F had no cross shore component (the wind always blew from the south). Furthermore, the model coordinates are directed such that y and v are the alongshore components, increasing towards the equator (thus towards the north), and

such that x and u are the cross shore components, increasing towards the coast (thus towards the east), as illustrated below:

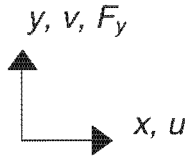

Following the above assumptions, the dominant terms for conservation of momentum in the cross shore direction (Equation (1)) then become:

(4) $$\frac{\partial u}{\partial t} + u\frac{\partial u}{\partial x} + g\frac{\partial \eta}{\partial x} - f.v + \frac{g.u|U|}{c^2(d+\eta)} = 0$$ (Cross shore geostrophy)

and the dominant terms for conservation of momentum in the alongshore direction (Equation (2)) then become:

(5) $$\frac{\partial v}{\partial t} + u\frac{\partial v}{\partial x} + f.u + \frac{g.v|U|}{c^2(d+\eta)} - \frac{F_y}{\rho(d+\eta)} = 0$$ (Wind forcing).

Equation (3) becomes:

(6) $$\frac{\partial \eta}{\partial t} + \frac{\partial[(d+\eta)u]}{\partial x} = 0$$ (Continuity).

Note that these equations do not contain any baroclinic (density variation) terms.

During a wind event, the dissipation terms grow as the alongshore current increases, until a steady state balance is achieved. As soon as a steady state is reached,

$$\frac{\partial}{\partial t} \to 0,$$

and the continuity equation (Equation (6)) gives

$$u \to 0, \text{ and } \frac{\partial u}{\partial x} \to 0.$$

Thus, from Equation (4):

(7) $$g\frac{\partial \eta}{\partial x} - f.v = 0 \quad \text{(Cross shore geostrophy)}$$

and from Equation (5):

(8) $$\frac{g.v^2}{c^2(d+\eta)} = \frac{F_y}{\rho(d+\eta)} \quad \text{(Wind forcing).}$$

Using the model constraints, the steady state values can be determined as

$$u_{ss} = 0$$

(10) $$v_{ss} = \sqrt{\frac{c^2 F_y}{\rho g}}$$

(11) $$\left.\frac{\partial \eta}{\partial x}\right|_{ss} = \frac{f v_{ss}}{g}.$$

Note that since $f < 0$ in the southern hemisphere,

$$\left.\frac{\partial \eta}{\partial x}\right|_{ss} < 0.$$

Air density (ρ_a) = 1.2, wind speed (U_{10}) = 10 m/s, and from the equation for the wind drag coefficient (Chapter 2.2.1), C_d = 0.0017. It thus follows (from the wind stress equation in Chapter 2.2.1) that $F_y = 1.2 \times 0.0017 \times 10^2 = 0.204$ and this gives the following value for the alongshore, steady state current v_{ss}:

$$v_{ss} = \sqrt{\frac{55^2 \times 0.204}{1024 \times 9.81}} = 0.248 \text{ m/s}$$

and thus

$$\left.\frac{\partial \eta}{\partial x}\right|_{ss} = \frac{-0.00008 \times 0.25}{9.81} = -2.04 \times 10^{-6}$$

These values can be checked against the model results. Figure 4-1 shows a spatial view of the modelled current velocities when a steady state has been achieved. The currents are predominantly

alongshore and uniform. In deeper waters, offshore of the 100 m depth contour, the currents seem to have a slight negative cross shore component, indicating that a steady state situation has not been completely reached, but this is considered an acceptable state for the purpose of this experiment.

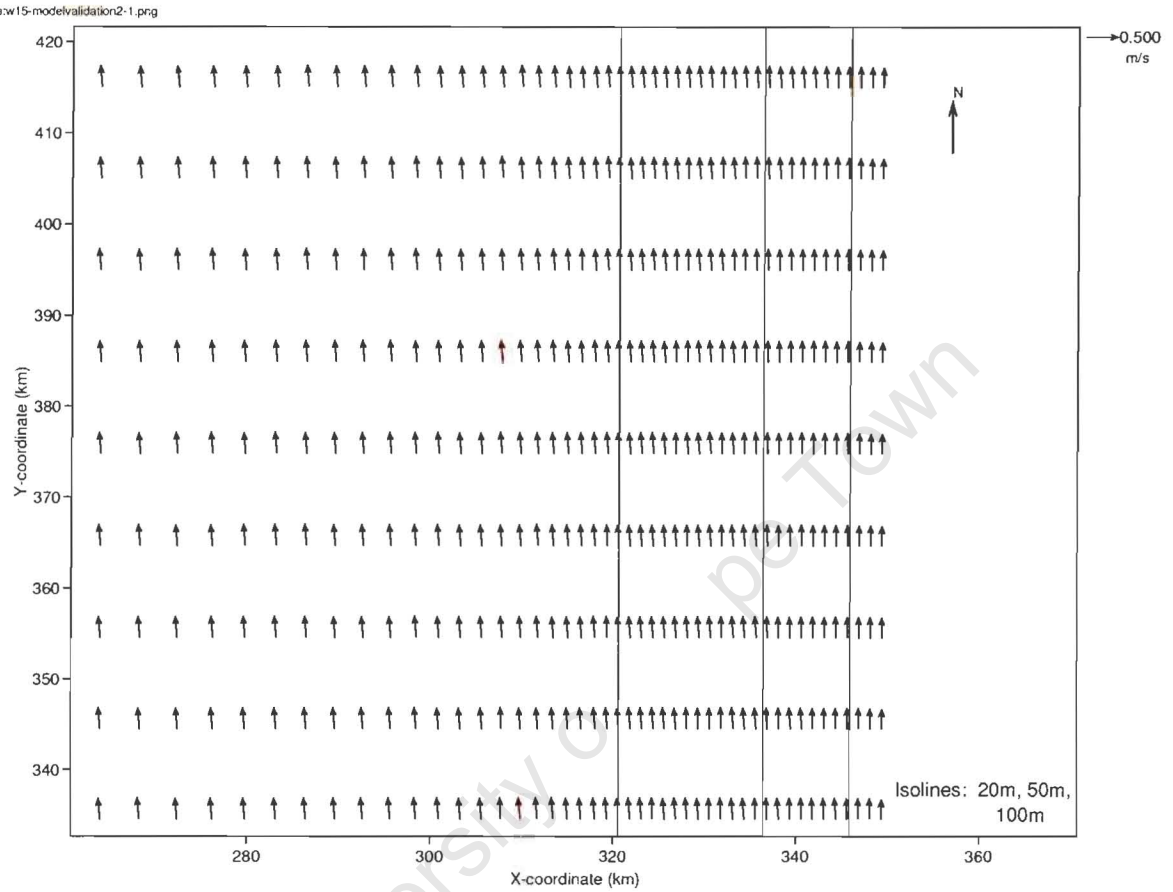

Figure 4-1 Reference Model Validation: Surface layer currents when steady state has been achieved (close-up view up to approximately 90 km offshore from the coast). The 20 m, 50 m and 100 m depth contours are indicated. The currents are uniform and alongshore.

Time series of the alongshore current speeds at a location close to the coast, is given in the top plot in Figure 4-2. This location is assumed representative of any location in the model, as Figure 4-1 indicated that the alongshore currents are very similar everywhere in the model. The chosen location is approximately 4 km offshore, in 35 m of water. The time series of the current speeds are plotted at three different water depths, namely at the surface (red), in the middle of the water column (blue), and near the bottom (green). The current speeds increase to a maximum while the wind is blowing, and then reduces again when the wind ceases. Steady state currents at all three depths are reached within one to two days after the wind started blowing. In the surface, middle and bottom layers the steady state current is 0.33 m/s, 0.24 m/s and 0.21 m/s respectively. Clearly, there is a vertical shear, leading to currents having lower speeds deeper down in the water column. Although the system is mixed (no

stratification) there are still many layers, which lead to the shear. The mean of these current speeds is 0.26 m/s, which agrees well with the theoretical steady state current speed of 0.248 m/s that was calculated above.

Figure 4-1 (bottom plot) shows a time series of the difference in the water levels at two locations in the model. These locations are in a straight cross shore line, one location being approximately 4 km from the coast, and the other being approximately 24 km offshore (the two locations are thus 20 km apart). When a steady state is reached, the difference in water levels is -0.0398 m, therefore:

$$\left.\frac{\partial \eta}{\partial x}\right|_{ss} (\text{model}) = -1.99\times10^{-6}.$$

This value agrees well with the theoretical steady state surface slope of -2.04×10^{-6} that was calculated above.

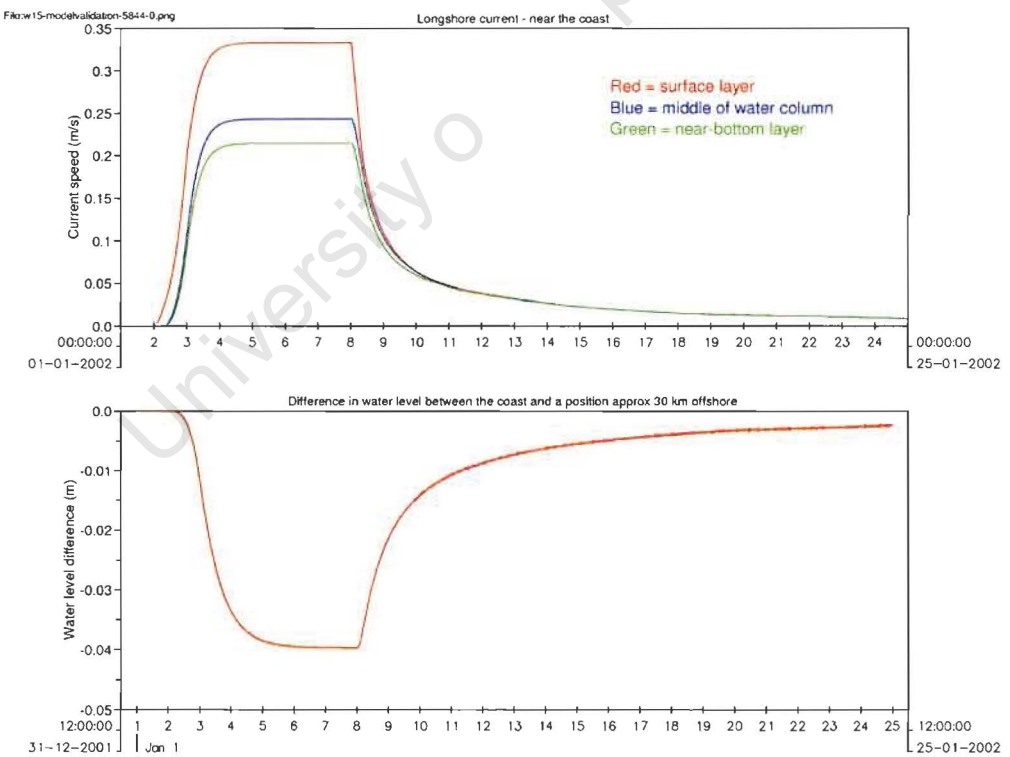

Figure 4-2 Reference Model Validation: Time series of alongshore currents at a location approximately 4 km offshore in 35 m of water, at three different depths (top plot). Time series of difference in water level between a location 4 km offshore and another location 24 km offshore (bottom plot).

The above calculations show that the modelled steady state values for alongshore current speeds and surface slope agree satisfactorily well with the theoretical steady state values, and therefore confidence has been achieved that the right type of inputs are given to the numerical model in order to study the nearshore poleward current.

Note that the above calculations were for the Reference Model, excluding stratification. Keep in mind that the purpose of these calculations was simply to test the basic model setup, and not to prove that the numerical model is working correctly (the assumption is made that the model is working properly). Due to the complexity that is added to the relevant equations when stratification is included, it was decided to follow the simpler approach. For the purpose of this thesis, it was thus assumed adequate to test the input parameters against the simplest model.

4.2 Reference Model Results

Table 4-1 gives a summary of the numerical experiments that were undertaken with the Reference Model. In all, there were three numerical experiments, each containing two or three comparative studies. The table indicates the name of each study, the wind time series that was applied (the single wind event or the multiple wind events), whether stratification was included, what bottom topography was applied (steep, medium or flat slope), and whether heat fluxes were included.

Table 4-1 Summary of Reference Model numerical experiments.

Numerical Experiment	*Study number*	*Name*	*Wind Time Series*	*Stratification Included (Yes/No)*	*Bottom Topography*	*Heat Flux Included (Yes/No)*
1	1	No Strat	Single wind event	No	Steep slope	No
	2	Strat	Single wind event	Yes	Steep slope	Yes
2	1	Steep Sl	Single wind event	Yes	Steep slope	Yes
	2	Med Sl	Single wind event	Yes	Medium slope	Yes
	3	Flat Sl	Single wind event	Yes	Flat inner shelf	Yes
3	1	Mult Wnd	Multiple wind events	Yes	Steep slope	Yes

The results from each numerical experiment will be presented individually in the following sections.

4.2.1 Results from Numerical Experiment 1

As described in Chapter 3.1.2, the aim of the first numerical experiment applying the Reference Model was to determine whether the presence of stratification is necessary for the formation of the poleward current. A detailed description of the set-up of the two test cases was given in Chapter 3.1.2, the one case excluding stratification and the other including stratification (see Table 4-1 for a summary of the setup). For the purpose of identification, the test cases will from now on be called the "No Strat" (no stratification) study and "Strat" (stratification included) studies respectively. The results from these case studies will be presented in this section.

The results will be presented by focussing on three stages during the model runs, namely:

- *During the wind event* (focussing on the stage when the wind is blowing, before the currents have reached a steady state);
- *Steady State* (focussing on the stage when the wind is still blowing, and the currents have reached steady state);
- *Relaxation* (focussing on the stage following the wind event).

During the wind event

It was clear from both case studies that initially only the inshore currents responded to the upwelling favourable wind. As the wind persisted and the water level at the coast dropped, the currents spread offshore gradually. This effect can be seen in Figure 4-3. This figure illustrates the development of alongshore currents for the "No Strat" study. A close up view of the coast up to 70 km offshore is given, showing the development of the surface currents while a 10 m/s southerly wind was blowing. The current field is plotted after 12, 18, 24 and 30 hours of persistent wind respectively. The 100 m depth contour is indicated in each case. These currents had a very strong alongshore component, as well as an offshore component at first, which later became negligible once a steady state had been reached.

The surface currents for the "Strat" study displayed the same behaviour, although the currents were slightly stronger and had a different cross shore profile than for the "No Strat" study. This difference in currents will be illustrated later.

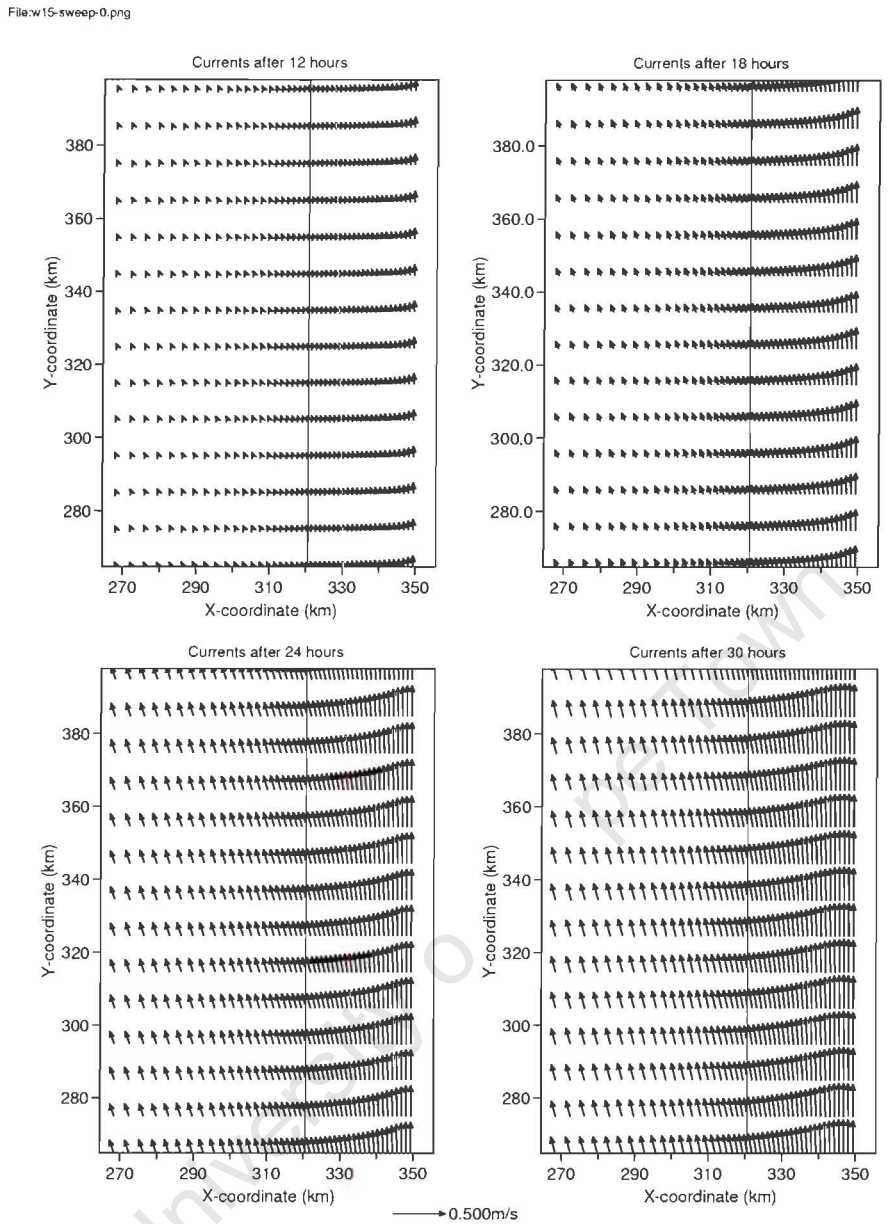

Figure 4-3 Reference Model - "No Strat" Study: Close up view of the coast up to 70 km offshore, showing the development of the surface currents while a 10 m/s southerly wind was blowing. The current field is plotted after 12, 18, 24 and 30 hours of wind respectively. The 100 m depth contour is indicated in each case.

Furthermore, for the "No Strat" case, the currents in the surface layer responded first to the wind, followed by the currents deeper in the water column. This indicated that, although the water column was mixed, there was still a shear between the different layers of the model, leading to a different response time in the different layers. The currents for the "Strat" case also responded in the surface layer first, after which the currents deeper down in the water column started to respond (as if the subsurface currents were 'dragged along' by the surface currents). Figure 4-4 shows a comparison between the currents for the "No Strat" study and the "Strat" study. Time series for the whole study

period are given at a location approximately 4 km offshore, in 35 m of water, at three different water depths for each study. The three water depths are the surface, the middle of the water column, and close to the bottom of the water column. In this plot, a positive current speed indicates equatorward flow, while a negative current speed indicates poleward flow.

By focussing on the first five days of each study (while the wind is blowing), it is clear from this figure that the currents for the "No Strat" study (top plot) as well as for the "Strat" study (bottom plot) responded in the surface layers first. The currents for the "No Strat" study were more steady and uniform than for the "Strat" study. The currents for the "Strat" study (bottom plot) reached a peak around the time when the wind reached its maximum of 10 m/s, reducing in speed and becoming more stable while the wind persisted. These currents showed more variability during the time that the wind persisted and the surface currents were stronger than for the "No Strat" study. The currents for the two studies showed the same relative behaviour throughout the water column.

The behaviour of the currents for the rest of the study period (also included in Figure 4-4) will be discussed later.

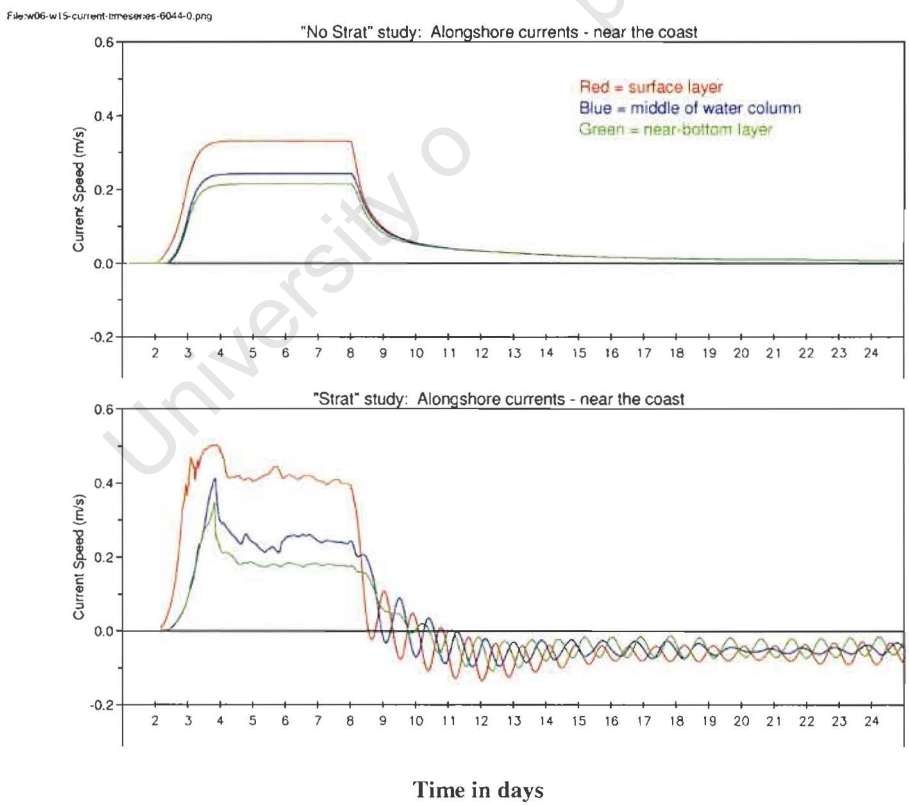

Figure 4-4 Reference Model: Comparison between the currents for the "No Strat" study (top) and the "Strat" study (bottom). Time series are given at the same location (4 km offshore, in 35 m of water) and at three different water depths for each study. The three water depths are the surface, the middle of the water column, and close to the bottom of the water column.

While the alongshore currents developed, upwelling of cold water into the surface layers took place at the coast for the "Strat" study. Whereas the isotherms were flat (horizontal) at the start of the study, this process of upwelling led to sloping isotherms, as will be illustrated later.

Steady state

Still focussing on the time when the wind persisted, for the "No Strat" study (Figure 4-4 top plot), the currents near the coast (throughout the water column) reached a steady state after approximately one and a half days. The surface currents reached the highest speeds (0.33 m/s), while the mid-water column currents and near-bottom currents reached 0.24 m/s and 0.21 m/s respectively. This steady state was maintained for the remainder of the time the wind continued.

For the "Strat" study (Figure 4-4 bottom plot), the nearshore currents reached a relatively steady state after approximately two and a half days. The surface currents had the highest speeds (0.41 m/s on average), while the mid-water column currents were 0.25 m/s on average. The near-bottom currents were 0.19 m/s on average. Although the currents seem to have reached a relatively steady state, there was still some variability in the currents. This is probably due a minor influence from the coastal boundary, as this location is relatively close to the boundary.

Figure 4-5 shows a comparison of surface currents between the "No Strat" study (left) and the "Strat" study (right) when a steady state has been achieved. The 100 m depth contour is indicated in each case, with the coastline being on the right hand side. The surface currents for the "No Strat" study are uniformly alongshore and equatorward. The currents for the "Strat" study are less uniform, showing stronger currents inshore of the inner shelf break and a surface jet around the 100 m depth contour.

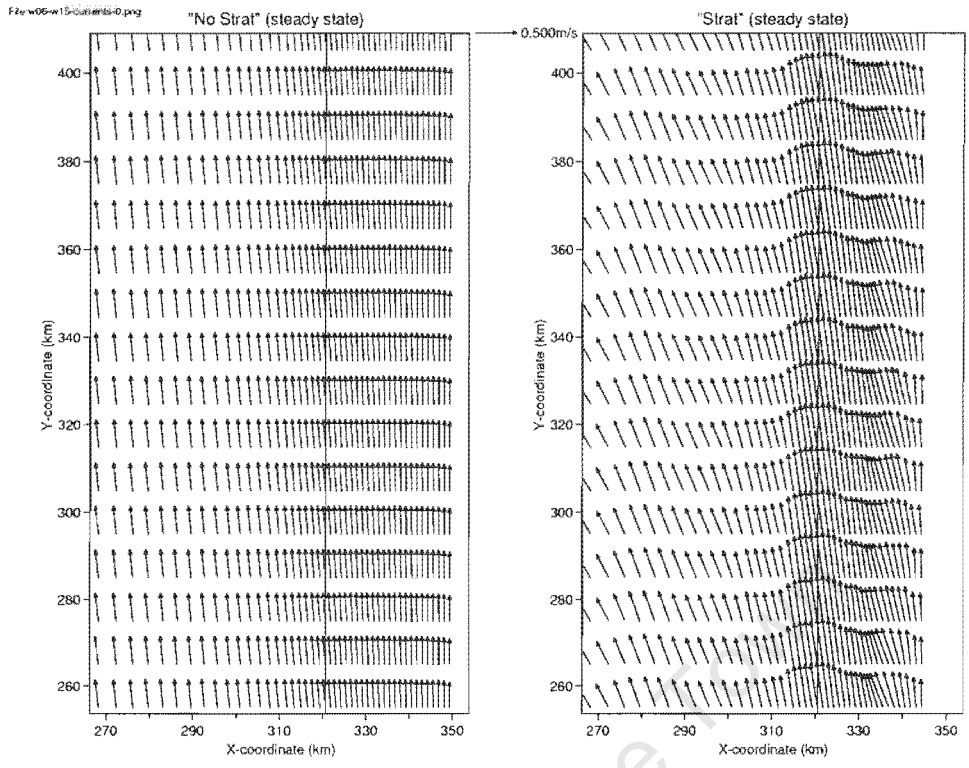

Figure 4-5 Reference Model: Comparison of surface currents for the "No Strat" study (left) and the "Strat" study (right) during the wind event, when a steady state has been achieved. The currents for the "Strat" study are less uniform and stronger, with evidence of a surface jet around the 100 m depth contour.

Figure 4-6 shows the surface currents (left), a vertical transect of temperature (top right) and a vertical cross-section of surface slope (bottom right) in a representative cross shore line in the "Strat" study when a relatively steady state in the currents has been achieved during the wind event. The 100 m depth contour is shown underneath the currents, indicating the position of the inner shelf break (this break can clearly be seen in the vertical section on the top right plot). The surface jet has reached speeds of approximately 0.6 m/s. Note the upwelling of cold water (less than 10.5 °C) to the surface in the inshore region (and the sloping isotherms that resulted from the upwelling), as well as the downward slope in the surface. Although the alongshore currents reached a steady state, the drop in water level and the upwelling continued to take place for as long as the wind persisted.

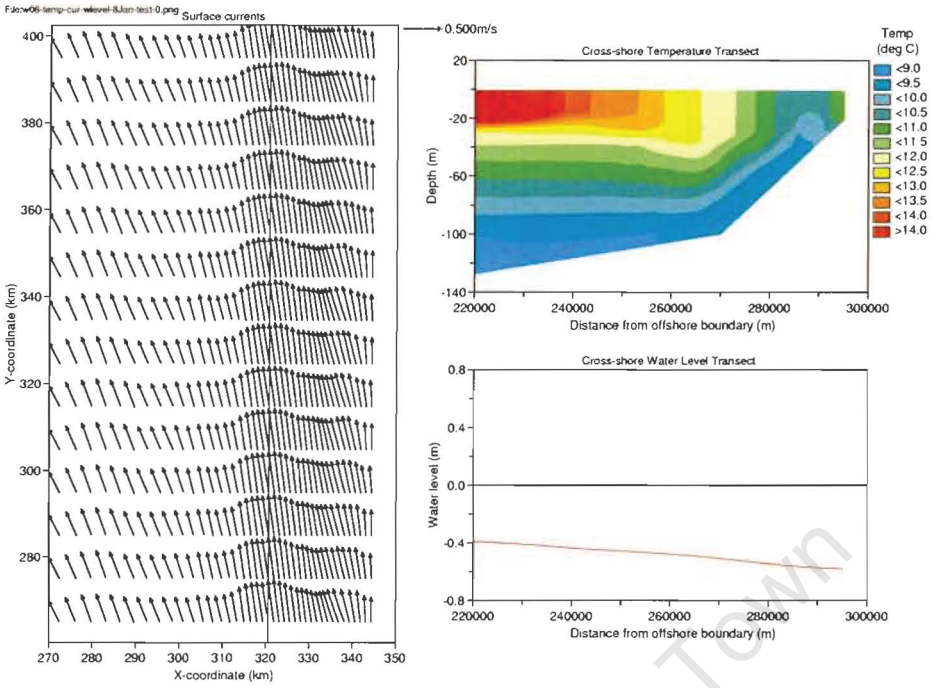

Figure 4-6 Reference Model – "Strat" study: Surface currents (left), vertical transect of temperature (top right) and vertical cross-section of surface slope (bottom right) in a representative cross shore line during the wind event, when a steady state has been achieved. The 100 m depth contour is shown underneath the currents, indicating the position of the inner shelf break (top right).

Relaxation

When the wind event came to an end, the alongshore currents for the "No Strat" study decayed immediately and approach 0 m/s as time passed (Figure 4-4 top plot). No evidence of the formation of a poleward current can be seen, as the current speeds stayed positive, indicating equatorward flow.

For the "Strat" study, however, interesting features were observed during a wind relaxation event. One of the outstanding features in Figure 4-4 (bottom plot), was the immediate reduction in current speeds when the wind relaxed, as well as the clear presence of inertial oscillations. Inertial oscillations normally become apparent when the sea surface is flattening out following a wind event. These oscillations were noted throughout the water column, and they were out of phase with each other at different water depths. As time passed, these oscillations dampened out considerably.

The reason why the inertial oscillations were absent during the wind relaxation phase in the "No Strat" study is not very clear. One possible reason could be that the vertical water column acts almost as a single body of water, and that this body of water cannot respond fast enough to the relaxation of the wind.

Another (important) feature that was evident from the "Strat" study time series is the negative direction that the currents throughout the water column assumed during wind relaxation, indicating the development of a poleward current. The surface current turned poleward first, after approximately one and a half days of wind relaxation, reaching a steady state after approximately eight days. The currents in the middle of the water column turned poleward after approximately two days of wind relaxation and the bottom currents turned poleward after approximately three days of wind relaxation. The currents throughout the water column reached steady state in more or less the same time. The poleward current was slightly stronger in the surface layers, becoming gradually weaker deeper down in the water column.

Figure 4-7 shows a comparison of the surface currents for the "No Strat" study (left plot) and the "Strat" study (right plot) when a steady state has been reached during wind relaxation. All the currents for the "No Strat" study have reduced to almost zero and no poleward flow was observed. This reduction in current speed started at the coast and gradually spread offshore. The current patterns for the "Strat" study, however, were distinctly different from the "No Strat" study. For the "Strat" study, Figure 4-7 shows that mainly three regions of current behaviour can be identified, namely an outer shelf region, a surface jet region, and an inner shelf region. An inshore poleward surface current of approximately 0.05 m/s can be seen. Note that the surface jet that was evident around the 100 m depth contour during the steady state situation has remained, but that its speed has reduced to approximately 0.3 m/s. The currents on the outer shelf are generally weak.

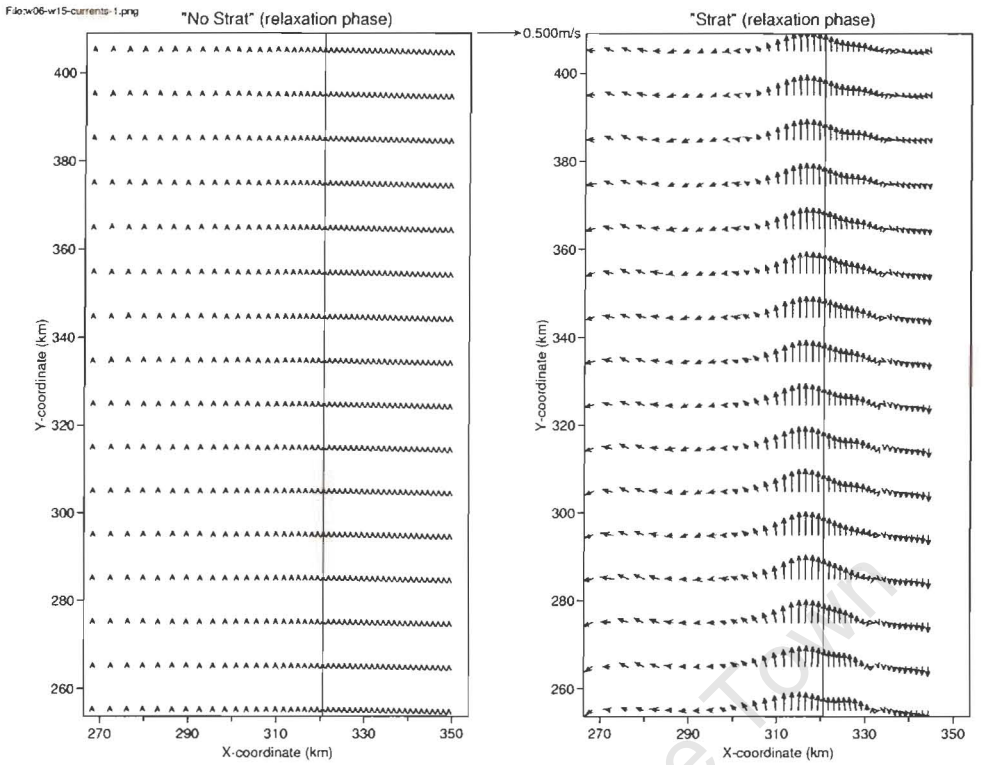

Figure 4-7 Reference Model: Comparison of surface currents for the "No Strat" study (left) and the "Strat" study (right) when a steady state has been reached during wind relaxation. All the currents for the "No Strat" study has reduced to almost zero, but the currents for the "Strat" study show a narrow inshore poleward current, and a surface equatorward jet around the 100 m depth contour.

Another perspective on the behaviour of the "Strat" currents can be seen in Figure 4-8. This figure indicates the surface currents (left), a vertical cross-section of temperature (top right) and a vertical cross-section of surface slope (bottom right) for the "Strat" study in a representative cross shore line when a steady state has been achieved during wind relaxation. The 100 m depth contour is shown underneath the currents, once again indicating the position of the inner shelf break.

From this figure it can be seen that the isotherms were relatively flat in the outer shelf region during the wind relaxation phase, and that this area thus assumed an oceanic character. It is also clear that the surface jet occurred in the region of the upwelling front, where the isotherms were sloping upwards towards the coast. This surface jet is associated with strong equatorward surface currents. In this case, the surface jet (width approximately 20 km) occurred on both sides of the inner shelf break. A nearshore poleward surface current of approximately 0.05 m/s was also visible. Note that the poleward surface current did not occur over the whole inner shelf region, but that it stayed confined to a region inshore of the surface jet (in this case approximately 10 km wide), where the isotherms have become flat and even reversed direction, becoming downward sloping towards the coast.

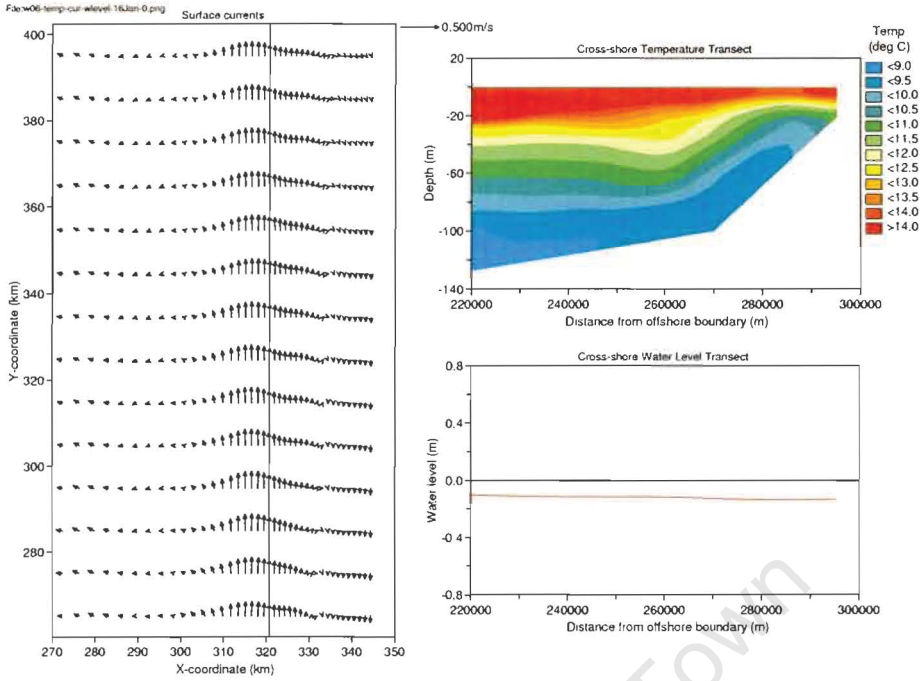

Figure 4-8 Reference Model – "Strat" study: Surface currents (left), vertical cross-section of temperature (top right) and vertical cross-section of surface slope (bottom right) in a representative cross shore line when a steady state has been achieved during wind relaxation. The 100 m depth contour is shown underneath the currents, indicating the position of the inner shelf break (top right).

This baroclinic adjustment during wind relaxation happens in conjunction with a barotropic adjustment. A comparison between Figures 4-6 and 4-8 shows that the surface slope has greatly flattened out during relaxation, although it has not returned to its original zero position yet. It should be stated that, during the wind event, both the "No Strat" study and the "Strat" study showed downward sloping surfaces over the whole cross-section. A close up view of the surface slope at the same cross-section, from the coast up to 35 km offshore, can be seen in Figure 4-9. This figure shows considerably more detail of the surface slopes when a steady state has been reached during the relaxation event (following the wind event) for the "No Strat" study (blue line) as well as the "Strat" study (red line). Immediately apparent is that, during wind relaxation, the surface slope for the "No Strat" study remained uniform and downward sloping. For the "Strat" study, however, this figure shows that the surface gradually changed (in an offshore to onshore direction) from downward sloping to upward sloping at a turning point approximately 12 - 15 km offshore. The nearshore surface thus has an upward slope in a band of approximately 10 km wide for the "Strat" study. This coincides with the width of the poleward surface current, as was illustrated in Figure 4-8.

Furthermore, the shelf break is situated approximately 30 km from the coast (approximately 270 km from the offshore boundary), so it can be seen that the surface jet around the shelf break is associated with the region where the surface slope is still downward towards the coast.

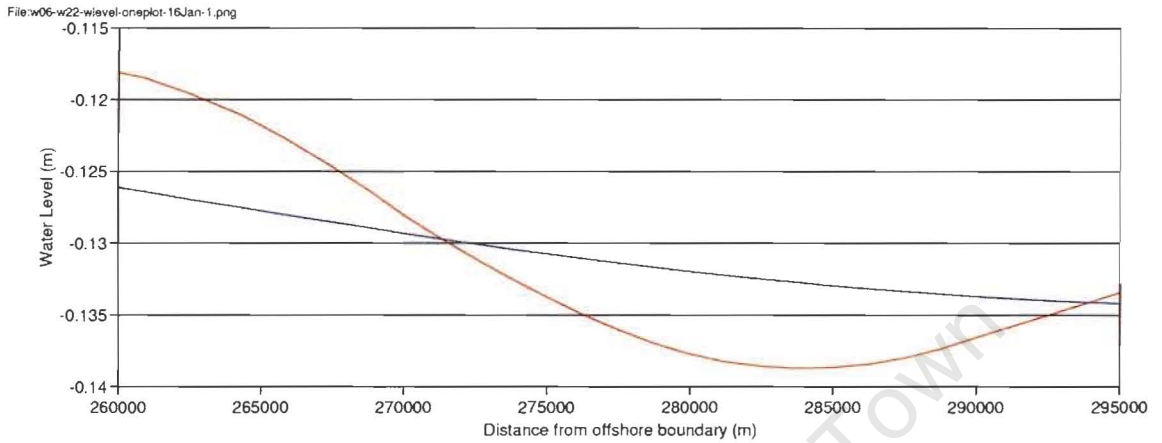

Figure 4-9 Reference Model: Comparison between surface slopes (from the coast to 35 km offshore) for the "No Strat" study (blue line) and the "Strat" study (red line) after eight days of wind relaxation. Note the upward sloping surface (approximately 10 km wide) close to the coast for the "Strat" study.

Note that the major adjustments in the subsurface isotherms and surface slope took place before the current turned poleward, indicating that these two forces probably are the main drivers of this current. When a steady state was reached during the wind relaxation event, the subsurface isotherms and the slope in the surface was in balance with each other. The only change that occurred from then onwards was that the water level kept on rising marginally, as indicated by Figure 4-10. This figure shows the daily water level for the "Strat" study for four days during the wind relaxation period, when a steady state in the poleward surface current has been reached, demonstrating the rise in water level, and the unchanged surface slopes. Investigation showed that the structure of the subsurface isotherms also remained unchanged in this region for the rest of the modelling period.

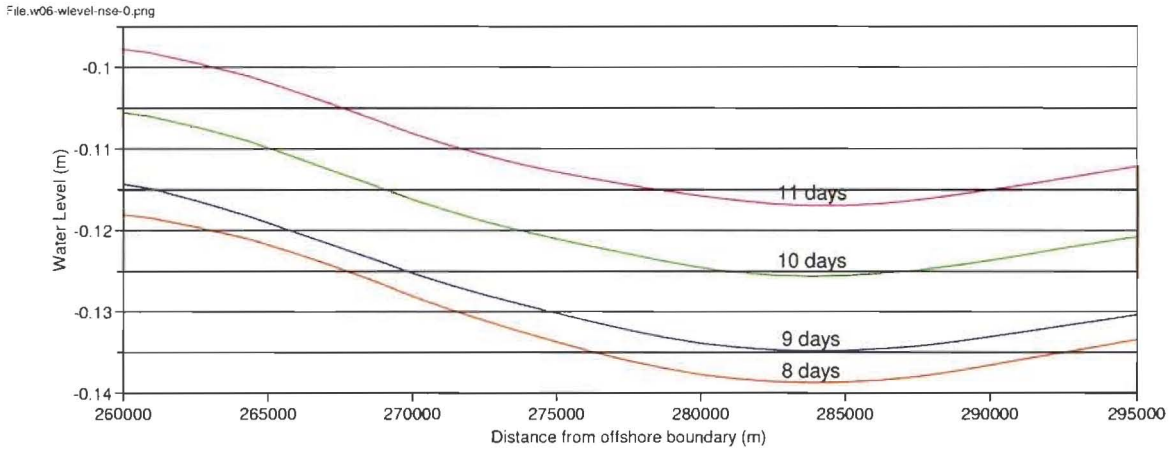

Figure 4-10 Reference Model: Comparison between surface slopes (from the coast to 35 km offshore) for the "Strat" study after eight days (red line), nine days (blue line), ten days (green line) and eleven days (magenta line) of wind relaxation. Note the rise in water level, although the surface slope stayed constant.

Some more interesting observations were made when comparing the behaviour of the nearshore surface currents with offshore surface currents, as well as offshore bottom currents. For this purpose, time series of current speed were studied at three different locations (representing typical current behaviour). The first position was approximately 4 km offshore, in 35 m of water, at the surface. This was the region where a poleward surface current was noted during wind relaxation. The second position was approximately 30 km offshore in 100 m of water, also at the surface, in the region of the surface jet. The third position was directly below the second position, near the bottom. A comparison between the time series at the above three locations can be seen in Figure 4-11.

It is clear that, when the wind ceased, the reduction in current speeds happened the fastest at the nearshore surface location (the shallower region). As discussed before (and once again clear from this figure), this surface current eventually turned poleward. There was a decay in the amplitude of the inertial oscillations as time passed (the inertial period being 22 hours in this region), but an increase in the amplitude can be seen towards the end of the model study (the last three days). The reason for this increase in inertial amplitude is not clear.

In the region of the surface jet, the currents started to reduce (gradually) once the wind relaxation event started, reaching a steady state after a few days (showing inertial oscillations), but never turning poleward. Also at this location, an increase in the inertial amplitude was noted towards the end of the simulation.

Interesting is the behaviour of the bottom currents, below the surface jet. The time series indicates

that the region of the surface jet was eventually associated with a net poleward undercurrent (also showing strong inertial oscillations). This undercurrent appeared a few days after the nearshore poleward current appeared. Once again, there seems to be an increase in the inertial amplitude towards the end of the simulation.

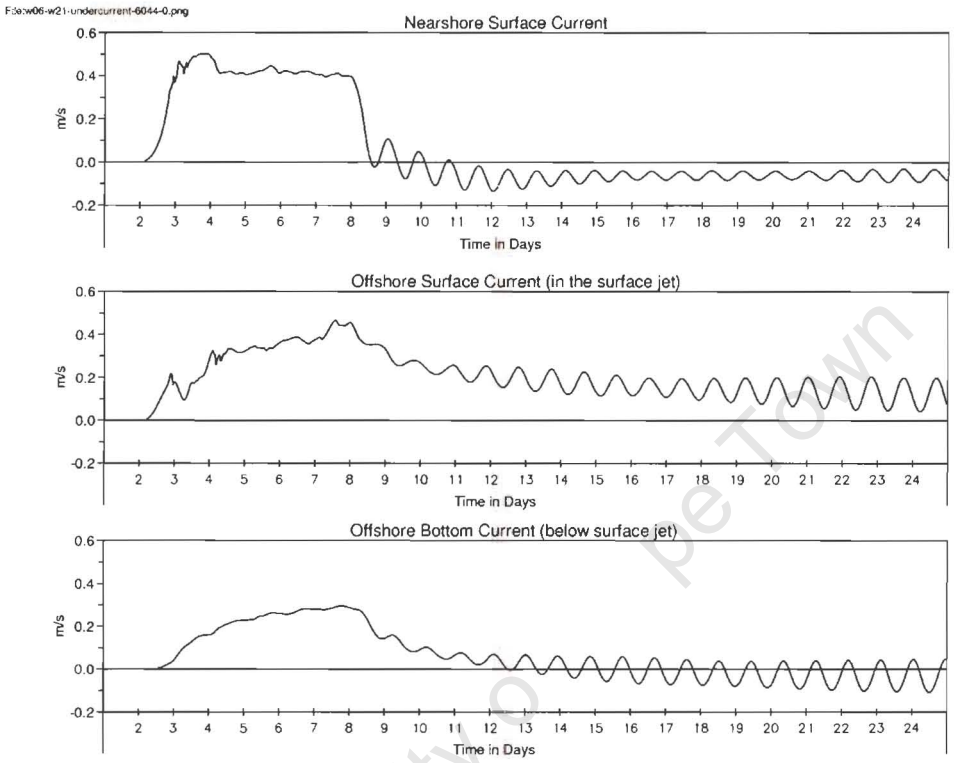

Figure 4-11 Reference Model – "Strat" study: Time series of nearshore surface currents, offshore surface currents and offshore bottom currents for the study period. Note the net poleward undercurrent that develops over time at the bottom.

In conclusion to this experiment, the presence of stratification is indeed necessary for the development of a poleward surface current. It appears that the baroclinic adjustment of the subsurface isotherms, as well as the concurrent barotropic adjustment in the surface slope that takes place during wind relaxation is important during the development of the nearshore poleward surface current. This perception is investigated in the next section.

4.2.2 Results from Numerical Experiment 2

The aim of this experiment was to determine what the importance of the slope of the inner shelf (thus the topography) is during the formation of the poleward current.

Three studies were undertaken (all three including stratification), and a detailed description of each study was given in Chapter 3.1.2. The only difference between the three studies was the slope of the inner shelf (see Figures 3-2(a) and (b)). Table 4-1 gave a summary of the setup of these three studies.

For the purpose of identification, the three studies will from now on be called the "Steep Sl" (steep slope) study, the "Med Sl" (medium slope) study and the "Flat Sl" (flat inner shelf) study respectively. The results from these studies will be presented in this section.

Once again, the results from these test cases will be presented by focussing on three stages during the model runs, namely:

- *During the wind event* (focussing on the stage when the wind is blowing, before the currents have reached a steady state);
- *Steady State* (focussing on the stage when the wind is still blowing, and the currents have reached steady state);
- *Relaxation* (focussing on the stage following the wind event).

During wind event

While the wind persisted, all three case studies showed the same response that was described in detail during Numerical Experiment 1 ("Strat" study). In summary:

- As the wind blew, the water level dropped at the coast;
- Initially, only the inshore currents responded to the drop in water level, and this response spread offshore gradually;
- The currents responded in the surface layer first, and thereafter in the deeper layers (in sequence);
- Equatorward, alongshore geostrophic currents developed as the wind persisted (the cross shore component of the currents became negligible over time);
- Upwelling of cold water at the coast took place while the wind was blowing.

Time series of surface currents for all three studies are shown in Figure 4-12. Time series for the "Steep Sl" study are given at a location approximately 4 km offshore, in 35 m of water. Time series for the "Med Sl" and "Flat Sl" are given at a location approximately 2.5 km offshore, in 30 m of water. The reason why the same location was not chosen for all three studies is because the width of the poleward current was significantly different for the "Med Sl" and "Flat Sl" studies (it was much narrower). It was thus necessary to choose a location closer to the coast.

The surface currents for all three studies reacted simultaneously to the drop in water level when the wind event started, reaching a peak at the time when the wind reached its peak of 10 m/s and then reducing in speed. It is clear, though, that the currents for the "Med Sl" and the "Flat Sl" studies show a significant amount of variability. This could most probably be ascribed to the fact that these two locations are very close to the coastal boundary (the area where the poleward current later developed) and some influence from the boundary might be present here during the period of wind forcing.

The behaviour of the currents for the rest of the study period will be discussed later.

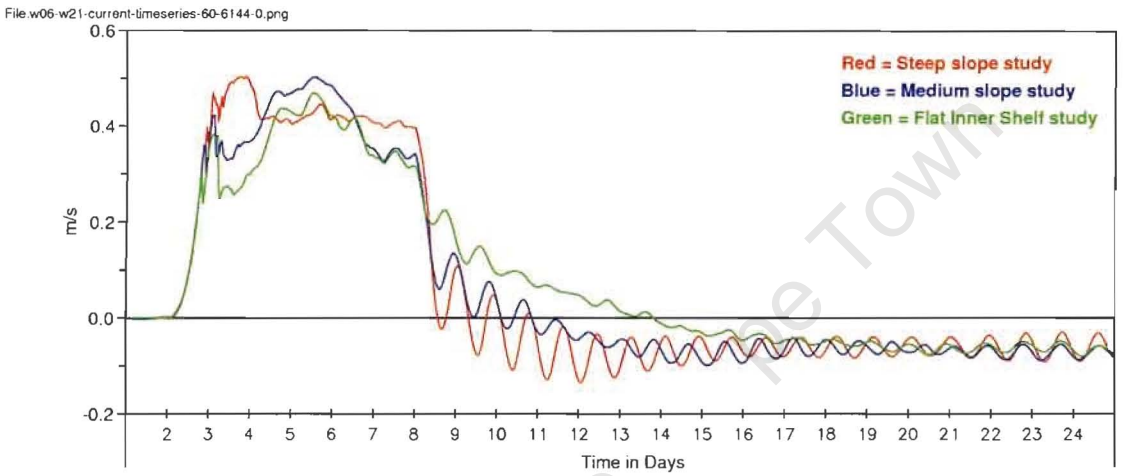

Figure 4-12 Reference Model: Comparison between the nearshore surface currents for the "Steep Sl" (red line), "Med Sl" (blue line) and "Flat Sl" (green line) studies. Time series for the "Steep Sl" study are given at a location approximately 4 km offshore, in 35 m of water. Time series for the "Med Sl" and "Flat Sl" studies are given at a location approximately 2.5 km offshore, in 30 m of water.

Steady state

As discussed during Numerical Experiment 1, for the "Steep Sl" study the nearshore currents reached a relatively steady state (throughout the water column) after approximately two and a half days. The surface currents reached speeds of 0.41 m/s on average. For the "Med Sl" and the "Flat Sl" studies, the surface currents showed still showed significant variability, probably due to boundary effects.

Figures 4-13(a), (b) and (c) illustrate the situation during the wind event, when a steady state has been achieved, for the "Steep Sl", the "Med Sl" and the "Flat Sl" studies respectively. For each study, the surface currents (left), a vertical transect of temperature (top right) and a vertical cross-section of surface slope (bottom right) in a representative cross shore line are shown.

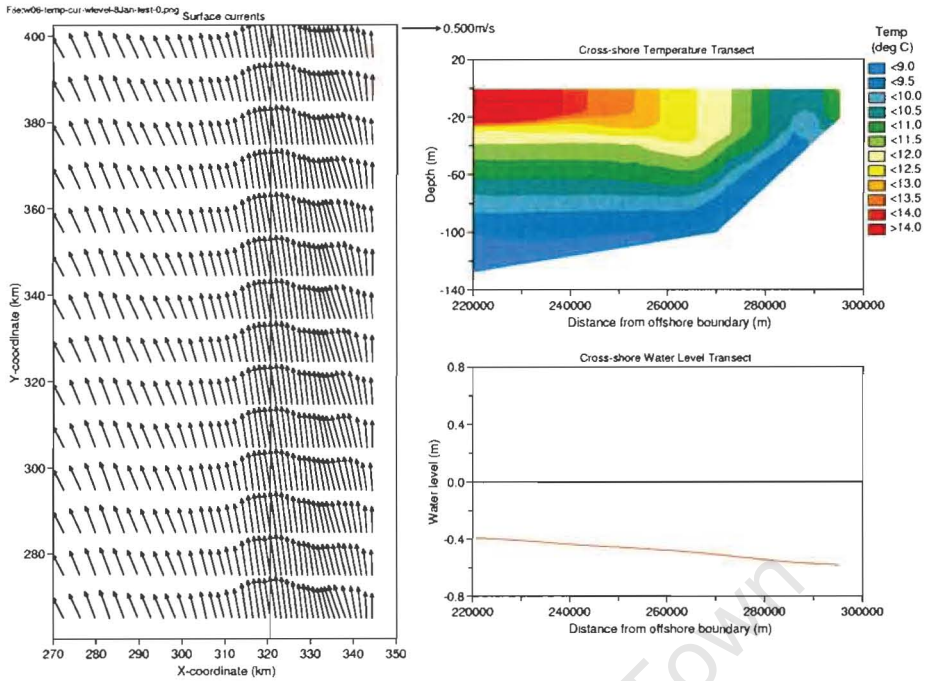

Figure 4-13(a) Reference Model – "Steep Sl" study: Surface currents (left), vertical transect of temperature (top right) and vertical cross-section of surface slope (bottom right) in a representative cross shore line during the wind event, when a steady state has been achieved. The 100 m depth contour is shown underneath the currents, indicating the position of the inner shelf break (top right).

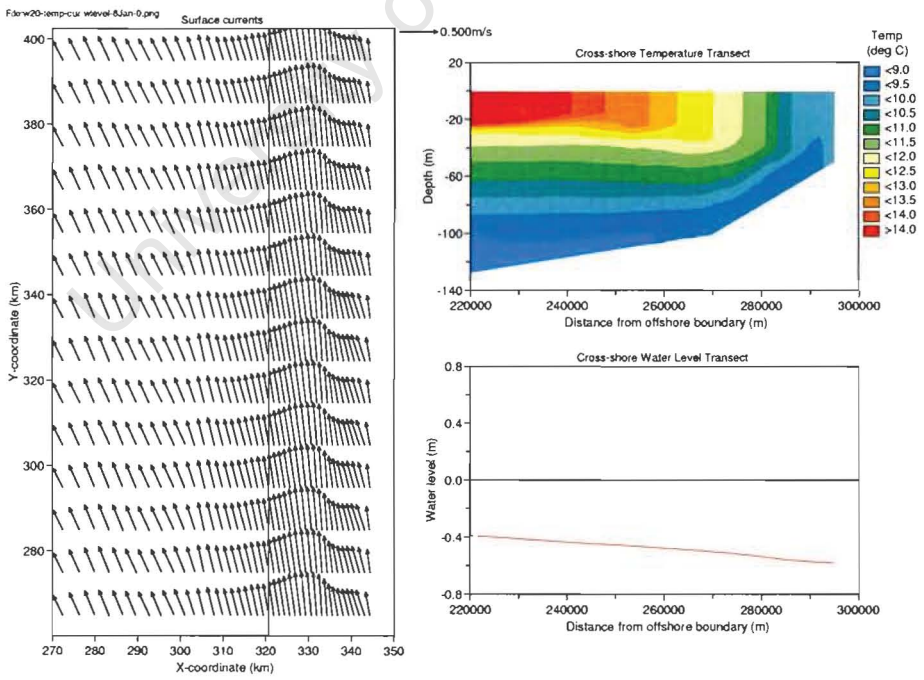

Figure 4-13(b) Reference Model – "Med Sl" study: Surface currents (left), vertical cross-section of temperature (top right) and vertical cross-section of surface slope (bottom right) in a representative cross shore line during the wind event, when a steady state has been achieved. The 100 m depth contour is shown underneath the currents, indicating the position of the inner shelf break (top right).

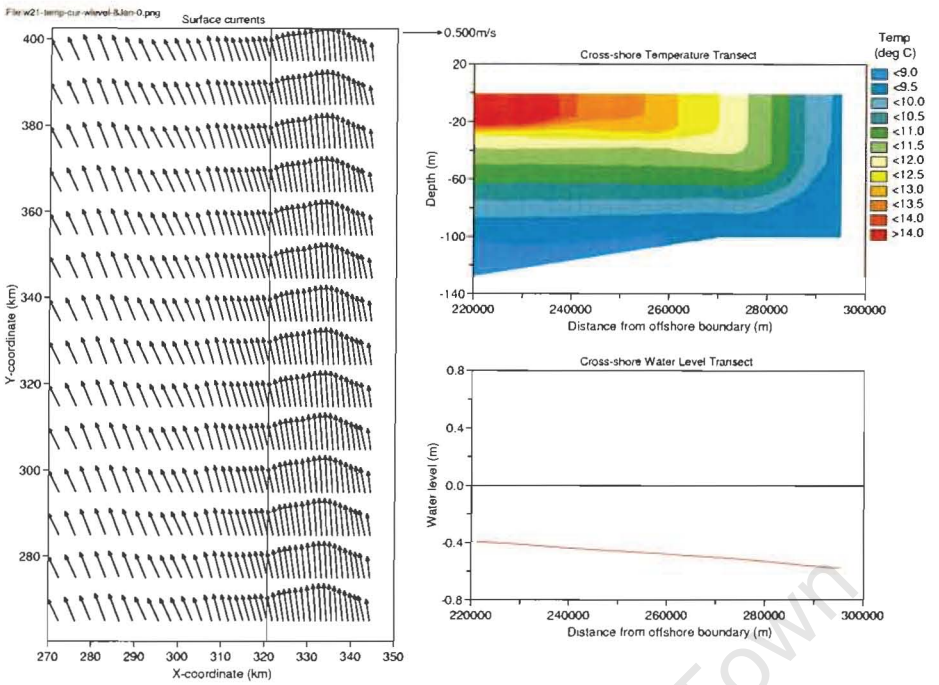

Figure 4-13(c) Reference Model – "Flat Sl" study: Surface currents (left), vertical cross-section of temperature (top right) and vertical cross-section of surface slope (bottom right) in a representative cross shore line during the wind event, when a steady state has been achieved. The 100 m depth contour is shown underneath the currents, indicating the position of the inner shelf break (top right).

A comparison between the above figures shows that, during steady state, there was a distinct difference between the three studies concerning the level of cold water intrusion close to the coast. The flatter the inner shelf slope, the more cold water moved in very close to the coast, reaching the surface and leading to a vertically mixed water column. Furthermore, the centre of the surface jet moved closer inshore the flatter the inner shelf slope was. This is an indication that the position of the temperature front was closer inshore the flatter the inner shelf slope was. For all three studies, these surface jets have reached speeds of approximately 0.6 m/s.

Relaxation

During the subsequent wind relaxation event, Figure 4-12 shows that inertial oscillations were present in the nearshore currents during all three studies. These oscillations were more visible the steeper the slope was.

Also, the surface currents for all three studies assumed a negative (poleward) direction during the study period. As discussed during Numerical Experiment 1, the "Steep Sl" study showed the first sign of nearshore poleward surface flow after approximately two days. The surface currents for the "Med Sl" study and the "Flat Sl" study started to turn poleward after three and five days respectively. This

figure thus indicates that the flatter the inner shelf slope was, the longer it took for the poleward current to start to develop. The poleward current, though, took more or less the same time (approximately eight days) to reach a fairly steady state. It should also be noted that the steady state speed of the poleward current, when compared to the "Steep Sl" study, was on average 0.05 m/s faster for the "Med Sl" study and 0.06 m/s faster for the "Flat Sl" study.

Figures 4-14(a), (b) and (c) illustrate the steady state situation during wind relaxation for the "Steep Sl", the "Med Sl" and the "Flat Sl" studies respectively. Once again, for each study, the surface currents (left), a vertical transect of temperature (top right) and a vertical cross-section of surface slope (bottom right) in a representative cross shore line are shown. Once more, for all three studies, mainly three regions of current behaviour can be identified, namely an outer shelf region, a surface jet region, and an inner shelf region.

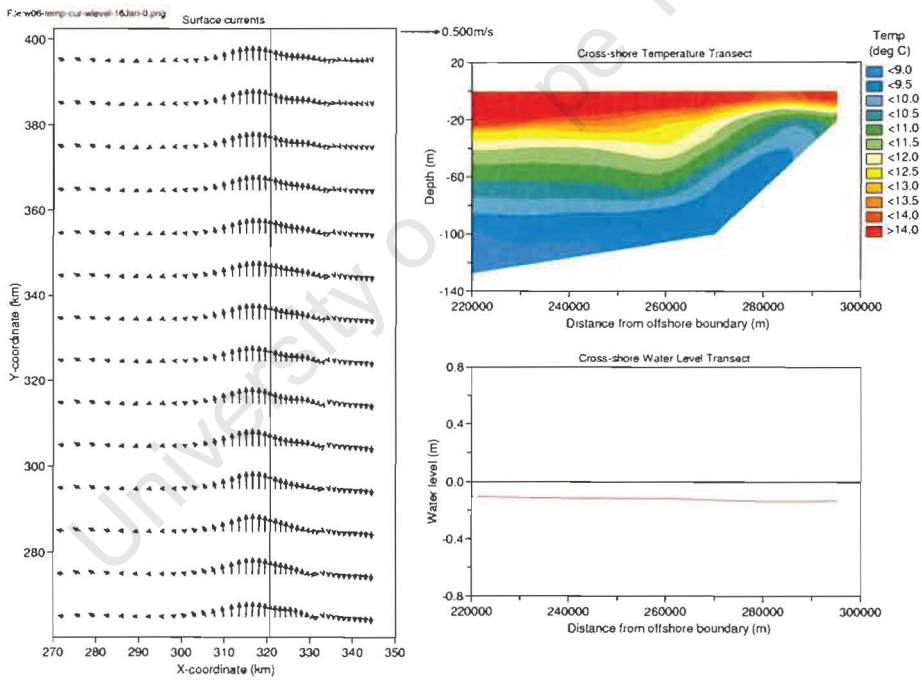

Figure 4-14(a) Reference Model – "Steep Sl" study: Surface currents (left), vertical cross-section of temperature (top right) and vertical cross-section of surface slope (bottom right) in a representative cross shore line when a steady state has been achieved during wind relaxation. The 100 m depth contour is shown underneath the currents, indicating the position of the inner shelf break (top right).

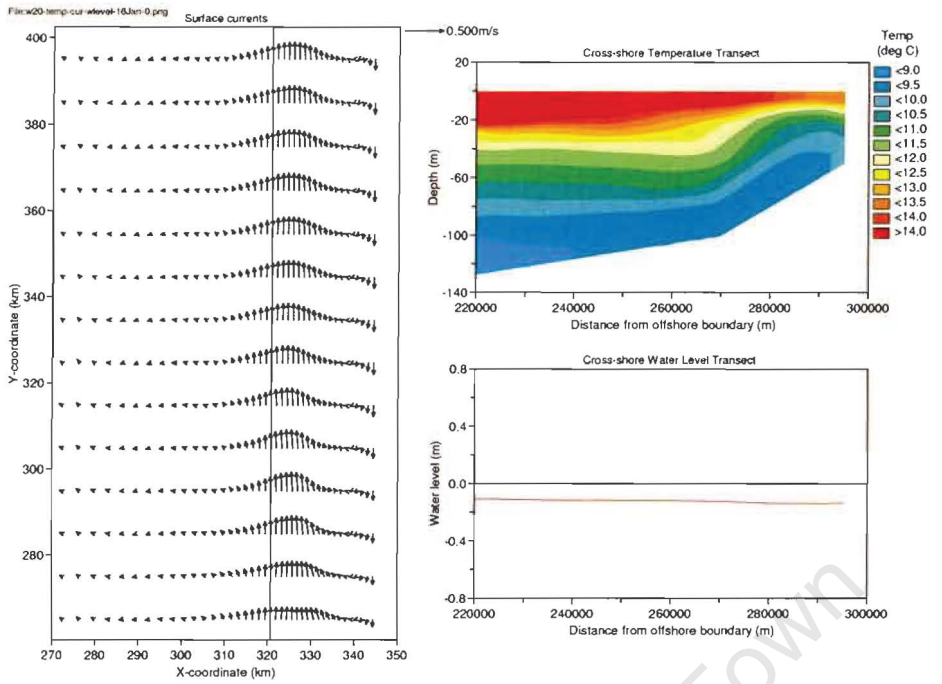

Figure 4-14(b) Reference Model – "Med Sl" study: Surface currents (left), vertical cross-section of temperature (top right) and vertical cross-section of surface slope (bottom right) in a representative cross shore line when a steady state has been achieved during wind relaxation. The 100 m depth contour is shown underneath the currents, indicating the position of the inner shelf break (top right).

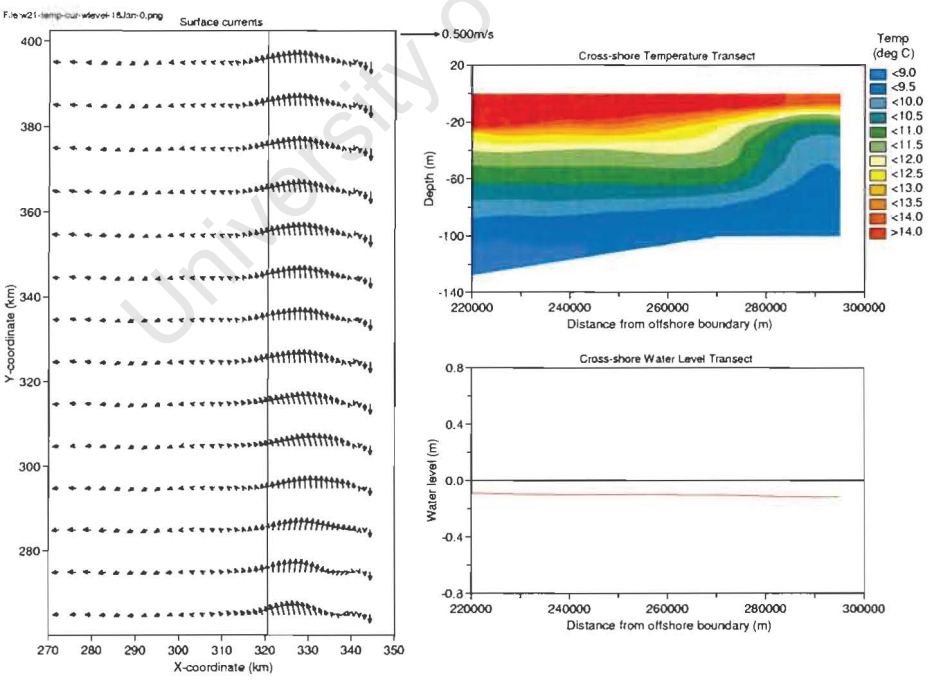

Figure 4-14(c) Reference Model – "Flat Sl" study: Surface currents (left), vertical cross-section of temperature (top right) and vertical cross-section of surface slope (bottom right) in a representative cross shore line when a steady state has been achieved during wind relaxation. The 100 m depth contour is shown underneath the currents, indicating the position of the inner shelf break (top right).

For the "Steep SI" study, from Figure 4-14(a) it can be seen that a steady nearshore poleward current of width approximately 10 km was present when a steady state has been achieved during wind relaxation. Offshore of the poleward current a surface jet can be seen in a wide band of approximately 20 km (10 km on either side of the 100 m depth contour). This jet, however, has reduced from 0.6 m/s (as was noted during the steady state situation) to approximately 0.3 m/s.

For the "Med SI" study, from Figure 4-14(b) it can be seen that a steady nearshore poleward current of width approximately 4 km was present when a steady state has been achieved during wind relaxation. Offshore of the poleward current a band of very weak currents (approximately 8 km wide) can be seen. Also, a surface jet of approximately 15 km wide can be seen just inshore of the 100 m depth contour, extending to slightly beyond the shelf break. This jet, however, has reduced from 0.6 m/s (as was noted during the steady state situation) to approximately 0.3 m/s.

For the "Flat SI" study, from Figure 4-14(c) a steady nearshore poleward current of width approximately 3 km was present when a steady state has been achieved during wind relaxation. A very narrow region of weak currents (approximately 3 km wide) can be seen just offshore of the poleward current. A wide surface jet of approximately 20 km wide can be seen offshore of the poleward current, up to the 100 m depth contour. This jet, however, has reduced from 0.6 m/s (as was noted during the steady state situation) to approximately 0.2 m/s.

From the above figures it can be seen that for each study, in the outer shelf region, the isotherms were relatively flat and that this area thus assumed an oceanic character. It is also clear that the surface jet (strong equatorward surface currents) in each study occurred in the region of the upwelling front, where the isotherms were sloping upwards towards the coast. Also, for each study the poleward surface current did not occur over the whole inner shelf region, but that it stayed confined to a region inshore of the surface jet. Important to note, however, is that although the position of the nearshore poleward surface current was always in the region inshore of the front, its width did not necessarily extend over this whole region, but sometimes only over a part of it, right against the coast. This coincided with the region where the subsurface isotherms' direction have reversed and have thus become downward sloping during wind relaxation (even though the downward slope was very subtle at times). Such an adjustment in the subsurface isotherms always took place in conjunction with an opposite adjustment in the surface slope, as will now be illustrated.

Figures 4-14(a), (b) and (c) also show that for all three studies the surface slope has greatly flattened out during relaxation, although it has not returned to its original zero position yet. Remember that all three studies showed downward sloping surfaces over the whole cross-section while the wind was

blowing. A close up view of the surface slope at the same cross-section as shown in the above figures, from the coast up to 35 km offshore, can be seen in Figure 4-15. This figure shows considerably more detail of the surface slopes during relaxation (following the wind event) for the "Steep Sl" study (red line), the "Med Sl" study (blue line) as well as for the "Flat Sl" study (green line). Immediately apparent is that, for all three studies, the surface slopes gradually changed (in an offshore to onshore direction) from downward sloping to upward sloping during wind relaxation. The nearshore surface has an upward slope in the nearshore area in a band of approximately 10 km, 5 km and 3 km wide for the "Steep Sl", "Med Sl" and "Flat Sl" studies respectively. This coincides with the width of the poleward surface current in each case, as was illustrated in Figures 4-14(a), (b) and (c). The upward sloping part of the surface was the steepest in the "Flat Sl" study, becoming gentler the steeper the inner shelf slope was.

Furthermore, for each study it can be seen that the surface jet offshore of the poleward surface current is associated with the region where the surface slope remained downward. The turning point from a downward to an upward surface slope appeared closer to the coast the flatter the inner shelf slope was. This is in agreement with the previous observation that the surface jet moved closer towards the coast the flatter the slope was.

Note that the area of very weak currents, normally seen in the region between the nearshore poleward surface current and the offshore surface jet is associated with a relatively flat surface slope.

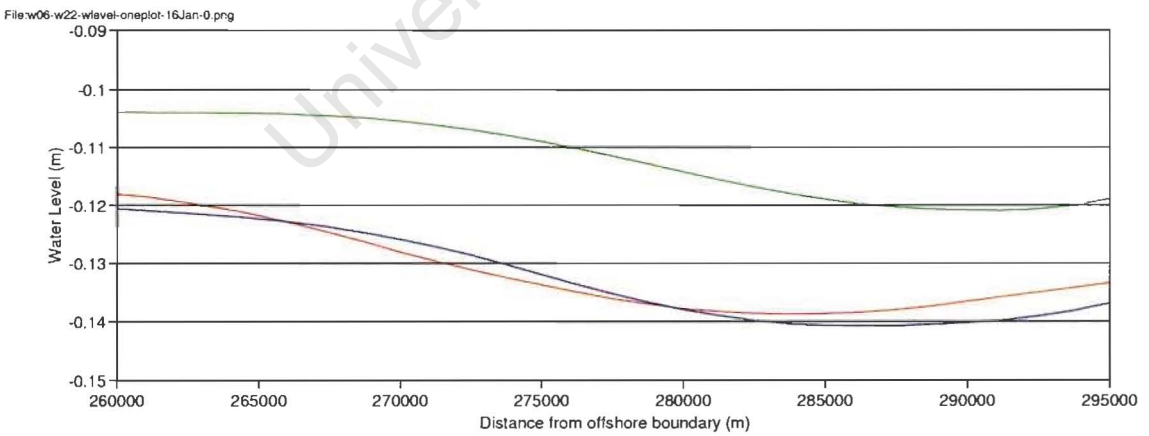

Figure 4-15 Reference Model: Comparison between surface slopes (from the coast to 35 km offshore) for the "Steep Sl" study (red line), the "Med Sl" study (blue line) and the "Flat Sl" study (green line) during wind relaxation. Note the difference in width of the upward sloping part of the surface slope close to the coast for the three studies.

When comparing the behaviour of the nearshore surface currents with offshore surface currents, as well as offshore bottom currents for all three studies, the same observations were made as during Numerical Experiment 1 (Chapter 4.2.1). For all three studies, when the wind ceased, the reduction in current speeds happened the fastest at the nearshore location (the shallower region), where the currents eventually turned poleward. Also, in the region of the surface jet, the currents started to reduce (gradually) once the wind relaxation event started, reaching a steady state after a few days (showing inertial oscillations), but never turning poleward. Below the surface jet, a net poleward undercurrent developed (showing inertial oscillations) a few days after the nearshore current turned poleward.

In summary, from the above results, the development of the nearshore poleward current for each study corresponds to the region where the subsurface isotherms have flattened out or reversed and where the surface has become upward sloping. The poleward current was narrower the flatter the bottom slope was, and it took longer to develop. Where the surface slope became flat during wind relaxation, the surface currents weakened tremendously (almost becoming 0 m/s). The position and width of the surface jet corresponded to the region where the surface was downward sloping (and the isotherms were upward sloping) towards the coast.

It is concluded that the inner shelf topography determines the position and strength of the temperature front, as well as the characteristics of the surface slope. This, in turn, determines the characteristics of the nearshore poleward current and the offshore surface jet.

Note that there is a slight instability in the surface jet in Figure 4-14(c). It can be seen that the surface jet seems to 'swerve around' and is not straight equatorward. This is due to the southern boundary of the model being ill posed by nature. This is a common modelling problem, which is not easily solved. For the purpose of this study, it is assumed that this instability did not influence the results in any significant way.

4.2.3 Results from Numerical Experiment 3

The aim of this experiment was to determine what happens to the poleward surface current when multiple wind events are simulated.

For the purpose of this experiment, the same model setup was applied as during the "Strat" study in Numerical Experiment 1, but this time a time series consisting of multiple wind events (as shown in Figure 3-3) was applied. Table 4-1 gave a summary of the setup of this study. This study will from now on be referred to as the "Mult Wnd" (multiple wind events) study. The study period was thirty days.

Figures 4-16(a), (b) and (c) illustrate the steady state situation during the first, second and third wind events respectively. For each case, the surface currents (left), a vertical transect of temperature (top right) and a vertical cross-section of surface slope (bottom right) in a representative cross shore line are shown.

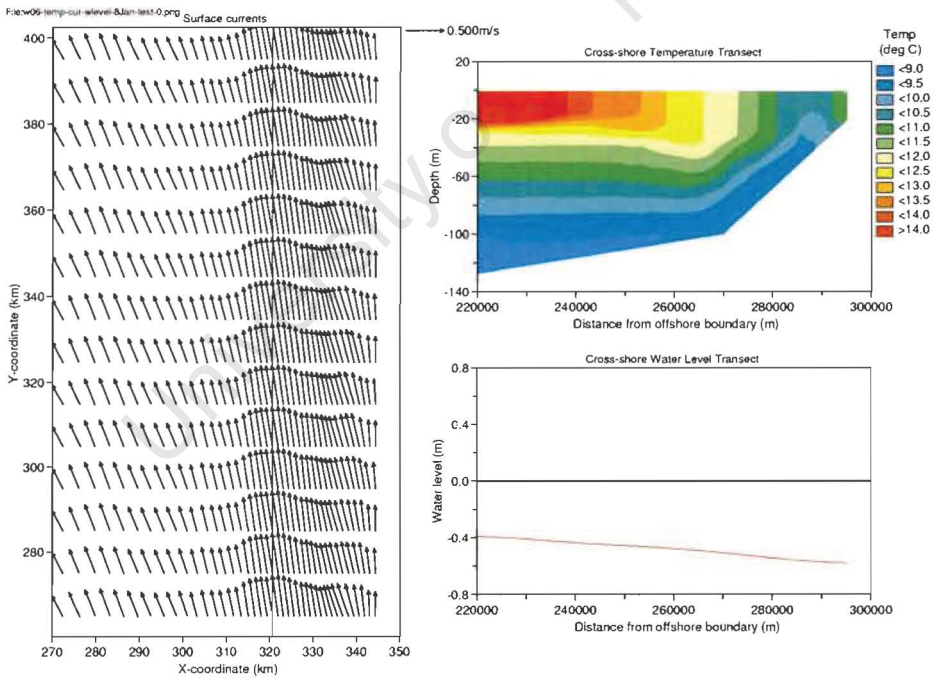

Figure 4-16(a) Reference Model – "Mult Wnd" study (during first wind event): Surface currents (left), vertical cross-section of temperature (top right) and vertical cross-section of surface slope (bottom right) in a representative cross shore line when a steady state has been achieved during the first wind event. The 100 m depth contour is shown underneath the currents, indicating the position of the inner shelf break (top right).

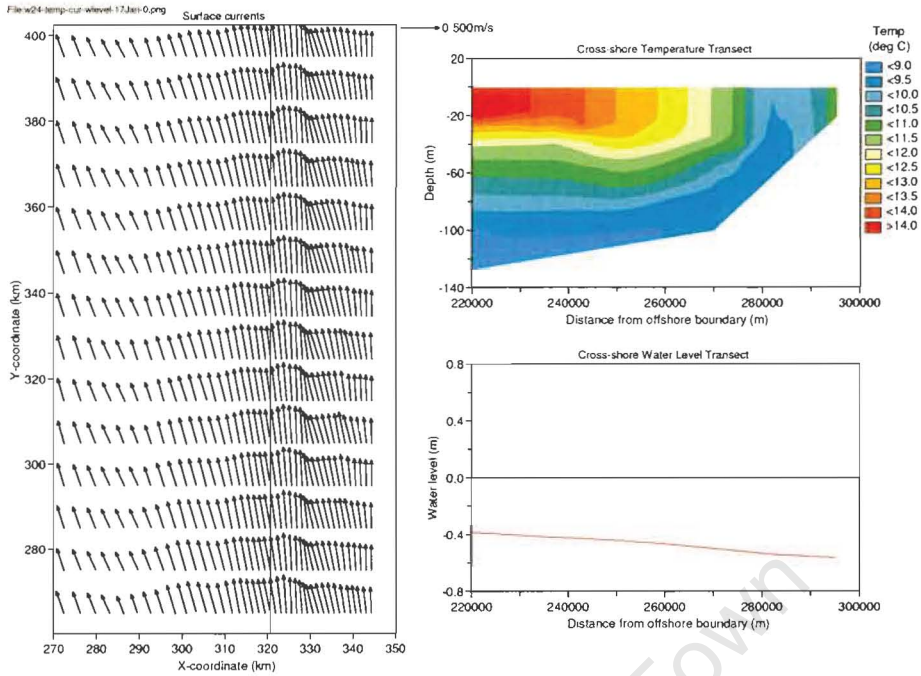

Figure 4-16(b) Reference Model – "Mult Wnd" study (during second wind event): Surface currents (left), vertical cross-section of temperature (top right) and vertical cross-section of surface slope (bottom right) in a representative cross shore line when a steady state has been achieved during the second wind event. The 100 m depth contour is shown underneath the currents, indicating the position of the inner shelf break (top right).

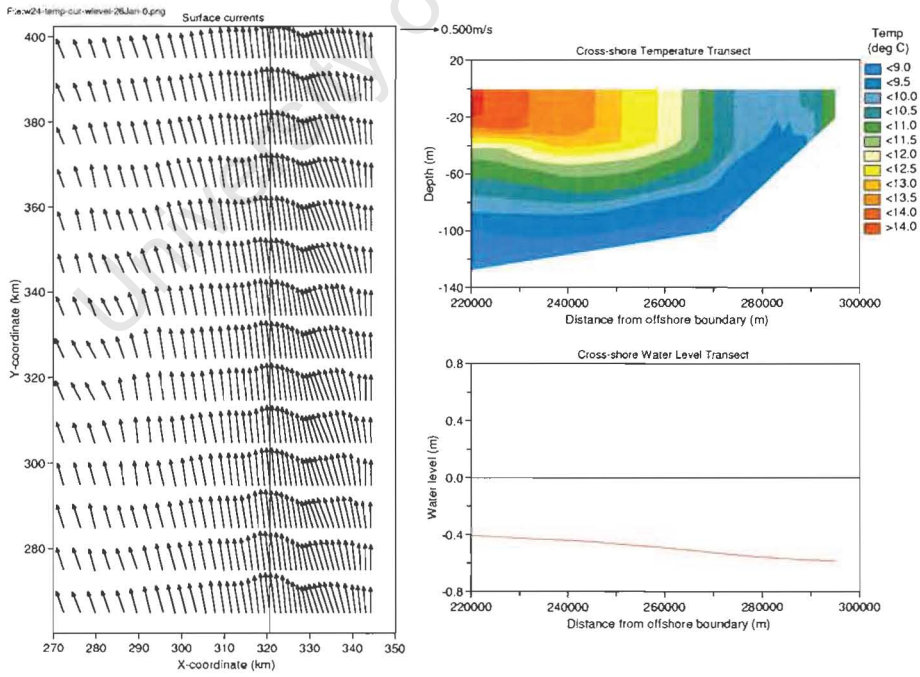

Figure 4-16(c) Reference Model – "Mult Wnd" study (during third wind event): Surface currents (left), vertical cross-section of temperature (top right) and vertical cross-section of surface slope (bottom right) in a representative cross shore line when a steady state has been achieved during the third wind event. The 100 m depth contour is shown underneath the currents, indicating the position of the inner shelf break (top right).

From the above figures, it was once again evident that an upwelling favourable wind caused a drop in water level at the coast, as well as the intrusion of cold bottom water into the nearshore environment and upwards towards the surface. Keeping in mind that this study started with the isotherms being horizontal (flat), the first wind event had a significant effect on the adjustment of the isotherms, with the effect being less dramatic during the subsequent wind events. It is clear that each successive wind event led to the cold bottom waters moving increasingly inshore and upwards, and as a result, the warm surface waters (as well as the subsurface temperature front) were pushed further and further offshore. Upwelling was therefore strengthened with each successive wind event. Also, during each wind event, the surface jet was correlated with the position of the temperature front, reaching speeds of between 0.5 and 0.6 m/s. Inshore of the surface jet, the currents were lower (0.3 m/s on average).

A much shorter time is needed for upwelling to develop than is needed to re-stratify the water column following an upwelling event. Therefore, every time the wind relaxed during this study, the upwelled cold bottom waters remained fairly close inshore and did not relax all the way back to its original location in the deeper offshore waters (although it did relax slightly). This is evident from Figures 4-17(a), (b) and (c), which illustrate the situation during the wind relaxation period following the first, second and third wind events respectively. Note that the interval between the three wind events was not long enough for the poleward current to reach a steady state.

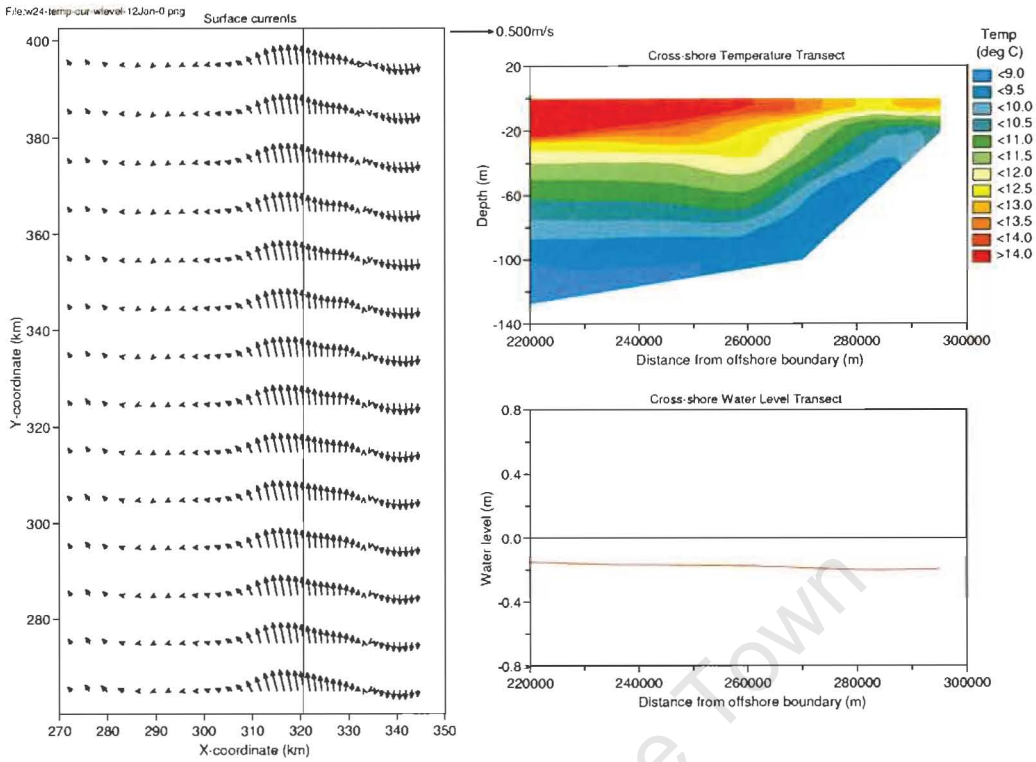

Figure 4-17(a) Reference Model – "Mult Wnd" study (following first wind event): Surface currents (left), vertical cross-section of temperature (top right) and vertical cross-section of surface slope (bottom right) in a representative cross shore during wind relaxation following the first wind event. The 100 m depth contour is shown underneath the currents, indicating the position of the inner shelf break (top right).

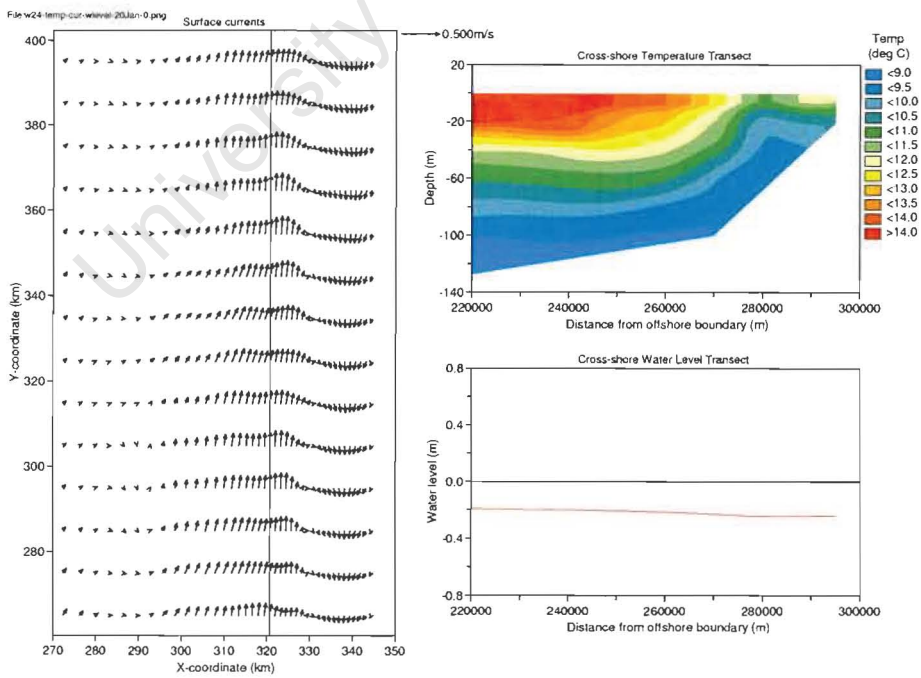

Figure 4-17(b) Reference Model – "Mult Wnd" study (following second wind event): Surface currents (left), vertical cross-section of temperature (top right) and vertical cross-section of surface slope (bottom right) in a representative cross shore during wind relaxation following the second wind event. The 100 m depth contour is shown underneath the currents, indicating the position of the inner shelf break (top right).

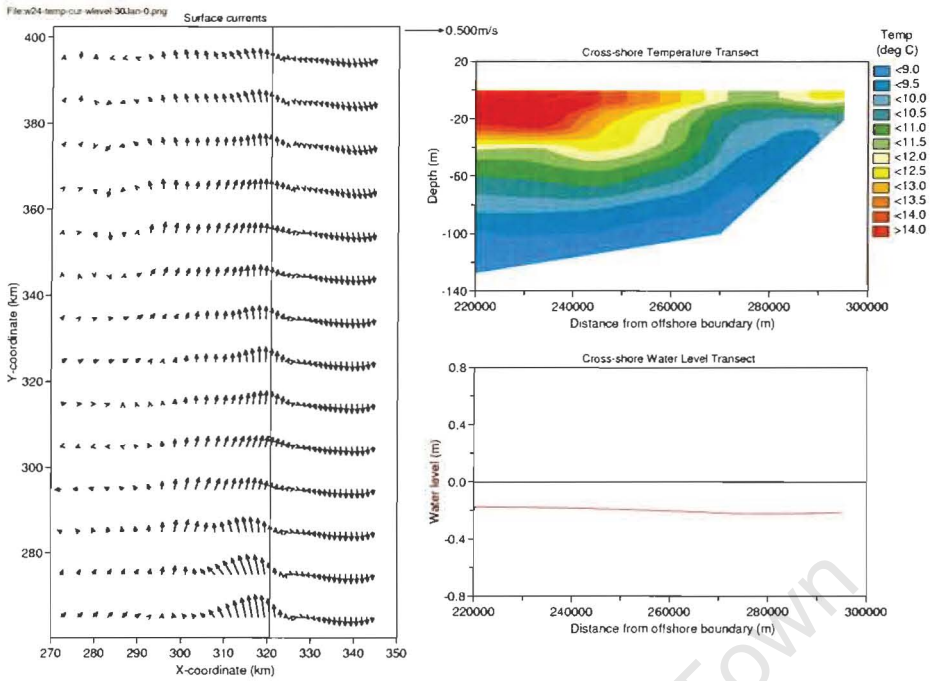

Figure 4-17(c) Reference Model – "Mult Wnd" study (following third wind event): Surface currents (left), vertical cross-section of temperature (top right) and vertical cross-section of surface slope (bottom right) in a representative cross shore line during wind relaxation following the third wind event. The 100 m depth contour is shown underneath the currents, indicating the position of the inner shelf break (top right).

Following each of the three wind events, a nearshore poleward surface current started to develop after approximately three to four days. This current became increasingly wider following each of the three wind events, and also slightly, but not significantly, weaker (reduced from approximately 0.08 m/s to 0.07 m/s, and thereafter to 0.06 m/s on average). The surface jet was still present in each case, but the speed of the jet currents have reduced to between 0.1 and 0.2 m/s.

It is important to note that, in Numerical Experiment 1 (the "Strat" study) in Chapter 4.2.1 and in Numerical Experiment 2 (the "Steep Sl", "Med Sl" and "Flat Sl" studies) in Chapter 4.2.2, the poleward current reached a steady state during relaxation following a wind event, and that it did not disappear again during the period of modelling. In this Numerical Experiment ("Mult Wnd" study), the poleward current immediately turned equatorward as soon as a new wind event started.

Figures 4-17(a), (b) and (c) also show that the surface slope has greatly flattened out during each wind relaxation event, although it has not returned to its original zero position. A close up view of the surface slope at the same cross-section as shown in the above figures, from the coast up to 35 km offshore, can be seen in Figure 4-18. This figure shows considerably more detail of the surface slopes during relaxation (following the wind event) for each of the three wind events. The red line indicates

the surface slope during relaxation following the first wind event, the blue line following the second event, and the green line following the third event.

Immediately apparent is that, during wind relaxation, the surfaces gradually changed (in an offshore to onshore direction) from downward sloping to upward sloping. The nearshore surface has an upward slope in the nearshore area in a band of approximately 10 km, 13 km and 15 km wide during the relaxation event following the first, second and third wind events respectively. This coincides with the width of the poleward surface current in each case, as was illustrated in Figures 4-17(a), (b) and (c). The upward sloping part of the surface, close to the coast, had essentially the same gradient for each study (thus, the slope had more or less the same steepness in each case). The very weak currents often noted in the region between the inshore poleward surface current and the offshore surface jet is once again associated with a flat surface (this is especially noticeable during the relaxation event following the third wind event). Furthermore, for each wind relaxation event it can be seen that the surface jet offshore of the poleward surface current once again is associated with the region where the surface slope remained downward.

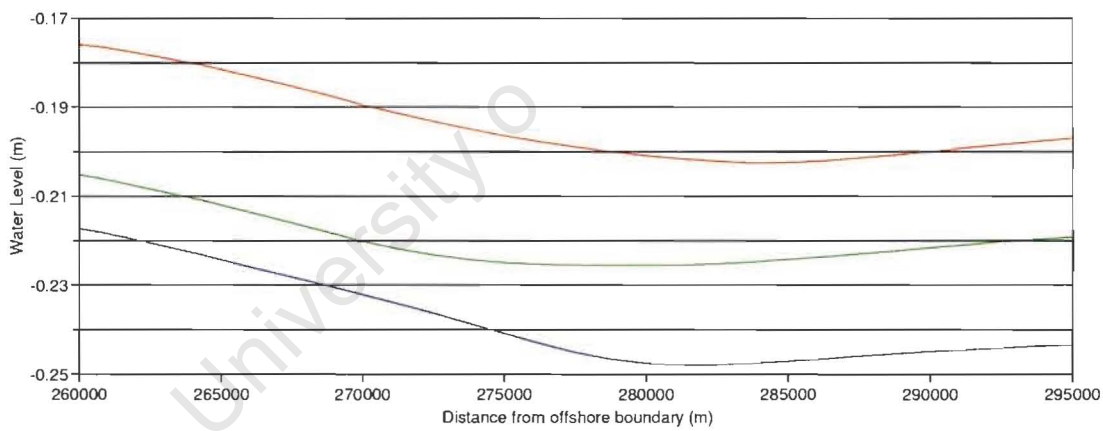

Figure 4-18 Reference Model "Mult Wnd" study: Comparison between surface slopes (from the coast to 35 km offshore) during relaxation following the first wind event (red line), the second wind event (blue line) and the third wind event (green line). Note that the width of the upward sloping part of the surface close to the coast increased after each successive wind event.

In conclusion, from this experiment it was evident that a wind time series simulating a 'real wind' led to the cold bottom waters moving increasingly inshore and upwards, and as a result, the warm surface waters (as well as the subsurface temperature front) were pushed further and further offshore. Upwelling was therefore strengthened with each successive wind event. Following each wind event, a narrow poleward surface current developed after about three to four days of relaxation, becoming progressively wider and slightly weaker following each successive wind event.

It should be noted that a so-called "spin up wind event" might be necessary when studies are undertaken with the more complex St Helena Bay model. An upwelling favourable wind that blows for a few days at the beginning of each study will ensure the initial intrusion of the cold bottom waters into the inshore region. This will set up a suitable initial condition to ensure that the temperature in the study represents the natural conditions as closely as possible.

Once again, an instability in the surface jet is noted in Figure 4-17(c), in which the offshore surface jet seems to "swerve around" and not move straight equatorward. This is once again due to the ill posed southern boundary. As before, it is assumed that this instability did not influence the results in any significant way.

5. RESULTS FROM THE ST HELENA BAY NUMERICAL MODEL

Three case studies were undertaken applying the St Helena Bay numerical model, and Table 5-1 below gives a summary of these studies.

Table 5-1 Summary of St Helena Bay numerical case studies.

Case	Winds
1	Measured St Helena Bay weather station winds
2	St Helena Bay weather station winds, reduced by 30%
3	Smoothed St Helena Bay weather station winds (diurnal component removed)

In studying the results from all three case studies, three specific regions were chosen as focus areas, namely (refer to Figure 1-1):

1. The area to the north of St Helena Bay, between Elands Bay and Lamberts Bay.
2. The eastern part of St Helena Bay.
3. The western part of St Helena Bay (including Cape Columbine).

The first region was chosen because it is far enough away from Cape Columbine so that the formation of the poleward current can take place without any influence from the Cape. The second region was in St Helena Bay, where a poleward current forms during wind relaxation, but it might be influenced by Cape Columbine. The third region was chosen because it is around Cape Columbine, and this is the region where thermistor chain data is available (see Figure 2-1).

In order to explore the formation of the poleward surface current effectively during the modelling period (January to mid February 2002 for each case), two prominent upwelling-relaxation events were chosen, namely:

1. The upwelling event that occurred from 19 – 24 January 2002, with the subsequent relaxation from 25 – 30 January 2002.
2. The upwelling event that occurred from 1 – 7 February 2002, with the subsequent relaxation from 8 – 11 February 2002.

The results from each separate case are presented in separate sections, as summarized in Table 5-2 below.

Table 5-2 Summary of presentation of St Helena Bay numerical model results.

Case	Upwelling/Relaxation Event	Focus Area
1	January	Lamberts Bay
	January	Eastern part of St Helena Bay
	February	Lamberts Bay
	February	Eastern part of St Helena Bay
	Full modelling period	Western part of St Helena Bay (comparison with thermistor chain data)
2	January	Lamberts Bay
	January	Eastern part of St Helena Bay
	February	Lamberts Bay
	February	Eastern part of St Helena Bay
	Full modelling period	Western part of St Helena Bay (comparison with thermistor chain data)
3	January	Lamberts Bay
	January	Eastern part of St Helena Bay
	February	Lamberts Bay
	February	Eastern part of St Helena Bay
	Full modelling period	Western part of St Helena Bay (comparison with thermistor chain data)

5.1 Results from Case 1

As described in Chapter 3.2.1, this study applied the measured St Helena Bay weather station winds (adjusted to 10 m above MSL) for the period January to mid February 2002.

One of the features that was most prominent during this case was the strong anti-cyclonic inertial oscillations that were present throughout the modelled period. The inertial oscillations had a period of approximately 22 hours. The currents in the deeper layers showed the same behaviour, although these currents were out of phase with the surface currents. This is in agreement with a study undertaken by Simpson *et al* (2002). According to this study, oscillations at, or close to, the inertial frequency become significantly enhanced in the vicinity of latitudes 30°N and S by a resonance in which the local inertial frequency coincides with that of diurnal forcing. Under these conditions, regular daily variations in wind stress tend to produce large anti-cyclonic motions that may extend throughout the water column. Figure 5-1(a) shows an example of the inertial oscillations in the surface layer of the St Helena Bay model. The surface currents are plotted every 6 hours.

These oscillatory movements push warm water back against the coast when the currents turn onshore, and pulls warm surface water away from the coast when the currents turn offshore, all during one inertial cycle. Even during a strong upwelling event, these currents strengthen and weaken upwelling

in the surface water, as seen in Figure 5-1(b). This figure shows a cross shore transect of temperature in the eastern part of St Helena Bay during the same upwelling event as illustrated in Figure 5-1(a). A sequence of four plots shows the strengthening and weakening of the upwelling during an inertial oscillation cycle, although there is a net increase in the strength of the upwelling.

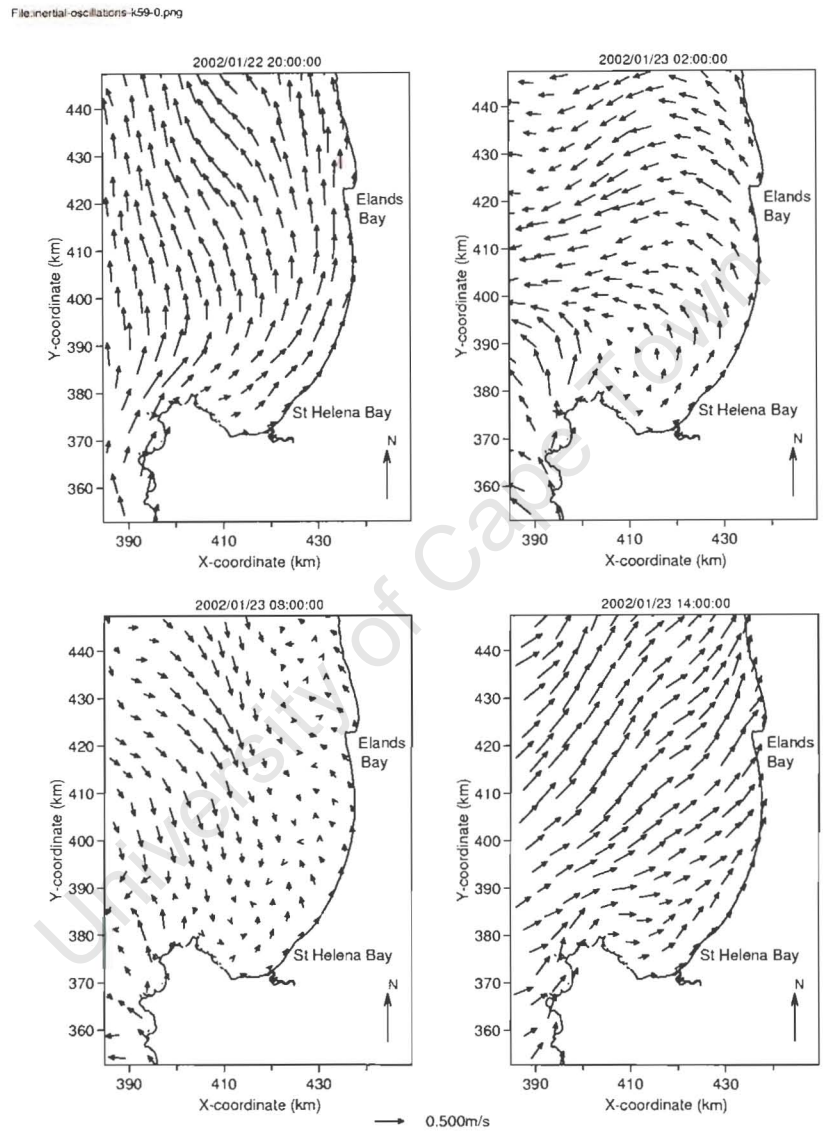

Figure 5-1(a) St Helena Bay model (St Helena Bay weather station winds): Surface currents plotted every 6 hours on 22 and 23 January 2002, illustrating the strong anti-cyclonic inertial oscillations.

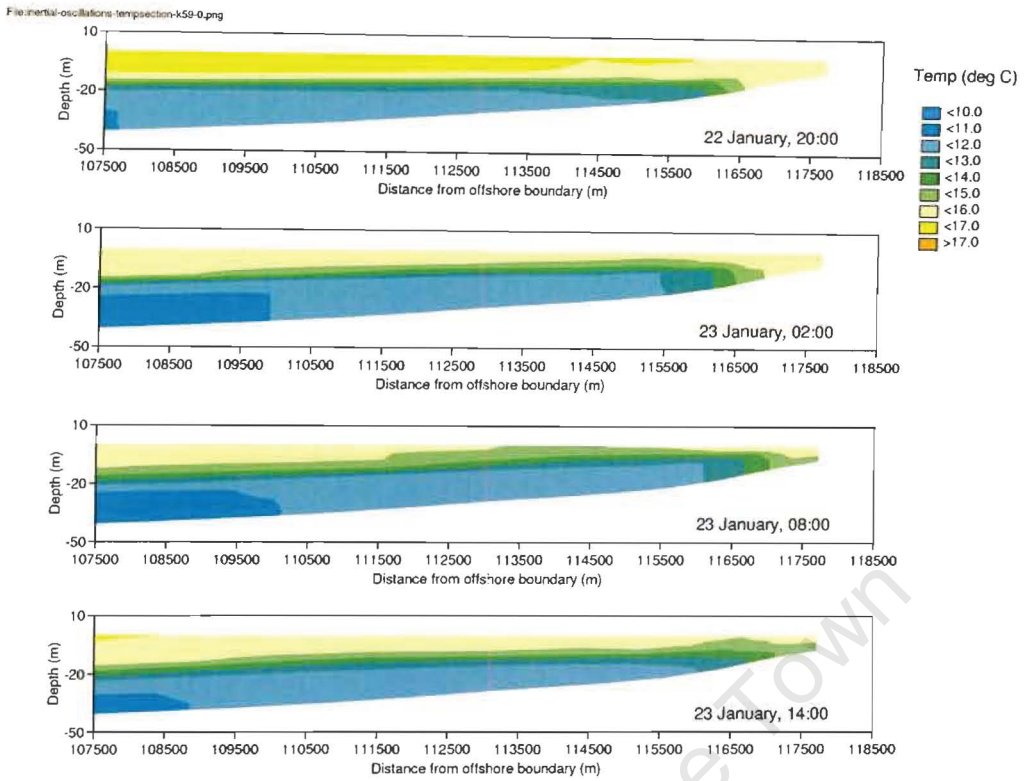

Figure 5-1(b) St Helena Bay model (St Helena Bay weather station winds): Cross shore transect of temperature in the eastern part of St Helena Bay plotted every 6 hours on the 22 and 23 January 2002, illustrating the strengthening and weakening of upwelling as a result of the inertial movements of the currents.

In the horizontal, Figure 5-2 illustrates the surface currents and temperature during a typical upwelling event (left), in this case on 24 January 2002, 18:00, and a subsequent wind relaxation event (right), on 30 January 2002, 02:00. During upwelling, cold water (less than 13°C) has reached the surface around Cape Columbine and on the West Coast, especially in the region between Lamberts Bay and Elands Bay. The currents are predominantly equatorward (0.4 m/s on average), but bends eastwards towards the West coast around Cape Columbine. A strong jet flows past Cape Columbine. The currents are weak in St Helena Bay.

During the subsequent wind relaxation event, the surface water has warmed and upwelling has completely subsided. The currents have significantly weakened (all currents are less than 0.2 m/s).

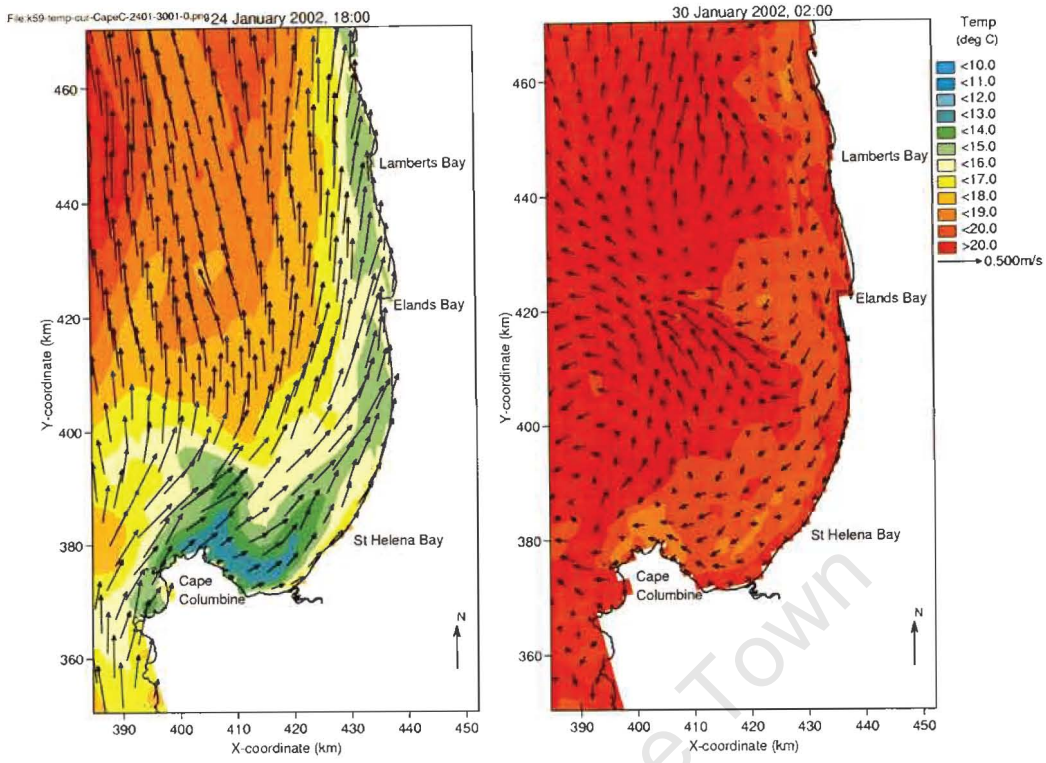

Figure 5-2 St Helena Bay model (St Helena Bay weather station winds): Surface currents and temperature during a typical upwelling event (left), in this case on 24 January 2002, 18:00, and a subsequent wind relaxation event (right), on 30 January 2002, 02:00. Note the upwelling of cold water around Cape Columbine and on the West Coast, especially in the region between Lamberts Bay and Elands Bay. During the wind relaxation event, the surface water warms to greater than 18°C.

Case 1: January Event – Lamberts Bay Region

Figures 5-3(a) – (c) shows the surface currents (left), a vertical transect of temperature (top right) and a vertical cross-section of surface slope (bottom right) along a profile line, indicated on the left hand plot, for certain times during the upwelling-relaxation event from 19 - 30 January 2002. In these figures, the focus area is the region between Elands Bay and Lamberts Bay, to the north of St Helena Bay.

Figure 5-3(a) illustrates a time of upwelling (23 January 2002, 20:00), with equatorward currents being forced by the upwelling favourable wind conditions. These currents are relatively weak (less than 0.2 m/s) at the coast and stronger (approximately 0.5 m/s) offshore. Cold water intrusion (water less than 15°C) into the surface waters at the coast can clearly be seen from the cross shore temperature transect. The water level has dropped by approximately 4 cm at the coast. Upwelling continued until the end of 25 January 2002.

Four hours later, however, on 27 January 12:00, a narrow, nearshore poleward current has formed. Figure 5-3(b) shows the poleward current (0.5 km wide), from north of Lamberts Bay to south of Elands Bay, protruding into St Helena Bay, with speeds of approximately 0.2 m/s. The surface waters have warmed to between 16°C and 19°C.

This poleward current persisted for the rest of the wind relaxation period (four days in total), continuing to strengthen, until it reached its peak on 29 January 2002, 14:00 (Figure 5-3(c)). At this stage, the poleward current was approximately 1 km wide and 0.3 m/s strong (strongest next to the coast). The surface waters have warmed to between 19°C and 20°C.

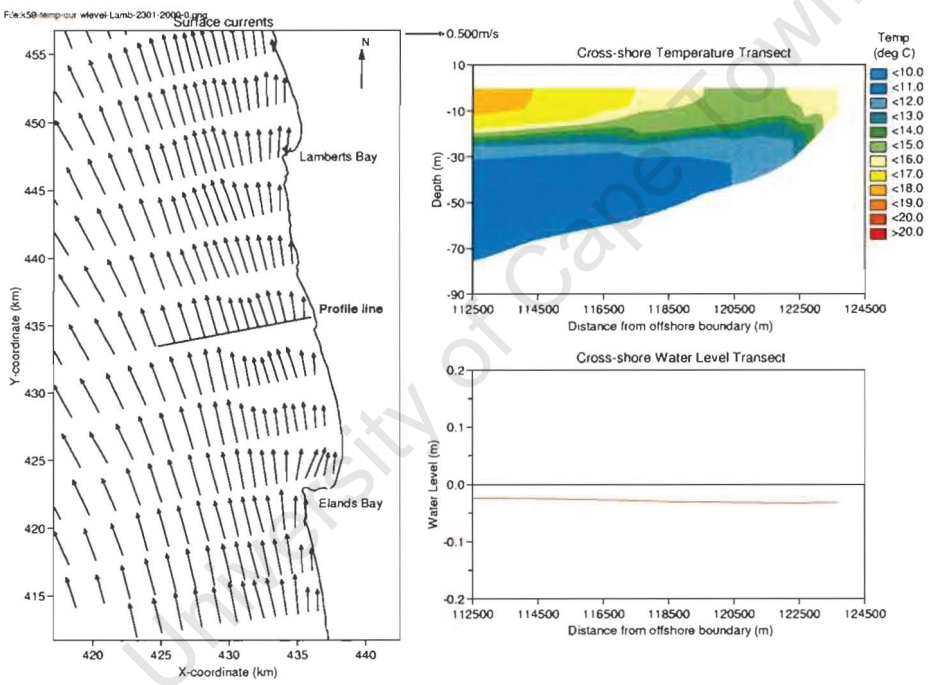

Figure 5-3(a) St Helena Bay model (St Helena Bay weather station winds) – Lamberts Bay region: Surface currents (left), vertical cross-section of temperature (top right) and vertical cross-section of surface slope (bottom right) along a profile line on 23 January 2002, 20:00 (a time of upwelling).

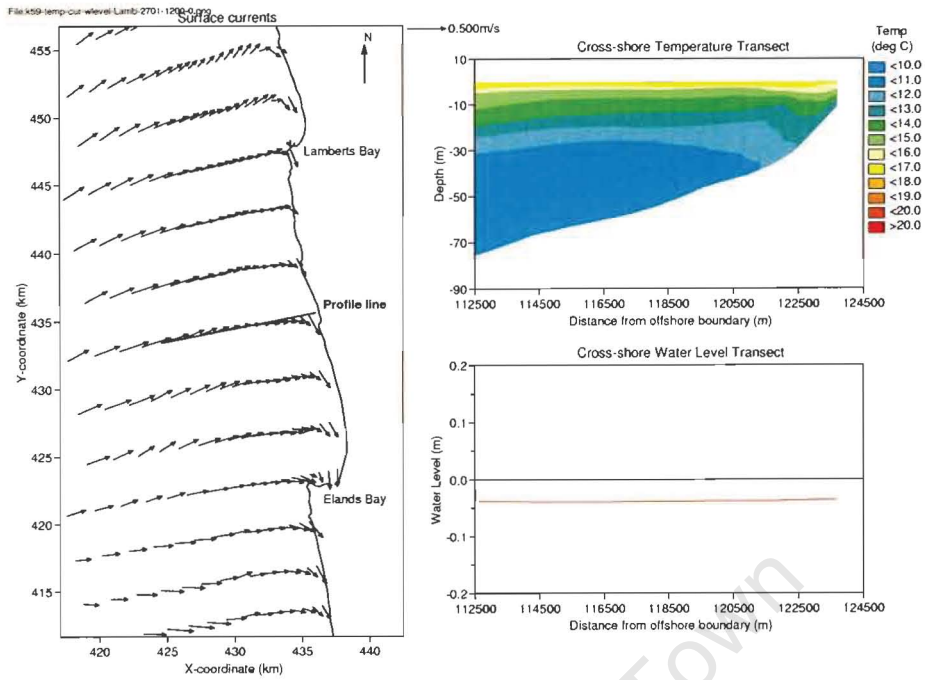

Figure 5-3(b) St Helena Bay model (St Helena Bay weather station winds) – Lamberts Bay region: Surface currents (left), vertical cross-section of temperature (top right) and vertical cross-section of surface slope (bottom right) along a profile line on 27 January 2002, 12:00 (a time of wind relaxation).

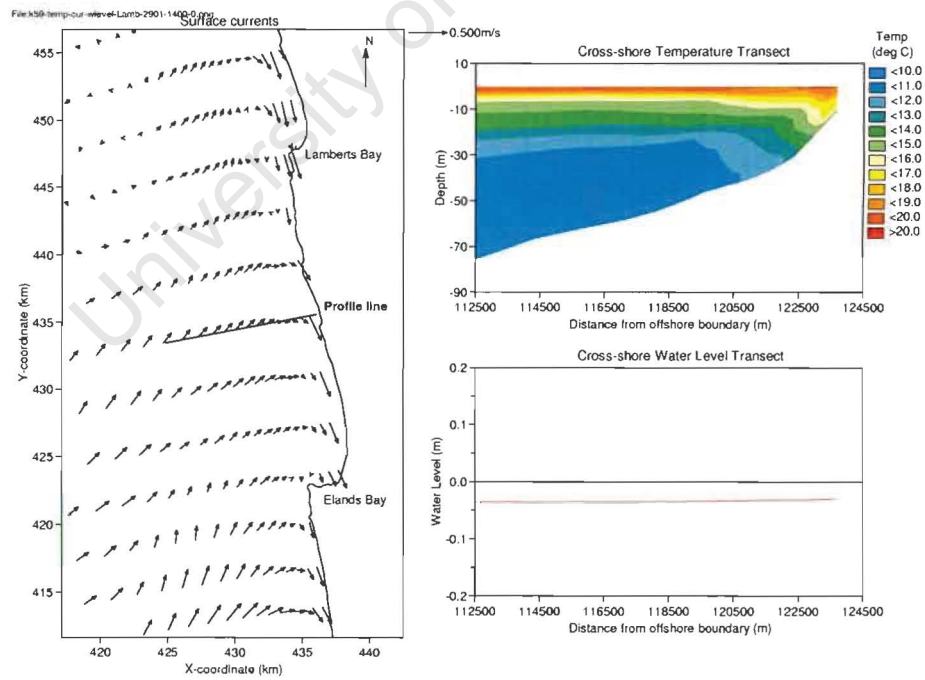

Figure 5-3(c) St Helena Bay model (St Helena Bay weather station winds) – Lamberts Bay region: Surface currents (left), vertical cross-section of temperature (top right) and vertical cross-section of surface slope (bottom right) along a profile line on 29 January 2002, 14:00 (close to the end of the wind relaxation event).

Figures 5-3(a)-(c) showed that the surface slope has greatly flattened out during each wind relaxation event, although it has not returned to its original zero position. A close up view of the surface slope at the same cross-section as shown in the above figures, from the coast up to approximately 1.7 km offshore, can be seen in Figure 5-4. This figure shows considerably more detail of the surface slopes at the same instances in time as shown in the above sequence of figures. The exact times are indicated on the figure.

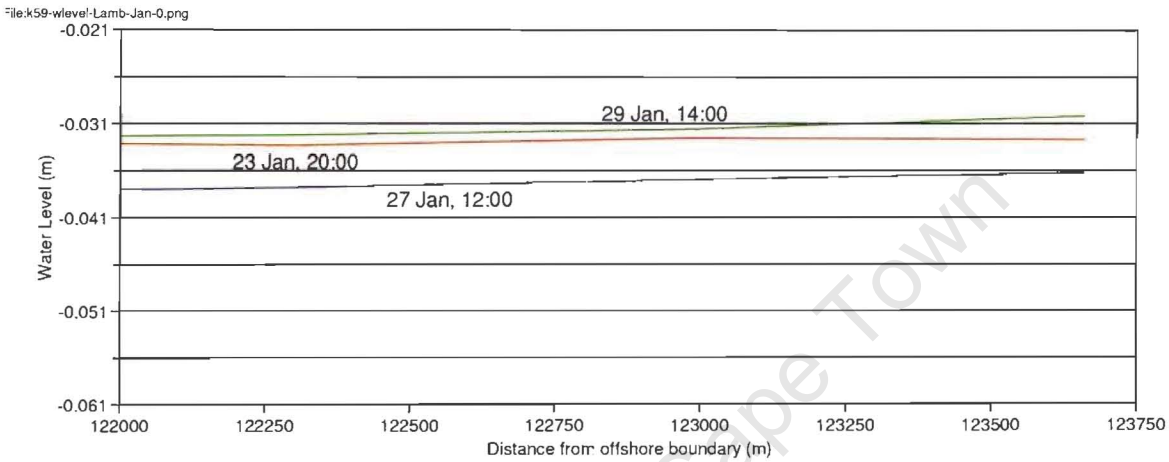

Figure 5-4 St Helena Bay model (St Helena Bay weather station winds) – Lamberts Bay region: Comparison between surface slopes (from the coast to 1.7 km offshore) for the January event. The time at which each surface slope is plotted, is indicated on the figure.

It is clear that, during upwelling, the surface was downward sloping close to the coast (red line). During wind relaxation, the surfaces became upward sloping close to the coast. On 29 January, the nearshore surface had an upward slope in the nearshore area in a band of approximately 1.2 km wide. The very weak currents noted in the region between the inshore poleward surface current and the offshore surface jet is associated with a relatively flat surface slope.

Case 1: January Event – Eastern part of St Helena Bay

Figures 5-5(a) – (c) shows the surface currents (left), a vertical transect of temperature (top right) and a vertical cross-section of surface slope (bottom right) along a profile line, indicated on the left hand plot, for certain times during the upwelling-relaxation event from 24 – 30 January 2002. In this case, the focus area is on the eastern part of St Helena Bay.

Figure 5-5(a) illustrates a time of upwelling (23 January 2002, 20:00), with equatorward currents being forced by the upwelling favourable wind conditions. These currents are relatively weak (less than 0.2 m/s) at the coast and in the southern parts of St Helena Bay, and stronger (approximately 0.5 m/s) offshore. Cold water intrusion (water less than 15°C) into the surface waters at the coast can clearly be seen from the cross shore temperature transect. The water level has dropped by approximately 4 cm at the coast. Upwelling continued until the end of 25 January 2002.

On 27 January 2002, 16:00 (Figure 5-5(b)), during the subsequent relaxation event, the wind speed has dropped and the warm surface waters are in the process of returning to the coast. Close to the coast, the surface waters are now between 18°C and 20°C. A narrow poleward current has formed close to the coast, in a band of approximately 0.5 km wide. The poleward current has a speed of approximately 0.2 m/s. The water level at the coast is 3 cm, and it seems to be almost horizontal. Cyclonic movement can be seen in the south of the Bay.

This poleward current persisted for the rest of the wind relaxation period (four days in total), continuing to strengthen and widen, until it reached its peak on 29 January 2002, 16:00 (Figure 5-5(c)). At this stage, the poleward current was approximately 1 km wide and 0.3 m/s strong (strongest next to the coast). The surface waters have warmed to greater than 20°C and the water level is 2 cm below MSL. In the south of the Bay, the cyclonic motion is still evident.

This appeared to be the steady state situation for the poleward current, and its strength and width remained unchanged for the rest of the upwelling event. The current only disappeared once the next upwelling event started.

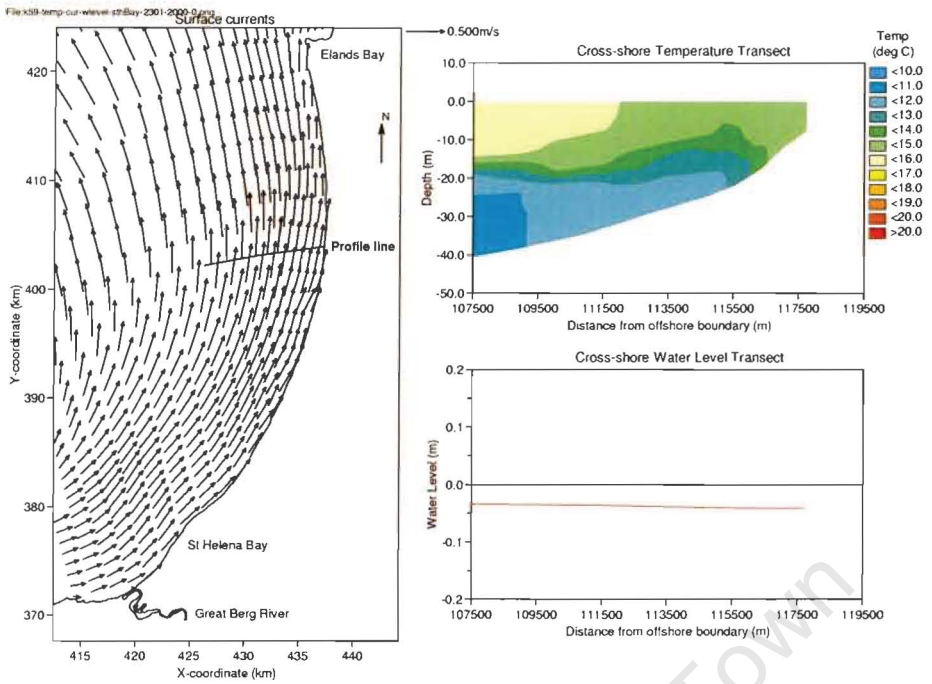

Figure 5-5(a) St Helena Bay model (St Helena Bay weather station winds) – Eastern part of St Helena Bay: Surface currents (left), vertical cross-section of temperature (top right) and vertical cross-section of surface slope (bottom right) along a profile line on 23 January 2002, 20:00 (a time of upwelling).

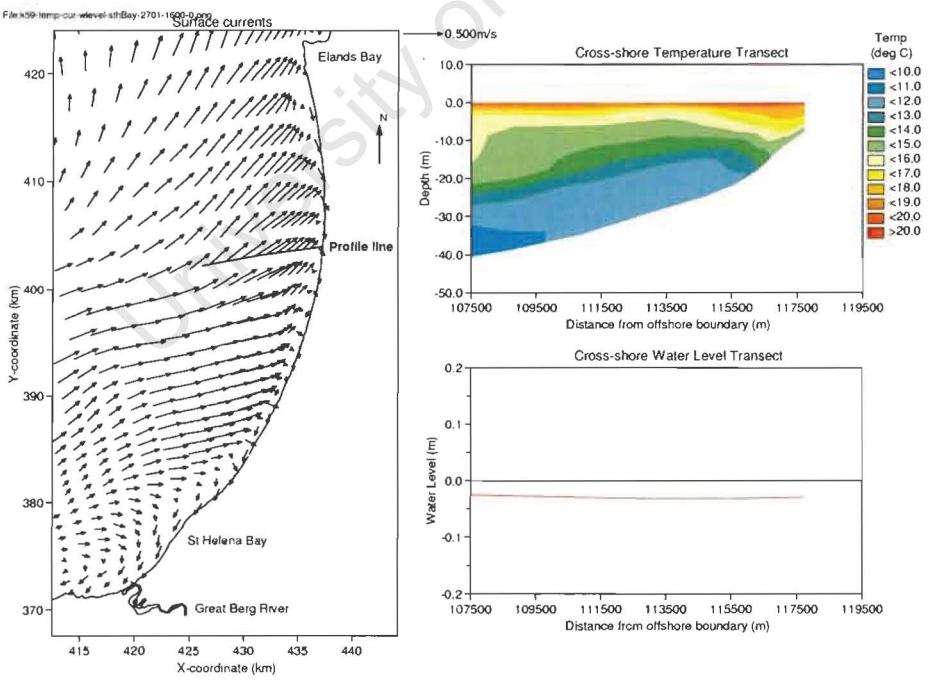

Figure 5-5(b) St Helena Bay model (St Helena Bay weather station winds) – Eastern part of St Helena Bay: Surface currents (left), vertical cross-section of temperature (top right) and vertical cross-section of surface slope (bottom right) along a profile line on 27 January 2002, 16:00 (a time of wind relaxation).

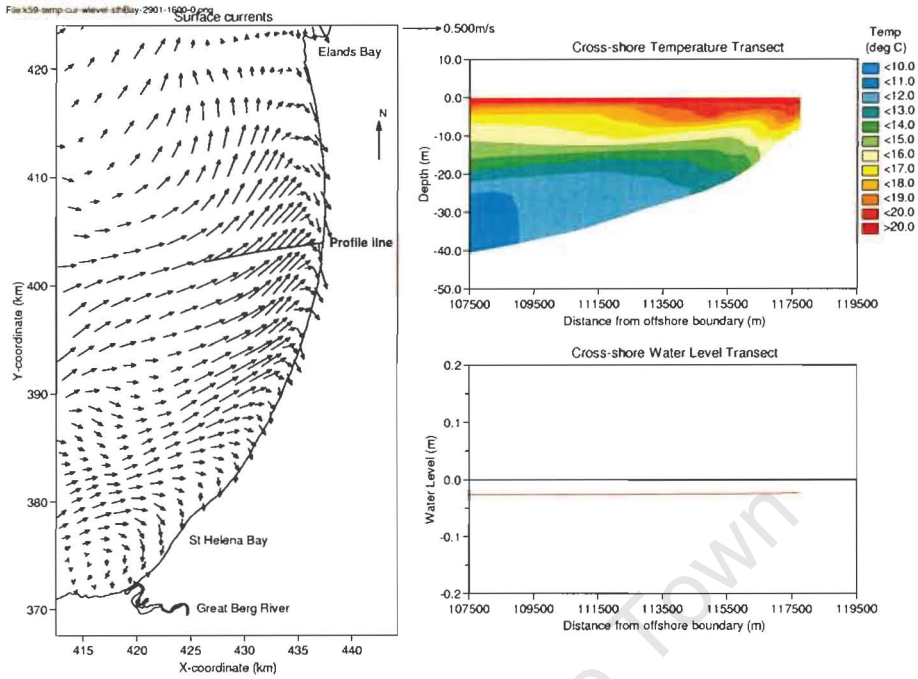

Figure 5-5(c) St Helena Bay model (St Helena Bay weather station winds) – Eastern part of St Helena Bay: Surface currents (left), vertical cross-section of temperature (top right) and vertical cross-section of surface slope (bottom right) along a profile line on 29 January 2002, 16:00 (a time of wind relaxation).

Figures 5-5(a)-(c) showed that the surface slope has greatly flattened out during each wind relaxation event, although it has not returned to its original zero position. A close up view of the surface slope at the same cross-section as shown in the above figures, from the coast up to approximately 1.7 km offshore, can be seen in Figure 5-6. This figure shows considerably more detail of the surface slope slopes at the same instances in time as shown in the above sequence of figures. The exact times are indicated on the figure.

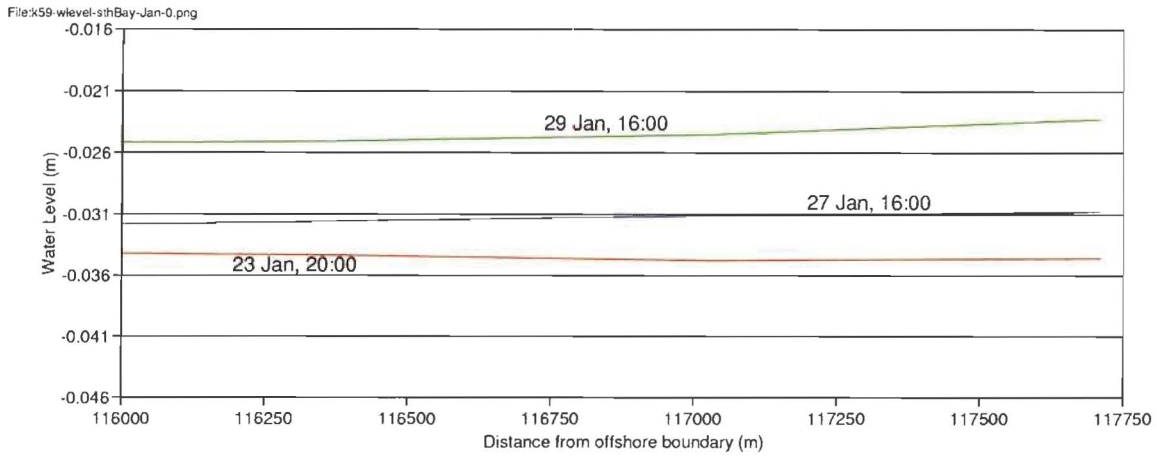

Figure 5-6 St Helena Bay model (St Helena Bay weather station winds) – Eastern part of St Helena Bay: Comparison between surface slopes (from the coast to 1.7 km offshore) for the January event. The time at which each surface slope is plotted, is indicated on the figure.

Immediately apparent is that, during wind relaxation, the surfaces gradually changed from downward sloping to upward sloping. On 29 January, the nearshore surface had an upward slope in the nearshore area in a band of approximately 0.75 km wide.

Case 1: February Event – Lamberts Bay Region

Figures 5-7(a) – (c) shows the surface currents (left), a vertical transect of temperature (top right) and a vertical cross-section of surface slope (bottom right) along a profile line, indicated on the left hand plot, for certain times during the upwelling-relaxation event from 1 – 11 February 2002. In these figures, the focus area is the region between Elands Bay and Lamberts Bay, to the north of St Helena Bay.

Figure 5-7(a) illustrates a time of upwelling (6 February 2002, 18:00), with equatorward currents being forced by the upwelling favourable wind conditions. These currents are relatively weak (less than 0.2 m/s) at the coast and stronger (up to 0.6 m/s) offshore. Cold water intrusion (water less than 12°C) into the surface waters at the coast can clearly be seen from the cross shore temperature transect. The water level has dropped by approximately 9 cm at the coast. Upwelling continued until 9 February 2002.

Following this lengthy upwelling event (from 1 – 9 February), the wind speed dropped for two days. This relaxation period was relatively short (two days). On 10 February 2002, 18:00 (Figure 5-7(b)), the currents have significantly reduced at the coast, and a narrow (0.5 km wide) poleward current can be seen close to the coast, in the region between Lamberts Bay and Elands Bay, protruding into

St Helena Bay. This current has a speed of approximately 0.1 m/s. At this stage, the surface waters have warmed to between 16°C and 17°C, and the water level was 5 cm below MSL.

Soon thereafter, another short (two day) upwelling event took place, during which the poleward current disappeared. This short upwelling event was followed by another short (two day) period of wind relaxation. Figure 5-7(c) illustrates the situation during the second short relaxation event (15 February 2002, 14:00). The wind speed has dropped and the surface waters have warmed to between 19°C and 20°C. The water level is 6 cm below MSL. In the nearshore area, in a band of approximately 1 km wide, a poleward surface current has formed (with current speed of between 0.2 m/s and 0.3 m/s).

This poleward current disappeared again towards the end of 15 February, when the next upwelling event started.

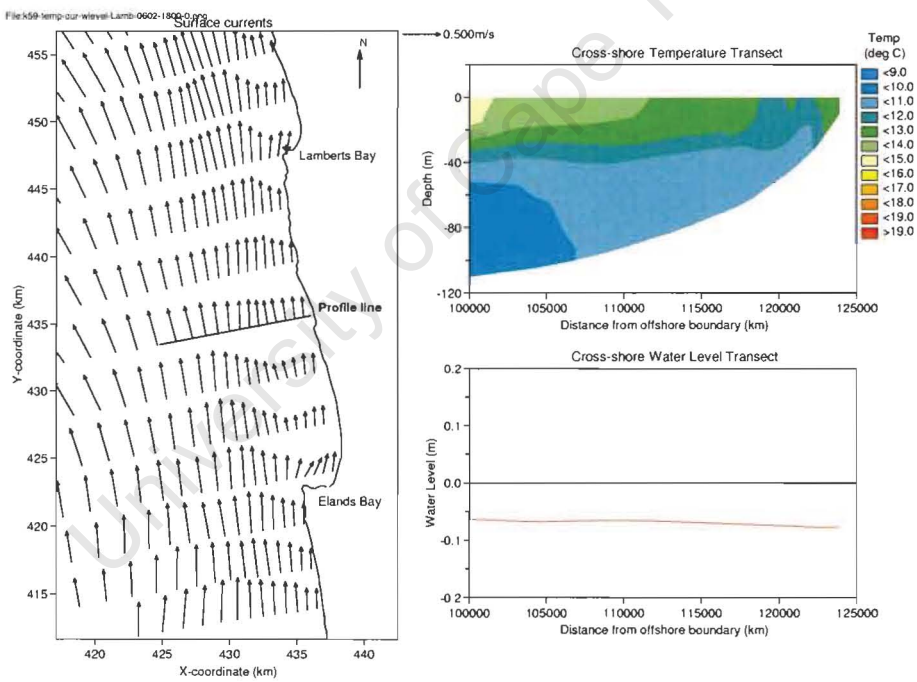

Figure 5-7(a) St Helena Bay model (St Helena Bay weather station winds) – Lamberts Bay region: Surface currents (left), vertical cross-section of temperature (top right) and vertical cross-section of surface slope (bottom right) along a profile line on 6 February 2002, 18:00 (a time of upwelling).

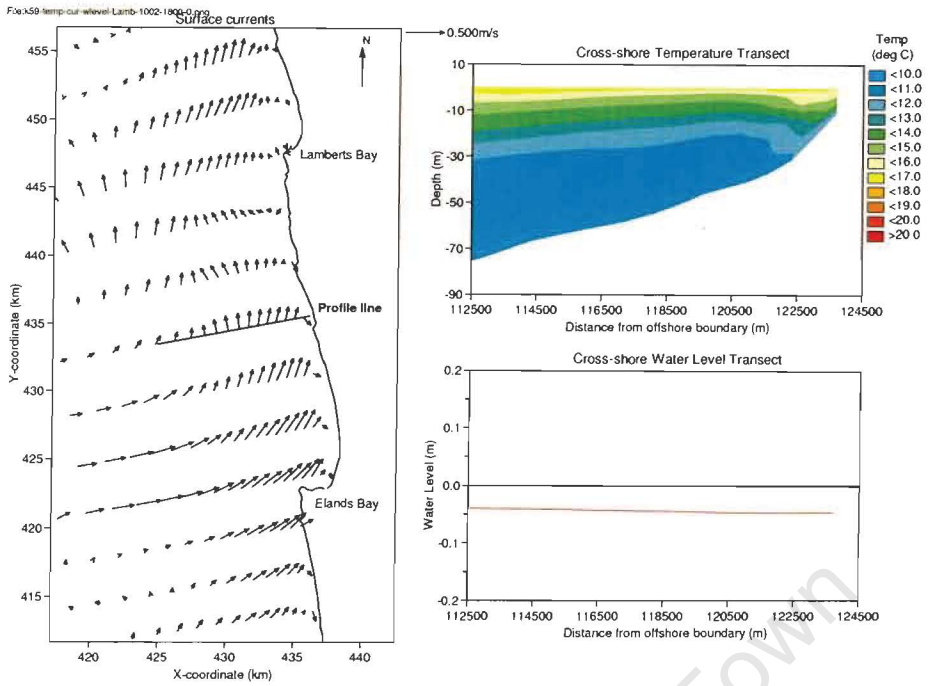

Figure 5-7(b) St Helena Bay model (St Helena Bay weather station winds) – Lamberts Bay region: Surface currents (left), vertical cross-section of temperature (top right) and vertical cross-section of surface slope (bottom right) along a profile line on 10 February 2002, 18:00 (a time of wind relaxation).

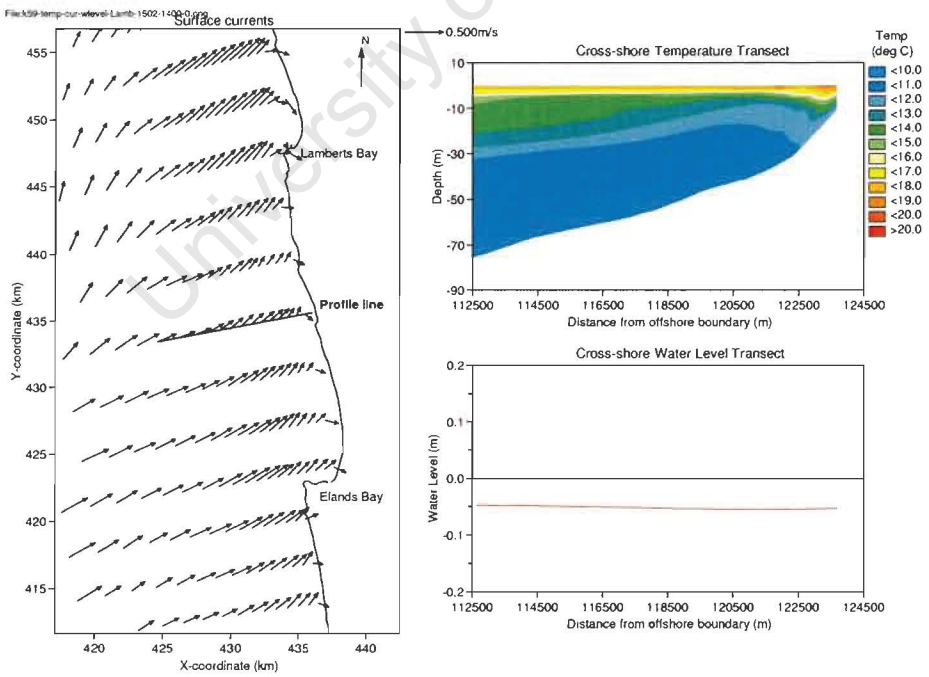

Figure 5-7(c) St Helena Bay model (St Helena Bay weather station winds) – Lamberts Bay region: Surface currents (left), vertical cross-section of temperature (top right) and vertical cross-section of surface slope (bottom right) along a profile line on 15 February 2002, 14:00 (a time of wind relaxation).

Figures 5-7(a)-(c) showed that the surface slope has greatly flattened out during each wind relaxation event, although it has not returned to its original zero position. A close up view of the surface slope at the same cross-section as shown in the above figures, from the coast up to approximately 1.7 km offshore, can be seen in Figure 5-8. This figure shows considerably more detail of the surface slopes at the same instances in time as shown in the above sequence of figures. The exact times are indicated on the figure.

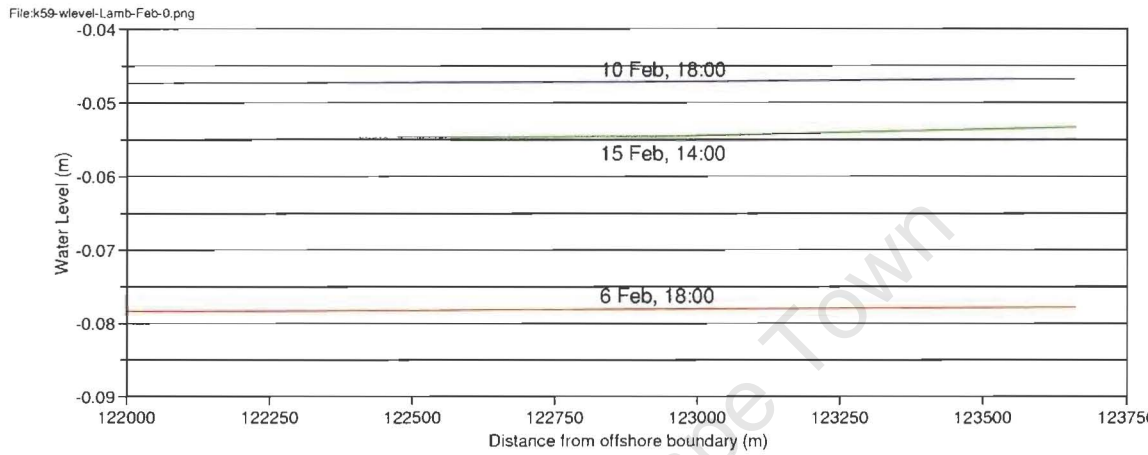

Figure 5-8 St Helena Bay model (St Helena Bay weather station winds) – Lamberts Bay region: Comparison between surface slopes (from the coast to 1.7 km offshore) for the February event. The time at which each surface slope is plotted, is indicated on the figure.

On 8 February, the nearshore surface seems to be slightly upward sloping, although an upweling event was taking place. This could be due to a momentary relaxation in wind speed. During wind relaxation, on 10 February, the nearshore surface slope seemed to be almost flat close to the coast (even slightly upward sloping). However, on 15 February, the surface had a clear upward slope in the nearshore area in a band of approximately 1 km wide.

Case 1: February Event – Eastern part of St Helena Bay

Figures 5-9(a) – (b) shows the surface currents (left), a vertical transect of temperature (top right) and a vertical cross-section of surface slope (bottom right) along a profile line, indicated on the left hand plot, for certain times during the upwelling-relaxation event from 1 – 11 February 2002. In this case, the focus area is on the eastern part of St Helena Bay.

Figure 5-9(a) illustrates a time of upwelling (6 February 2002, 14:00), with equatorward currents being forced by the upwelling favourable wind conditions. These currents are weaker (less than

0.3 m/s) at the coast and in the southern parts of St Helena Bay, and stronger (approximately 0.4 m/s) offshore. Cold water intrusion (water less than 13°C) into the surface waters at the coast can clearly be seen from the cross shore temperature transect. The water level has dropped by approximately 13 cm at the coast. Upwelling continued until 9 February.

On 10 February 2002, 16:00 (Figure 5-9(b)), during the subsequent wind relaxation event, the wind speed has dropped and the warm surface waters are in the process of returning to the coast. Close to the coast, the surface waters are now between 17°C and 19°C. The current speeds have dropped to below 0.2 m/s, although stronger currents seem to come from the direction of Cape Columbine. Cyclonic motion can be seen in St Helena Bay. The water level at the coast is 6 cm below MSL. At this time, a narrow, nearshore poleward current is visible, from south of Elands Bay into St Helena Bay, with speeds of approximately 0.1 m/s.

This poleward current disappeared as soon as the next (two day) upwelling event started, and no poleward motion in this focus region was detected for the rest of the modelling period.

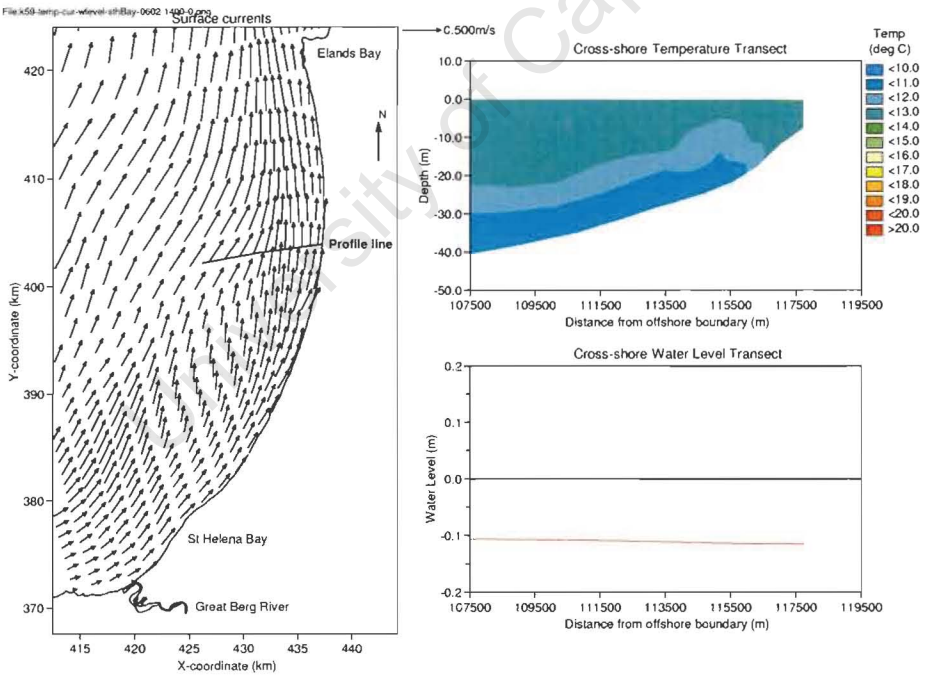

Figure 5-9(a) St Helena Bay model (St Helena Bay weather station winds) – Eastern part of St Helena Bay: Surface currents (left), vertical cross-section of temperature (top right) and vertical cross-section of surface slope (bottom right) along a profile line on 6 February 2002, 14:00 (a time of upwelling).

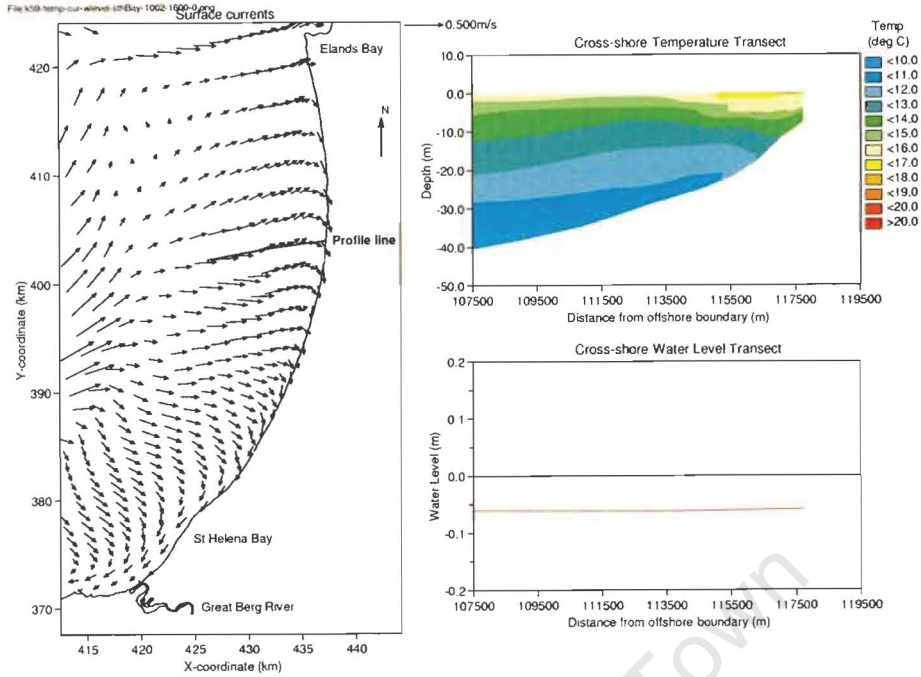

Figure 5-9(b) St Helena Bay model (St Helena Bay weather station winds) – Eastern part of St Helena Bay: Surface currents (left), vertical cross-section of temperature (top right) and vertical cross-section of surface slope (bottom right) along a profile line on 10 February 2002, 16:00 (a time of wind relaxation).

Figures 5-9(a)-(b) showed that the surface has greatly flattened out during each wind relaxation event, although it has not returned to its original zero position. A close up view of the surface slope at the same cross-section as shown in the above figures, from the coast up to approximately 1.7 km offshore, can be seen in Figure 5-10. This figure shows considerably more detail of the surface slopes at the same instances in time as shown in the above sequence of figures. The exact times are indicated on the figure.

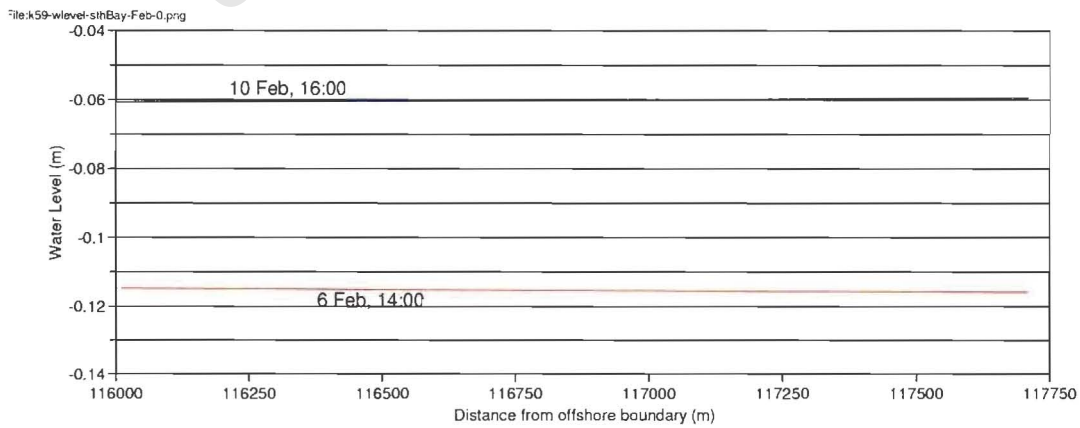

Figure 5-10 St Helena Bay model (St Helena Bay weather station winds) – Eastern part of St Helena Bay: Comparison between surface slopes (from the coast to 1.7 km offshore) for the February event. The time at which each surface slope is plotted, is indicated on the figure.

From the above figure, on 6 February, the surface slope was slightly downward towards the coast. On 10 February (during wind relaxation), the surface was slightly upward sloping towards the coast.

Case 1: Western Part of St Helena Bay

For the western part of St Helena Bay, in the vertical, a comparison of the modelled and measured temperatures at the thermistor chain's location for January 2002 (Figure 2.1) for Case 1 is shown in Figure 5-11(a).

Overall, the model represents the 6 - 8 day event scale warming and cooling well, although the modelled temperatures seem to be colder than the measured temperatures in the top half of the water column for most of the simulation time. The modelled temperatures also show less diurnal variability than the measured temperatures. In general, the modelled temperatures in St Helena Bay are within 2°C - 3°C of the measured values when the St Helena Bay weather station winds are applied.

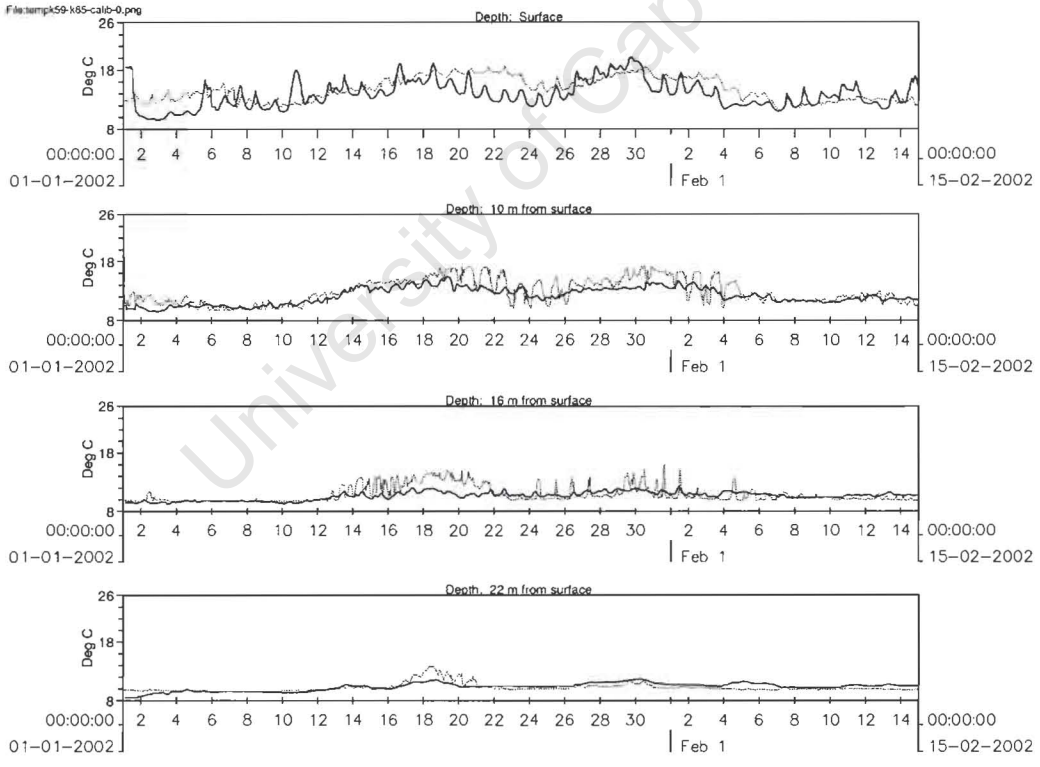

Figure 5-11(a) St Helena Bay model (St Helena Bay weather station winds): Comparison between measured (dotted) and modelled (solid) temperatures at different depths in the western part of St Helena Bay for January to mid February 2002.

Another way of comparing the measured and the modelled temperatures is by calculating the temperature anomalies. These anomalies were calculated by applying the following formula:

$$\text{Anomaly} = (\text{Measurement} - \text{Model})/(\text{Measurement}) \times 100.$$

Figure 5-11(b) shows the anomalies for temperature for Case 1 for the period January to mid February 2002. At the surface, the figure shows a mostly positive anomaly ranging between -20% and 20% for most of the simulation period.

At 10 m and 16 m from the surface, the figure shows highly variable anomalies, mostly ranging between -20% and 20%. When focussing on the lower frequency values, thus the event scale rather than the diurnal/inertial scale, there is very good agreement between the measured and modelled temperatures.

At the bottom, the figure shows relatively weak anomalies, ranging between -10% and 10% for most of March and April 2002.

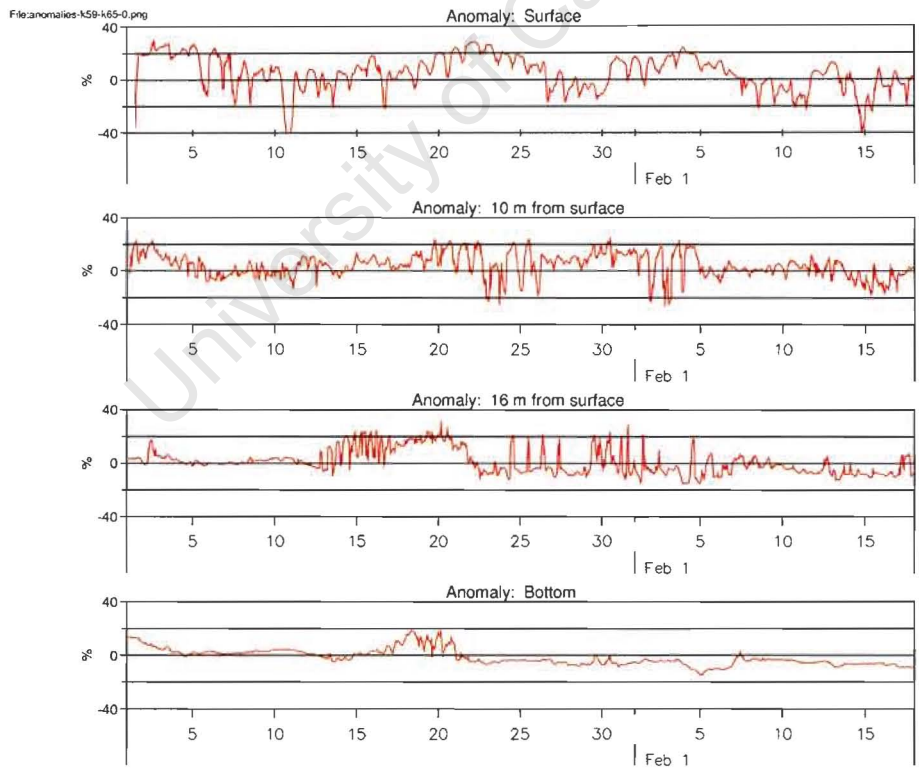

Figure 5-11(b) St Helena Bay model (St Helena Bay weather station winds): Anomalies for temperature for the period January to mid February 2002, at different depths. Here a positive anomaly indicates that the measured temperature was higher than the modelled temperature.

Overall, Figure 5-11(b) indicates that there is a relatively good concordance between measured and modelled temperatures in all the layers of the water column.

5.2 Results from Case 2

As described in Chapter 3.2.2, during this study, the measured St Helena Bay weather station winds (adjusted to 10 m above MSL) were applied, but this time the wind speeds were reduced by 30 %. This was done in order to apply a wind time series that were an approximate representation of the winds in the eastern part of St Helena Bay, as well as in the Lamberts Bay region.

During Case 1, strong anti-cyclonic inertial oscillations were present throughout the modelled period. Anti-cyclonic inertial oscillations were also present in Case 2, although the currents were generally weaker (due to the "low wind scenario" that was applied).

In the horizontal, Figure 5-12 illustrates the surface currents and temperature during a typical upwelling event (left), in this case on 24 January 2002, 14:00, and a subsequent wind relaxation event (right), on 30 January 2002, 02:00. During upwelling, relatively cold water (less than 16°C) has reached the surface around Cape Columbine and on the West Coast, especially in the region south of Elands Bay. At this stage, the currents were predominantly northward (0.3 m/s on average), but weaker in St Helena Bay. During the subsequent wind relaxation event, the surface water has warmed and the currents have significantly weakened (all currents are less than 0.1 m/s). Upwelling has completely subsided.

A comparison between Figure 5-2 and 5-12 shows that, during the upwelling events, the surface currents and the level of upwelling are significantly stronger when the measured St Helena Bay weather station winds are applied, as opposed to the reduced St Helena Bay winds. During relaxation, the currents are also stronger when the measured St Helena Bay weather station winds are applied.

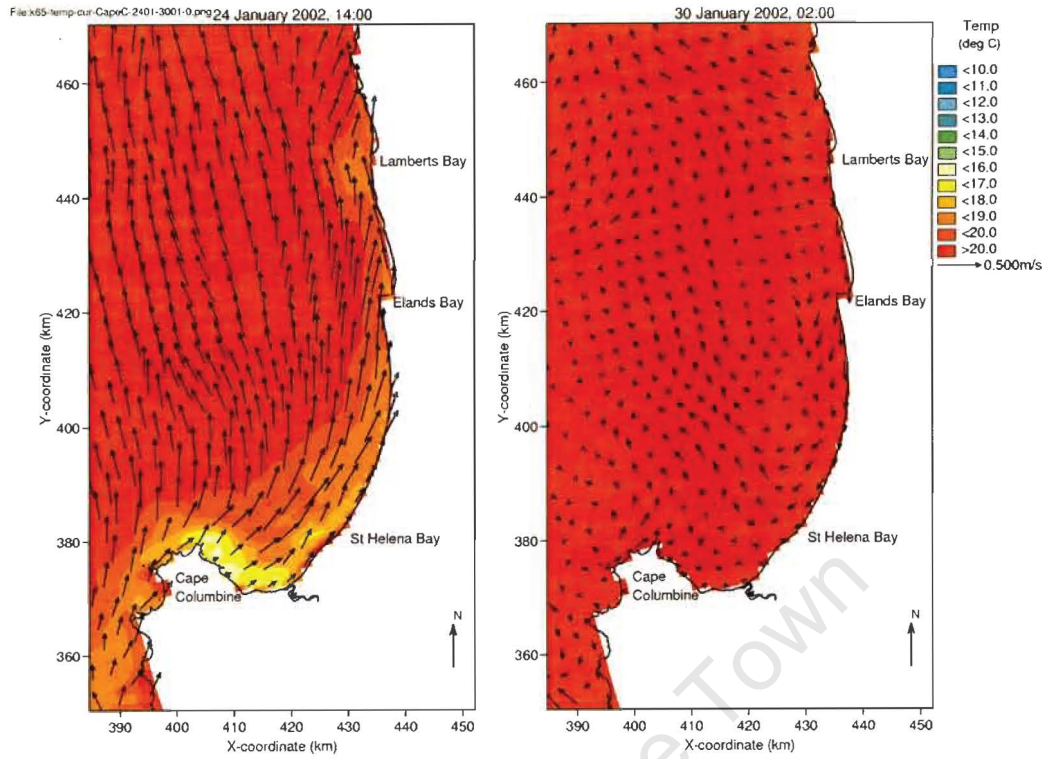

Figure 5-12 St Helena Bay model (St Helena Bay weather station winds, reduced by 30%): Surface currents and temperature during a typical upwelling event (left), in this case on 24 January 2002, 14:00, and a subsequent wind relaxation event (right), on 30 January 2002, 02:00. Note the upwelling of cold water around Cape Columbine and on the West Coast, especially in the region between Lamberts Bay and Elands Bay.

Case 2: January Event – Lamberts Bay Region

Figures 5-13(a) – (b) shows the surface currents (left), a vertical transect of temperature (top right) and a vertical cross-section of surface slope (bottom right) along a profile line, indicated on the left hand plot, for certain times during the upwelling-relaxation event from 19 - 30 January 2002. In these figures, the focus area is the region between Elands Bay and Lamberts Bay, to the north of St Helena Bay.

Figure 5-13(a) illustrates a time of upwelling (24 January 2002, 18:00), with equatorward currents being forced by the upwelling favourable wind conditions. These currents are relatively uniform and 0.3 m/s – 0.4 m/s on average. Cold water intrusion (water less than 17°C) into the surface waters at the coast can be seen from the cross shore temperature transect. The water level has dropped by approximately 3 cm at the coast. Upwelling continued until the end of 25 January 2002.

Two days later, on 27 January 2002, 14:00 (Figure 5-13(b)), during the subsequent wind relaxation event, the current speeds have dropped. The surface waters have warmed to greater than 20°C and the surface slope is relatively horizontal, and at 3 cm below MSL. A narrow poleward current of approximately 0.75 km wide and with a speed of 0.2 m/s can be seen from north of Lamberts Bay to south of Elands Bay, protruding into St Helena Bay. This poleward current persisted until the next upwelling event started on 30 January.

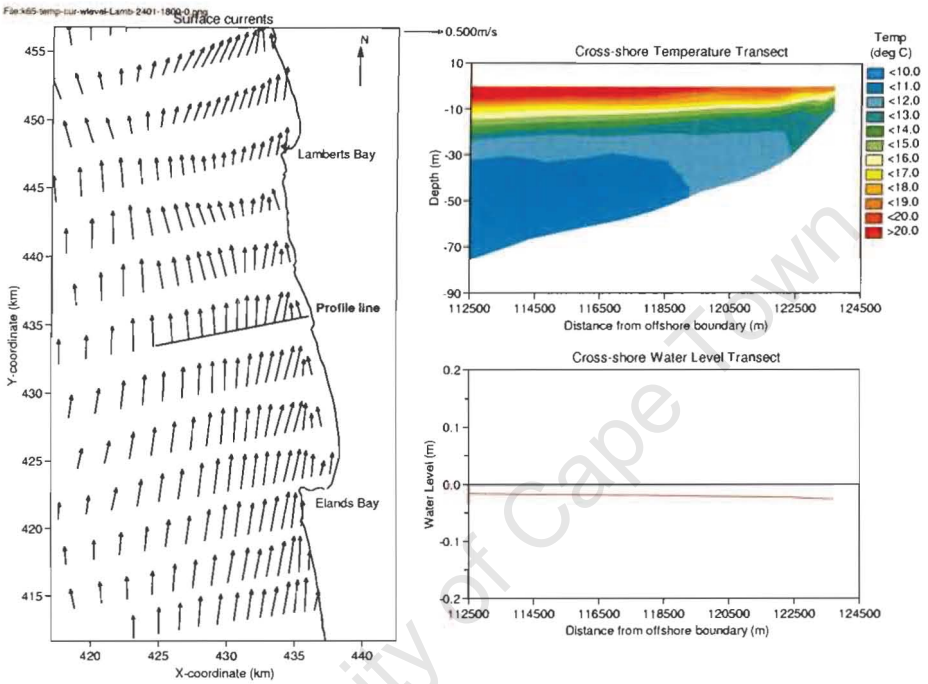

Figure 5-13(a) St Helena Bay model (St Helena Bay weather station winds, reduced by 30%) – Lamberts Bay region: Surface currents (left), vertical cross-section of temperature (top right) and vertical cross-section of surface slope (bottom right) along a profile line on 24 January 2002, 18:00 (a time of upwelling).

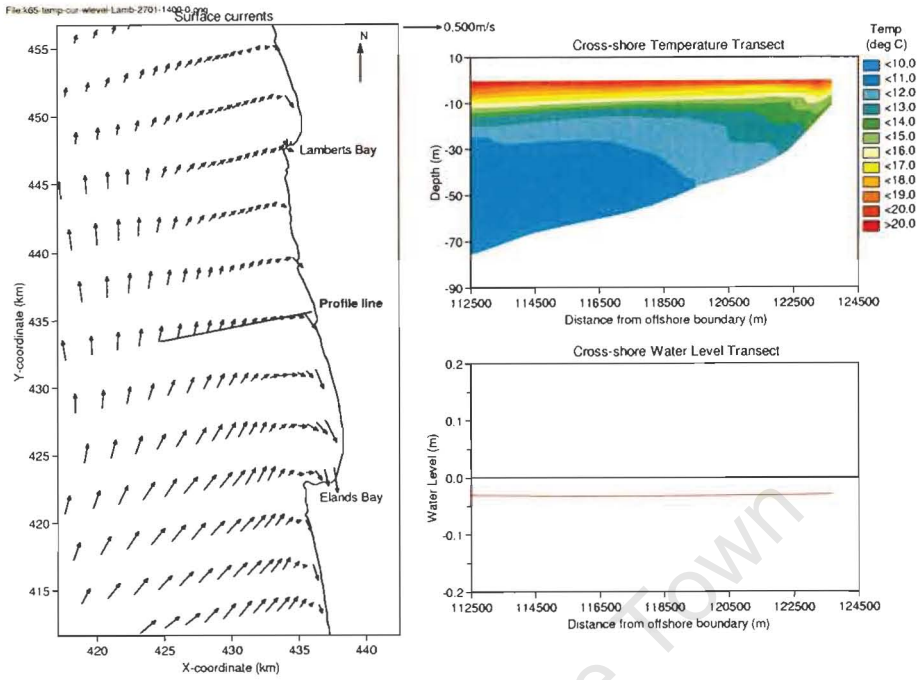

Figure 5-13(b) St Helena Bay model (St Helena Bay weather station winds, reduced by 30%) – Lamberts Bay region: Surface currents (left), vertical cross-section of temperature (top right) and vertical cross-section of surface slope (bottom right) along a profile line on 27 January 2002, 14:00 (a time of wind relaxation).

Figures 5-13(a)-(b) shows that the surface slope has greatly flattened out during each wind relaxation event, although it has not returned to its original zero position. A close up view of the surface slope at the same cross-section as shown in the above figures, from the coast up to approximately 1.7 km offshore, can be seen in Figure 5-14. This figure shows considerably more detail of the surface slopes at the same instances in time as shown in the above sequence of figures. The exact times are indicated on the figure.

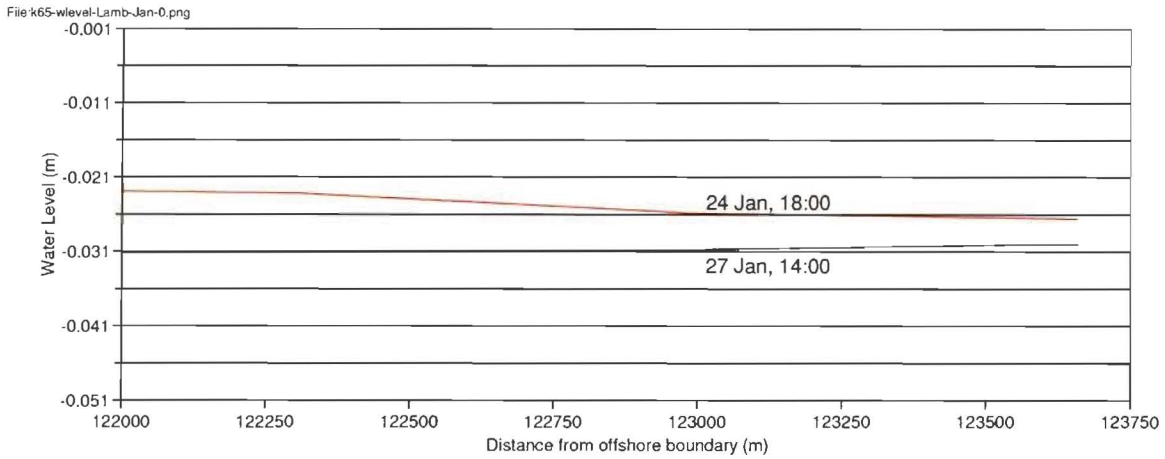

Figure 5-14 St Helena Bay model (St Helena Bay weather station winds, reduced by 30%) – Lamberts Bay region: Comparison between surface slopes (from the coast to 1.7 km offshore) for the January event. The time at which each surface slope is plotted, is indicated on the figure.

The surface changed from downward sloping during upwelling (24 January) to slightly upward sloping close to the coast (27 January) during wind relaxation. This upward sloping part of the surface was visible over a cross-sectional width of approximately 0.75 km.

Case 2: January Event – Eastern part of St Helena Bay

Figures 5-15(a) – (c) shows the surface currents (left), a vertical transect of temperature (top right) and a vertical cross-section of surface slope (bottom right) along a profile line, indicated on the left hand plot, for certain times during the upwelling-relaxation event from 24 – 30 January 2002. In this case, the focus area is on the eastern part of St Helena Bay.

Figure 5-15(a) illustrates a time of upwelling (24 January 2002, 16:00), with equatorward currents being forced by the upwelling favourable wind conditions. On average, these currents are 0.3 m/s - 0.4 m/s strong and weaker at the coast. Cold water intrusion (water less than 16°C) into the surface waters at the coast can be seen from the cross shore temperature transect. The water level has dropped by approximately 3 cm at the coast. Upwelling continued until the end of 25 January 2002.

On 28 January 2002, 12:00 (Figure 5-15(b)), during the subsequent wind relaxation event, the wind speed has dropped and the warm surface waters have returned to the coast. Close to the coast, the surface waters are now between 19°C and 20°C. The current speeds have dropped, and the surface slope at the coast is almost horizontal, and at 3 cm below MSL. From Elands Bay to south of the profile line, a narrow poleward current of width 1.5 km and average speed of 0.2 m/s, is visible. In the south of the Bay, cyclonic motion can be seen.

This poleward current continued to strengthen and widen, until it reached its peak on 29 January 2002, 10:00 (Figure 5-15(c)). At this stage, the poleward current was approximately 2 km wide and 0.2 m/s – 0.3 m/s in strength. The surface waters have warmed to greater than 20°C. In the south of the Bay, cyclonic motion can still be seen.

This current disappeared soon hereafter, once the next upwelling event started.

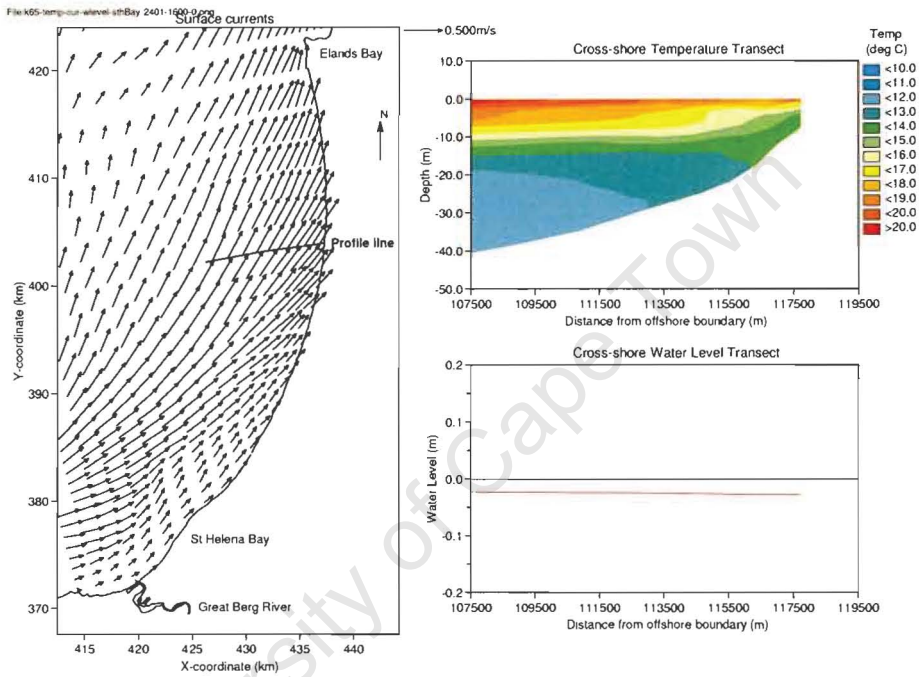

Figure 5-15(a) St Helena Bay model (St Helena Bay weather station winds, reduced by 30%) – Eastern part of St Helena Bay: Surface currents (left), vertical cross-section of temperature (top right) and vertical cross-section of surface slope (bottom right) along a profile line on 24 January 2002, 16:00 (a time of upwelling).

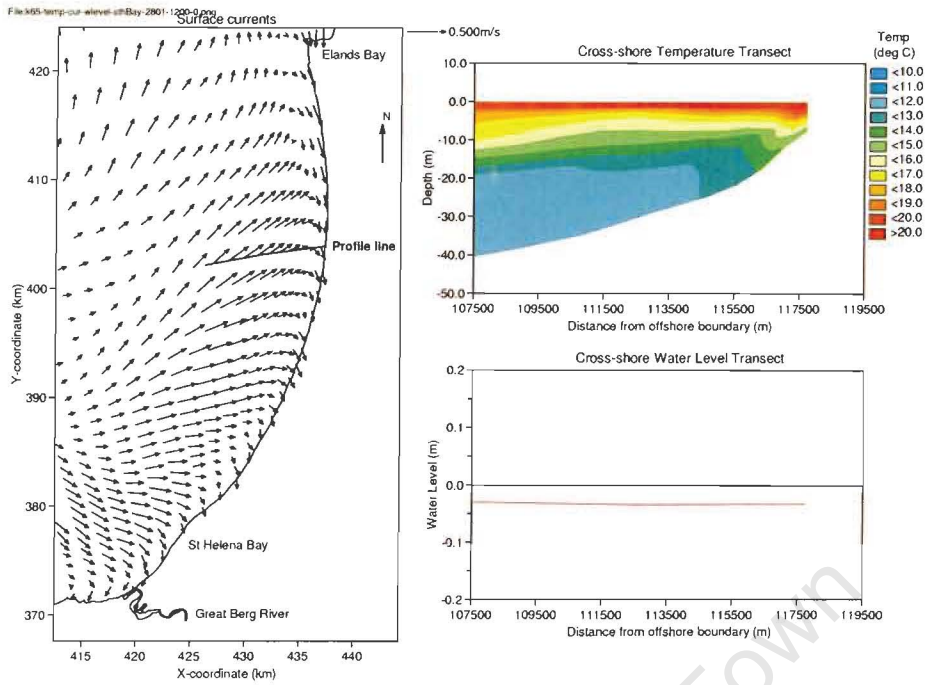

Figure 5-15(b) St Helena Bay model (St Helena Bay weather station winds, reduced by 30%) – Eastern part of St Helena Bay: Surface currents (left), vertical cross-section of temperature (top right) and vertical cross-section of surface slope (bottom right) along a profile line on 28 January 2002, 12:00 (a time of wind relaxation).

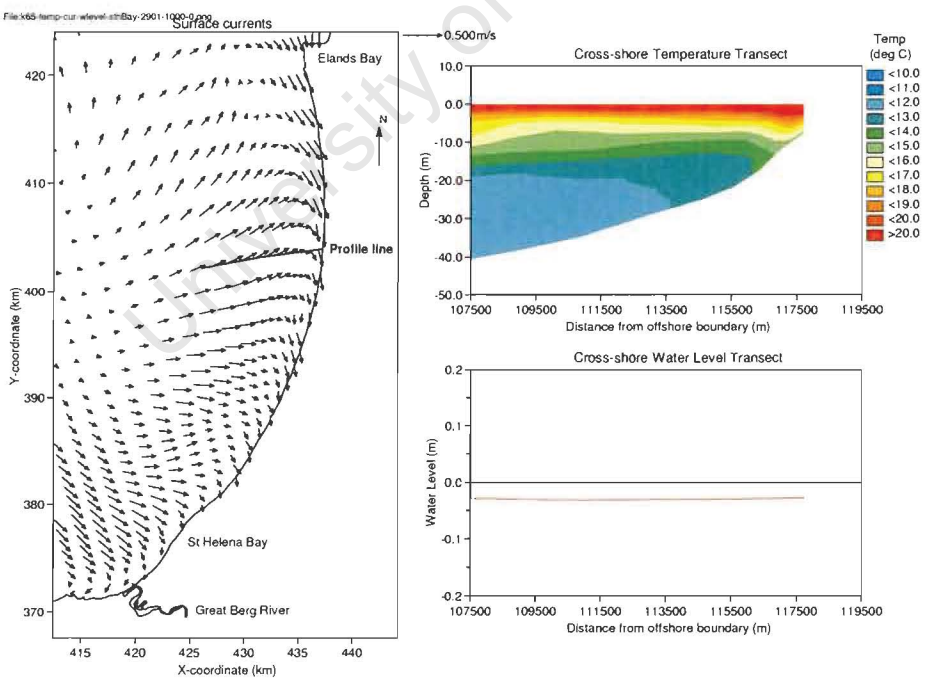

Figure 5-15(c) St Helena Bay model (St Helena Bay weather station winds, reduced by 30%) – Eastern part of St Helena Bay: Surface currents (left), vertical cross-section of temperature (top right) and vertical cross-section of surface slope (bottom right) along a profile line on 29 January 2002, 10:00 (a time of wind relaxation).

Figures 5-15(a)-(d) showed that the surface slope has greatly flattened out during each wind relaxation event, although it has not returned to its original zero position. A close up view of the surface slope at the same cross-section as shown in the above figures, from the coast up to approximately 1.7 km offshore, can be seen in Figure 5-16. This figure shows considerably more detail of the surface slopes at the same instances in time as shown in the above sequence of figures. The exact times are indicated on the figure.

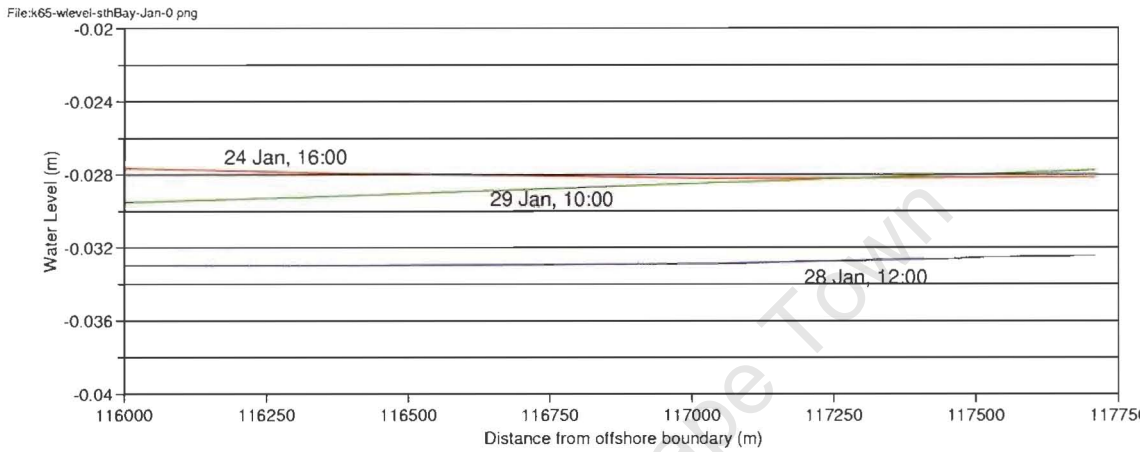

Figure 5-16 St Helena Bay model (St Helena Bay weather station winds, reduced by 30%) – Eastern part of St Helena Bay: Comparison between surface slopes (from the coast to 1.7 km offshore) for the January event. The time at which each surface slope is plotted, is indicated on the figure.

During wind relaxation, the surface became upward sloping at the coast (27 January). This upward sloping part of the surface slope gradually increased in gradient and width while the relaxation event persisted (29 January).

Case 2: February Event – Lamberts Bay Region

Figures 5-17(a) – (b) shows the surface currents (left), a vertical transect of temperature (top right) and a vertical cross-section of surface slope (bottom right) along a profile line, indicated on the left hand plot, for certain times during the upwelling-relaxation event from 1 – 11 February 2002. In these figures, the focus area is the region between Elands Bay and Lamberts Bay, to the north of St Helena Bay.

Figure 5-17(a) illustrates a time of upwelling (6 February 2002, 14:00), with equatorward currents being forced by the upwelling favourable wind conditions. These currents vary in strength (between 0.2 m/s and 0.5 m/s). Cold water intrusion (water less than 14°C) into the surface waters at the coast can be seen from the cross shore temperature transect. The water level has dropped by approximately 6 cm at the coast. Upwelling continued until 9 February 2002.

Following this lengthy upwelling event (from 1 – 9 February), the wind speed dropped for two days. This wind relaxation period was relatively short (two days) and no poleward current was noted during this time. Another short (two day) upwelling event followed. During the subsequent wind relaxation event, on 14 February 2002, 14:00 (Figure 5-17(b)), the currents have reduced, and a poleward current has formed from north of Lamberts Bay all the way down into St Helena Bay. This current is 3 - 4 km wide and 0.4 m/s in strength. The surface water at the coast is now between 19°C and 20°C, and the water level is 4 cm below MSL.

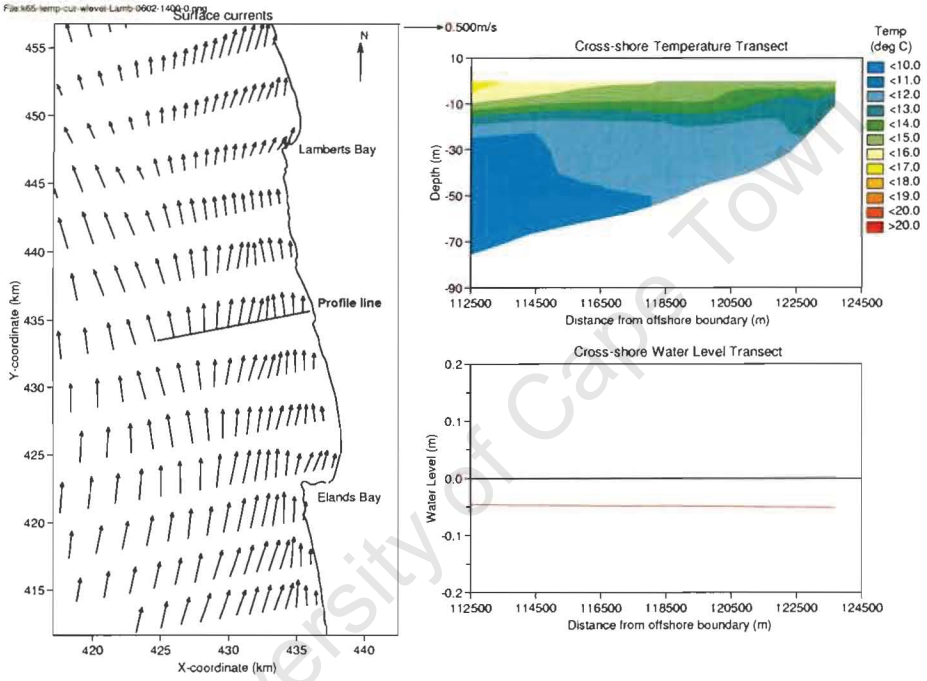

Figure 5-17(a) St Helena Bay model (St Helena Bay weather station winds, reduced by 30%) – Lamberts Bay region: Surface currents (left), vertical cross-section of temperature (top right) and vertical cross-section of surface slope (bottom right) along a profile line on 6 February 2002, 14:00 (a time of upwelling).

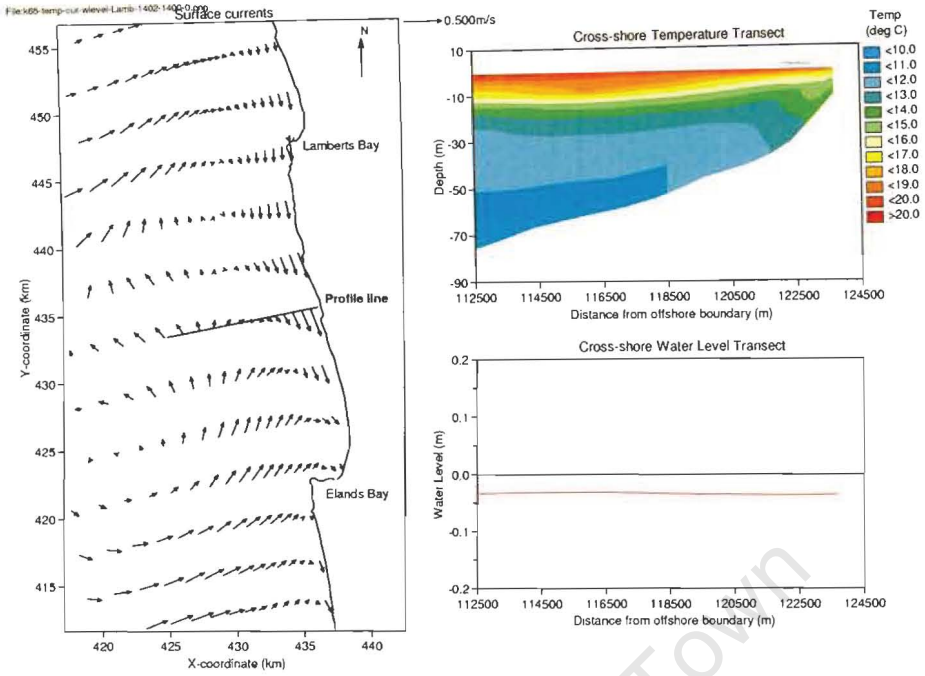

Figure 5-17(b) St Helena Bay model (St Helena Bay weather station winds, reduced by 30%) – Lamberts Bay region: Surface currents (left), vertical cross-section of temperature (top right) and vertical cross-section of surface slope (bottom right) along a profile line on 14 February 2002, 14:00 (a time of wind relaxation).

Figures 5-17(a)-(b) showed that the surface slope has greatly flattened out during each wind relaxation event, although it has not returned to its original zero position. A close up view of the surface slope at the same cross-section as shown in the above figures, from the coast up to approximately 1.7 km offshore, can be seen in Figure 5-18. This figure shows considerably more detail of the surface slopes at the same instances in time as shown in the above sequence of figures. The exact times are indicated on the figure.

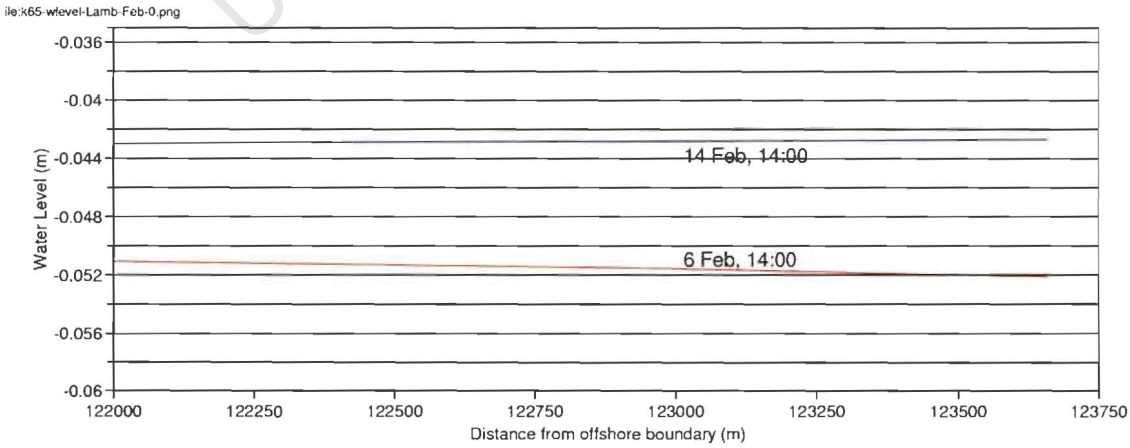

Figure 5-18 St Helena Bay model (St Helena Bay weather station winds, reduced by 30%) – Lamberts Bay region: Comparison between surface slopes (from the coast to 1.7 km offshore) for the February event. The time at which each surface slope is plotted, is indicated on the figure.

During upwelling (6 February), the surface was downward sloping towards the coast. On 14 February, during wind relaxation, the surface slope has become very slightly upward sloping over the whole cross-sectional area, thus over a band of width at least 1.7 km.

Case 2: February Event – Eastern part of St Helena Bay

Figures 5-19(a) – (b) shows the surface currents (left), a vertical transect of temperature (top right) and a vertical cross-section of surface slope (bottom right) along a profile line, indicated on the left hand plot, for certain times during the upwelling-relaxation event from 1 – 11 February 2002. In this case, the focus area is on the eastern part of St Helena Bay.

Figure 5-19(a) illustrates a time of upwelling (6 February 2002, 16:00), with equatorward currents being forced by the upwelling favourable wind conditions. These currents are relatively uniform and its strength ranges from 0.3 m/s to 0.4 m/s. Cold water intrusion (water less than 13°C) into the surface waters at the coast can be seen from the cross shore temperature transect. The water level has dropped by approximately 5 cm at the coast. Upwelling continued until 9 February 2002.

Following this lengthy upwelling event (from 1 – 9 February), the wind speed dropped for two days. This wind relaxation period was relatively short (two days) and no poleward current was noted during this time. Another short (two day) upwelling event followed. During the subsequent wind relaxation event, on 14 February 2002, 18:00 (Figure 5-19(b)), the wind speed has dropped and the warm surface waters have returned to the coast. Close to the coast, the surface waters are now greater than 20°C. The current speeds have dropped, and the water level is at 3 cm below MSL. Just south of Elands Bay a narrow poleward current can be seen, but the extent of this current is minimal (it barely reaches the profile line). This current is approximately 0.5 km wide and has a speed of 0.3 m/s.

In general, the modelled temperatures in St Helena Bay are too warm when the reduced St Helena Bay weather station winds were applied. Especially the surface temperatures do not agree well with the measurements.

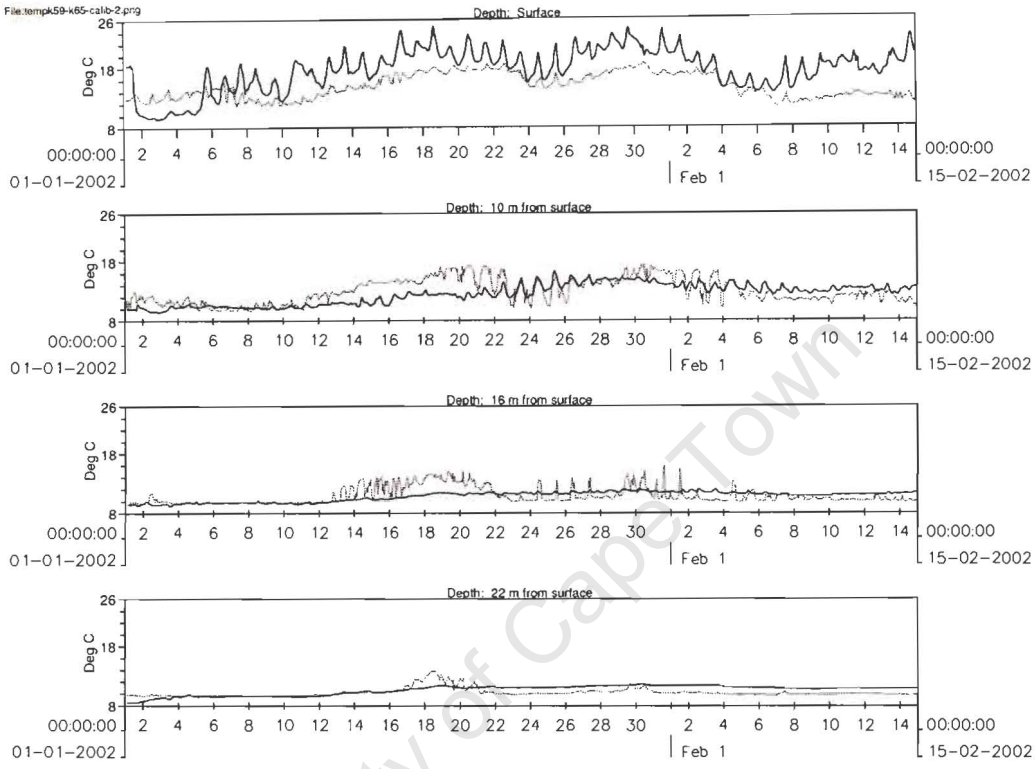

Figure 5-21(a) St Helena Bay model (St Helena Bay weather station winds, reduced by 30%): Comparison between measured (dotted) and modelled (solid) temperatures at different depths in the western part of St Helena Bay for January to mid February 2002.

Figure 5-21(b) shows the anomalies for temperature for Case 2 for the period January to mid February 2002. These anomalies were calculated by applying the following formula:

$$\text{Anomaly} = (\text{Measurement} - \text{Model})/(\text{Measurement}) \times 100.$$

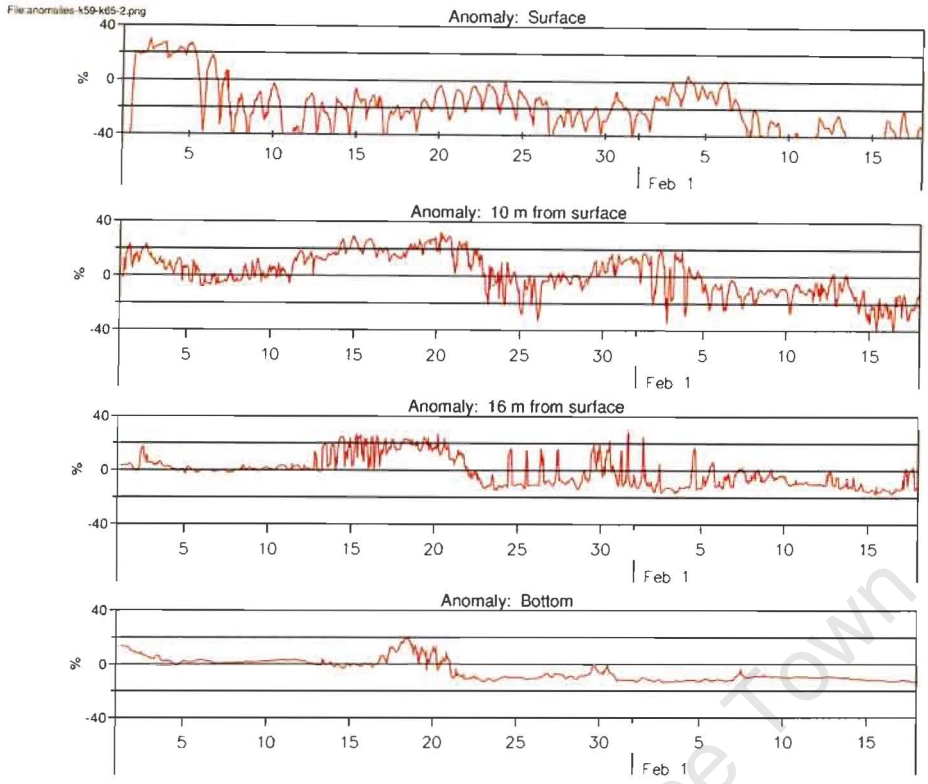

Figure 5-21(b) St Helena Bay model (St Helena Bay weather station winds, reduced by 30%): Anomalies for temperature for the period January to mid February 2002, at different depths. Here a positive anomaly indicates that the measured temperature was higher than the modelled temperature.

At the surface, the figure shows a mostly negative anomaly ranging between 0% and -40% for most of the simulation period. Towards mid February, the anomalies become increasingly negative, reaching values of approximately -60%.

At 10 m and 16 m from the surface, the figure shows highly variable anomalies, ranging between 20% and -20% for most of the simulation period.

At the bottom, the figure shows anomalies of between 0% and -20% for most of the simulation time.

Overall, Figure 5-21(b) indicates that there is a relatively good correlation between measured and modelled temperatures in all the layers of the water column, although it is not as good as what was seen during Case 1.

5.3 Results from Case 3

As described in Chapter 3.2.2, this study applied the smoothed St Helena Bay weather station winds (adjusted to 10 m above MSL).

As mentioned in Chapter 5.1, one of the features that was most prominent when the measured St Helena Bay weather station winds were applied, was the strong anti-cyclonic inertial oscillations that were present throughout the modelled period. Smoothing the winds out (and thus removing the seabreeze component of the wind) has led to a considerable dampening in the strength of the inertial currents. In fact, the inertial oscillations have almost disappeared.

In the horizontal, Figure 5-22 illustrates the surface currents and temperature during a typical upwelling event (left), in this case on 24 January 2002, 18:00, and a subsequent wind relaxation event (right), on 28 January 2002, 02:00. During upwelling, cold water (less than 13°C) has reached the surface around Cape Columbine, into St Helena Bay, as well as along the West Coast. The currents are weak (mostly less than 0.2 m/s). During wind relaxation, the currents have weakened and any sign of upwelling has disappeared.

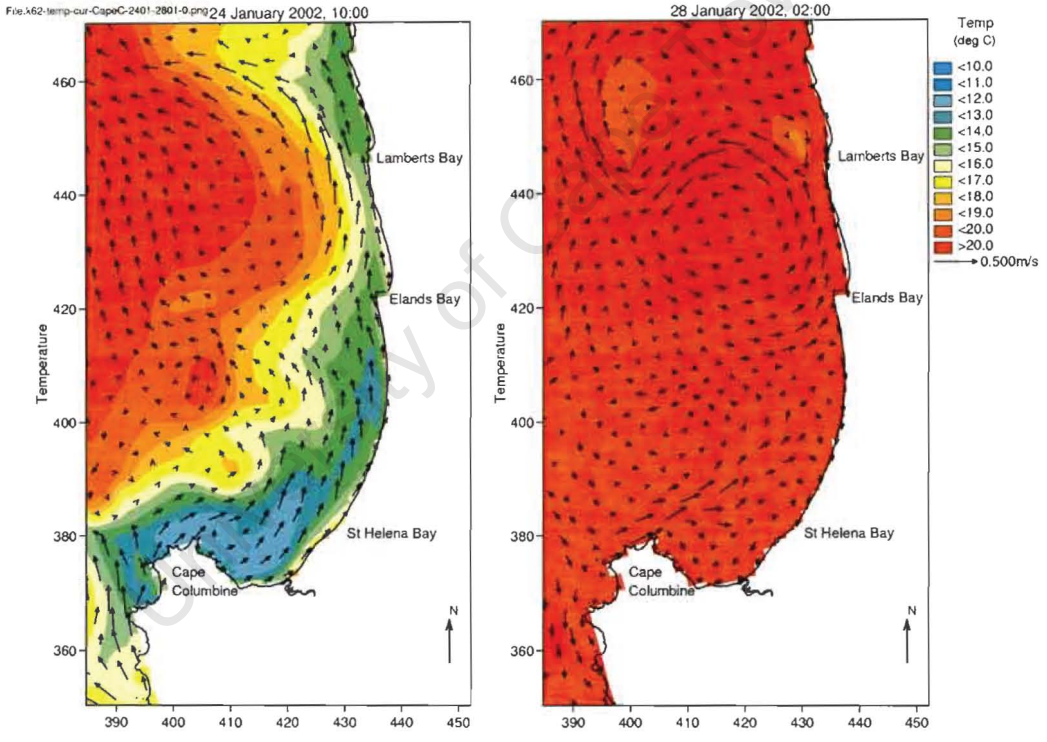

Figure 5-22 St Helena Bay model (smoothed St Helena Bay weather station winds): Surface currents and temperature during a typical upwelling event (left), in this case on 24 January 2002, 18:00, and a subsequent wind relaxation event (right), on 28 January 2002, 02:00. Note the upwelling of cold water around Cape Columbine into St Helena Bay, and along the West Coast.

Case 3: January Event – Lamberts Bay Region

Figures 5-23(a) – (b) shows the surface currents (left), a vertical transect of temperature (top right) and a vertical cross-section of surface slope (bottom right) along a profile line, indicated on the left hand plot, for certain times during the upwelling-relaxation event from 19 - 30 January 2002. In these figures, the focus area is the region between Elands Bay and Lamberts Bay, to the north of St Helena Bay.

Figure 5-23(a) illustrates a time of upwelling (23 January 2002, 08:00) nearshore currents are between 0.2 m/s and 0.5 m/s. Cold water intrusion (water less than 16°C) into the surface waters at the coast can be seen from the cross shore temperature transect. The water level has dropped by approximately 3 cm at the coast. Upwelling continued until the end of 25 January 2002.

On 29 January 2002, 12:00 (Figure 5-23(b)), during the subsequent wind relaxation event, the wind speed has dropped and the surface waters have warmed up to over 20°C at the coast. The surface is in the process of flattening out again. A nearshore poleward current can be seen all along the coastline in the region of focus, all the way south into St Helena Bay. This current has a speed of approximately 0.3 m/s and is approximately 0.75 km wide. The poleward current persisted disappeared when the next upwelling event started.

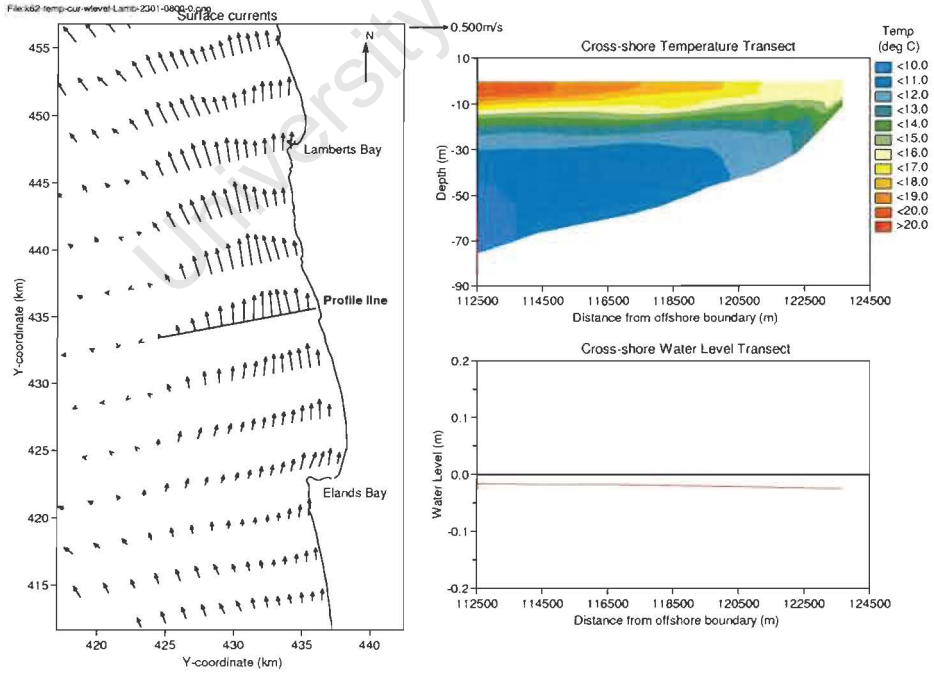

Figure 5-23(a) St Helena Bay model (smoothed St Helena Bay weather station winds) – Lamberts Bay region: Surface currents (left), vertical cross-section of temperature (top right) and vertical cross-section of surface slope (bottom right) along a profile line on 23 January 2002, 08:00 (a time of upwelling).

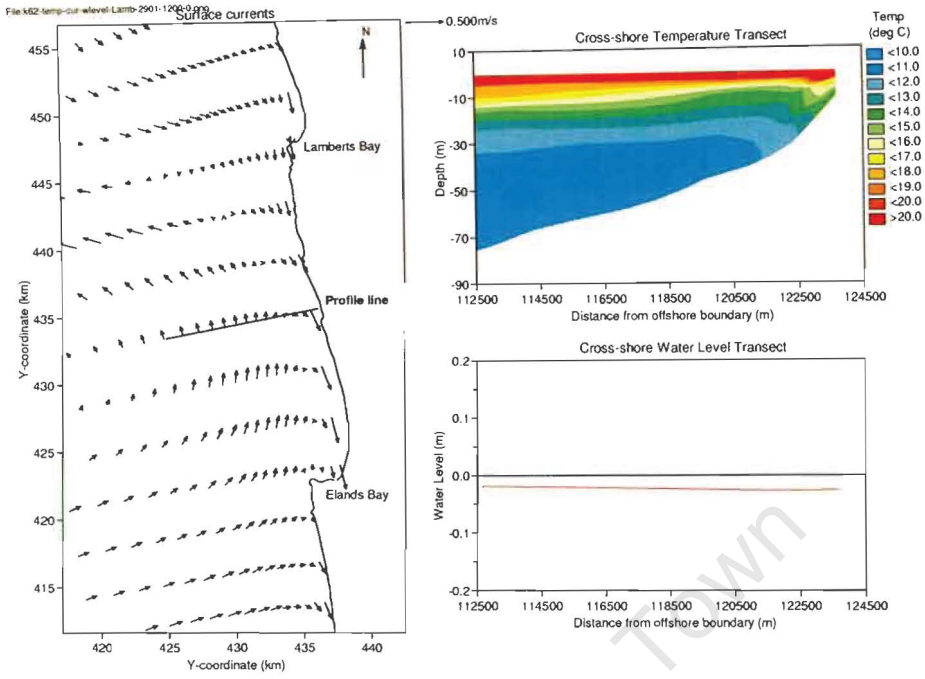

Figure 5-23(b) St Helena Bay model (smoothed St Helena Bay weather station winds) – Lamberts Bay region: Surface currents (left), vertical cross-section of temperature (top right) and vertical cross-section of surface slope (bottom right) along a profile line on 29 January 2002, 12:00 (a time of wind relaxation).

Figures 5-23(a)-(b) showed that the surface slope has greatly flattened out during each wind relaxation event, although it has not returned to its original zero position. A close up view of the surface slope at the same cross-section as shown in the above figures, from the coast up to approximately 1.7 km offshore, can be seen in Figure 5-24. This figure shows considerably more detail of the surface slopes at the same instances in time as shown in the above sequence of figures. The exact times are indicated on the figure.

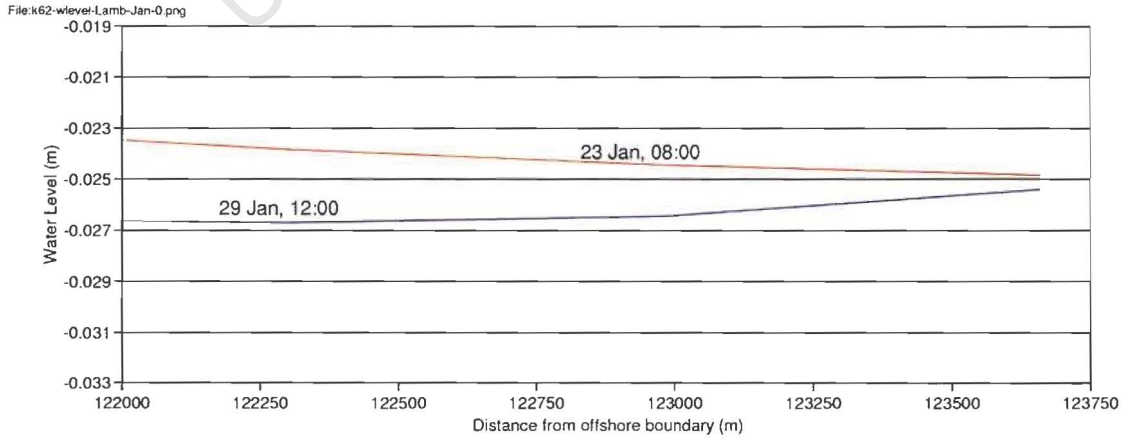

Figure 5-24 St Helena Bay model (smoothed St Helena Bay weather station winds) – Lamberts Bay region: Comparison between surface slopes (from the coast to 1.7 km offshore) for the January event. The time at which each surface slope is plotted, is indicated on the figure.

Immediately apparent is that, during wind relaxation, the surface gradually changed from downward sloping to upward sloping. On 29 January, when the nearshore poleward surface current was at its strongest, the surface near the coast was upward sloping in a band of approximately 0.75 km wide.

Case 3: January Event – Eastern part of St Helena Bay

Figures 5-25(a) – (c) shows the surface currents (left), a vertical transect of temperature (top right) and a vertical cross-section of surface slope (bottom right) along a profile line, indicated on the left hand plot, for certain times during the upwelling-relaxation event from 24 – 30 January 2002. In this case, the focus area is on the eastern part of St Helena Bay.

Figure 5-25(a) illustrates a time of upwelling (24 January 2002, 00:00). The currents are relatively weak (less than 0.2 m/s on average). Cold water intrusion (water less than 15°C) into the surface waters at the coast can be seen from the cross shore temperature transect. The water level has dropped by approximately 4 cm at the coast. Upwelling continued until the end of 25 January 2002.

During the subsequent wind relaxation event, on 27 January 2002, 08:00 (Figure 5-25(b)), the wind speed has dropped and the surface waters have warmed to between 19°C and 20°C. Overall, the current speeds have dropped. The water level at the coast is 3 cm. A narrow poleward current can be seen along the coast, from Elands Bay to just south of the profile line. This current is approximately 1 km wide and has an average speed of 0.3 m/s. Also, relatively strong currents seem to come from the direction of Cape Columbine, moving eastward.

Two days later, on 29 January 06:00, Figure 5-25(c) shows that this nearshore poleward current has widened to approximately 2 km and has a speed of 0.3 m/s on average. The surface waters have warmed to greater than 20°C at the coast, and the surface slope has remained unchanged, at 3 cm below MSL.

The current only disappeared once the next upwelling event started.

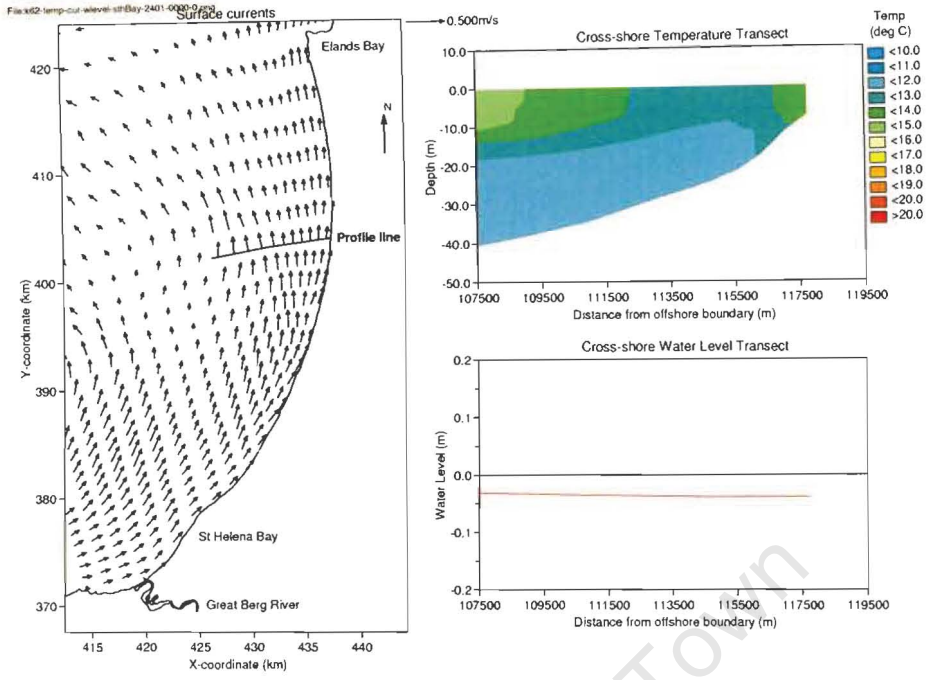

Figure 5-25(a) St Helena Bay model (smoothed St Helena Bay weather station winds) – Eastern part of St Helena Bay: Surface currents (left), vertical cross-section of temperature (top right) and vertical cross-section of surface slope (bottom right) along a profile line on 24 January 2002, 00:00 (a time of upwelling).

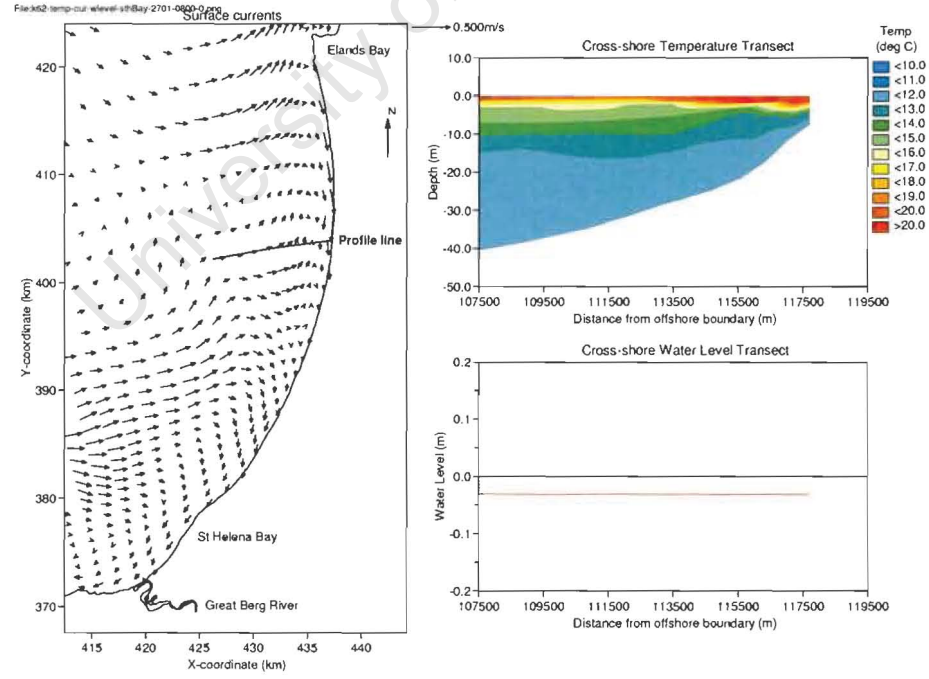

Figure 5-25(b) St Helena Bay model (smoothed St Helena Bay weather station winds) – Eastern part of St Helena Bay: Surface currents (left), vertical cross-section of temperature (top right) and vertical cross-section of surface slope (bottom right) along a profile line on 27 January 2002, 08:00 (during a wind relaxation event).

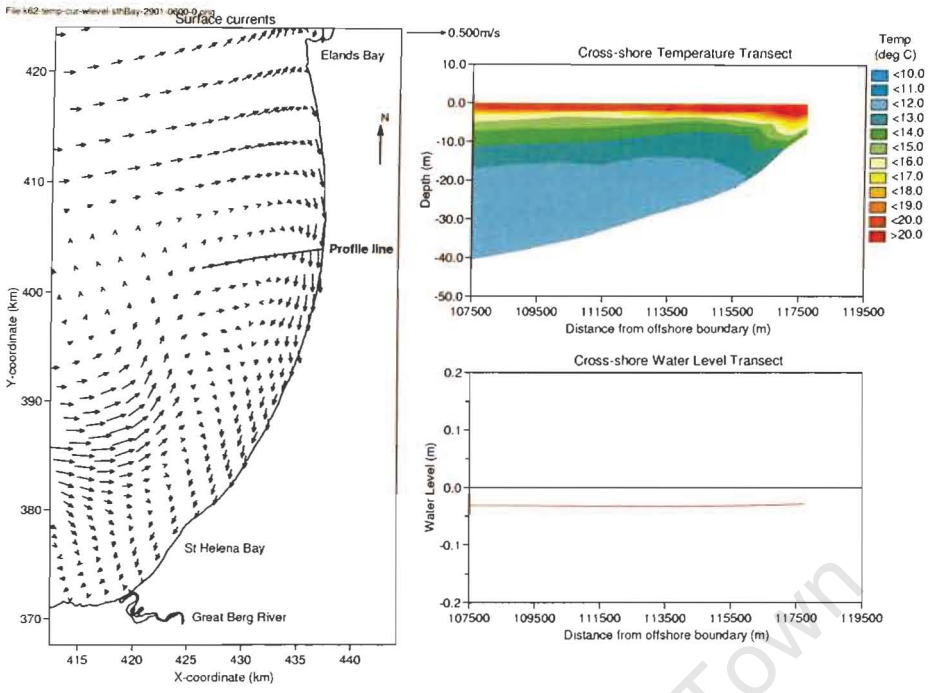

Figure 5-25(c) St Helena Bay model (smoothed St Helena Bay weather station winds) – Eastern part of St Helena Bay: Surface currents (left), vertical cross-section of temperature (top right) and vertical cross-section of surface slope (bottom right) along a profile line on 29 January 2002, 06:00 (a time of wind relaxation).

Figures 5-25(a)-(c) showed that the surface slope has greatly flattened out during each wind relaxation event, although it has not returned to its original zero position. A close up view of the surface slope at the same cross-section as shown in the above figures, from the coast up to approximately 1.7 km offshore, can be seen in Figure 5-26. This figure shows considerably more detail of the surface slopes at the same instances in time as shown in the above sequence of figures. The exact times are indicated on the figure.

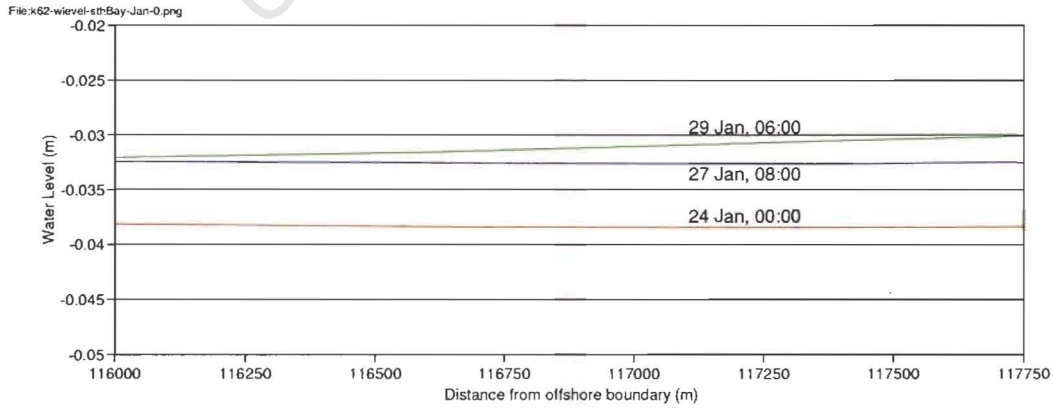

Figure 5-26 St Helena Bay model (smoothed St Helena Bay weather station winds) – Eastern part of St Helena Bay: Comparison between surface slopes (from the coast to 1.7 km offshore) for the January event. The time at which each surface slope is plotted, is indicated on the figure.

During the upwelling event, on 24 January, the surface slope was relatively flat (but slightly downward sloping). During wind relaxation, the surface slopes gradually started to flatten out, and then changed from downward sloping to upward sloping. On 29 January, the time when the poleward current was at its widest, the surface slope was upwards towards the coast over the whole width of this cross-section (thus in a band of at least 1.7 km wide).

Case 3: February Event – Lamberts Bay Region

Figures 5-27(a) – (b) shows the surface currents (left), a vertical transect of temperature (top right) and a vertical cross-section of surface slope (bottom right) along a profile line, indicated on the left hand plot, for certain times during the upwelling-relaxation event from 1 – 11 February 2002. In these figures, the focus area is the region between Elands Bay and Lamberts Bay, to the north of St Helena Bay.

Figure 5-27(a) illustrates a time of upwelling (6 February 2002, 16:00). These currents have average speeds of 0.3 m/s – 0.4 m/s. Cold water intrusion (water less than 15°C) into the surface waters at the coast can be seen from the cross shore temperature transect. The water level has dropped by approximately 8 cm at the coast. Upwelling continued until 9 February 2002.

Following this lengthy upwelling event (from 1 – 9 February), the wind speed dropped for two days. On 10 February 2002, 22:00, a weak poleward current of 0.5 km wide and 0.1 m/s – 0.2 m/s strong has formed from Lamberts Bay to south of the profile line (Figure 5-27(b)). The surface waters at the profile line have warmed to between 19°C and 20°C and the water level has flattened out to 5 cm below MSL. Soon thereafter, though, another short (two day) upwelling event took place, which made the (weak) poleward current disappear. This short upwelling event was followed by another short (two day) period of wind relaxation. No poleward current was noted again during the rest of the modelling period for this case.

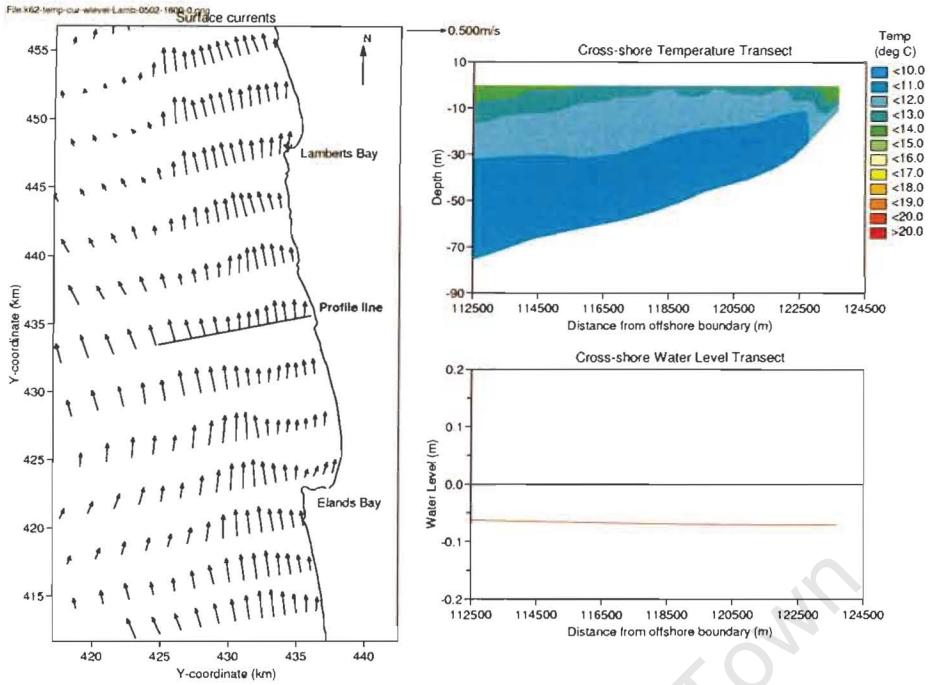

Figure 5-27(a) St Helena Bay model (smoothed St Helena Bay weather station winds) – Lamberts Bay region: Surface currents (left), vertical cross-section of temperature (top right) and vertical cross-section of surface slope (bottom right) along a profile line on 6 February 2002, 16:00 (a time of upwelling).

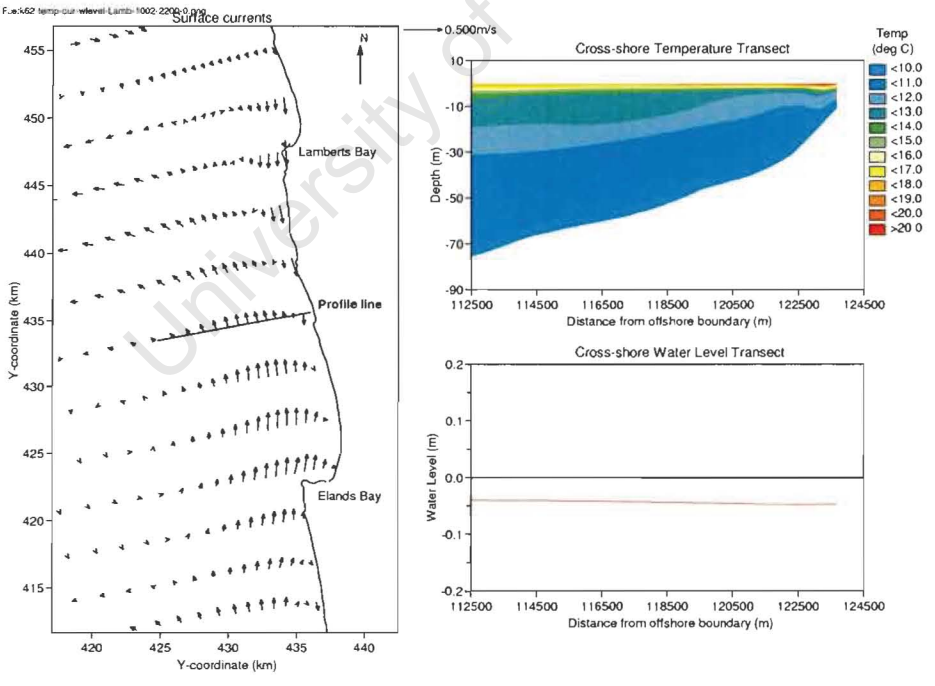

Figure 5-27(b) St Helena Bay model (smoothed St Helena Bay weather station winds) – Lamberts Bay region: Surface currents (left), vertical cross-section of temperature (top right) and vertical cross-section of surface slope (bottom right) along a profile line on 10 February 2002, 22:00 (a time of wind relaxation).

Figures 5-27(a)-(b) showed that the surface slope has greatly flattened out during each wind relaxation event, although it has not returned to its original zero position. A close up view of the surface slope at the same cross-section as shown in the above figures, from the coast up to approximately 1.7 km offshore, can be seen in Figure 5-28. This figure shows considerably more detail of the surface slopes at the same instances in time as shown in the above sequence of figures. The exact times are indicated on the figure.

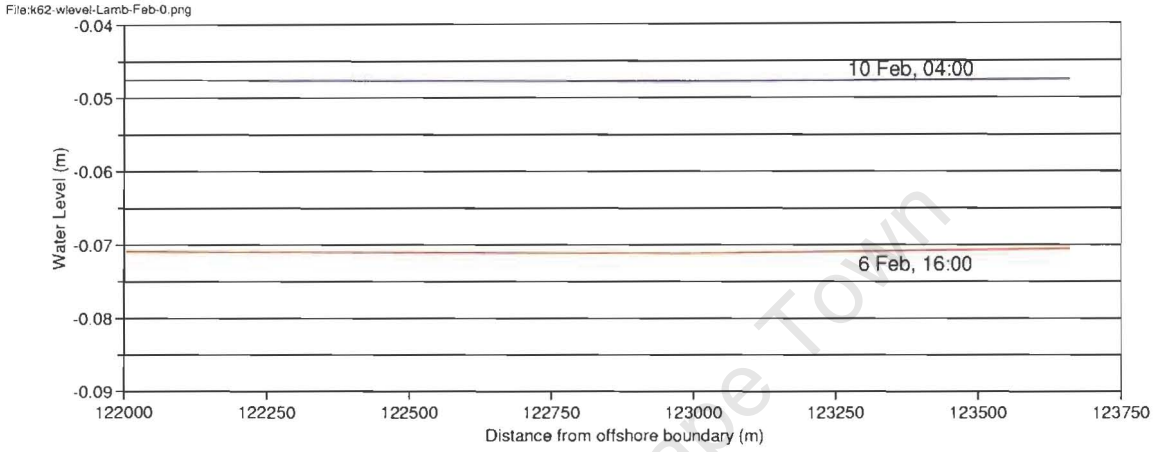

Figure 5-28 St Helena Bay model (smoothed St Helena Bay weather station winds) – Lamberts Bay region: Comparison between surface slopes (from the coast to 1.7 km offshore) for the February event. The time at which each surface slope is plotted, is indicated on the figure.

The surface was fairly flat and even slightly upward sloping very close to the coast during the time of upwelling. During the wind relaxation period, the surface was slightly upward sloping towards the coast in a band of width approximately 0.5 km.

Case 3: February Event – Eastern part of St Helena Bay

Figures 5-29(a) – (b) shows the surface currents (left), a vertical transect of temperature (top right) and a vertical cross-section of surface slope (bottom right) along a profile line, indicated on the left hand plot, for certain times during the upwelling-relaxation event from 1 – 11 February 2002. In this case, the focus area is on the eastern part of St Helena Bay.

Figure 5-29(a) illustrates a time of upwelling (6 February 2002, 12:00), with equatorward currents (generally between 0.2 m/s and 0.4 m/s) being forced by the upwelling favourable wind conditions. Cold water intrusion (water less than 13°C) into the surface waters at the coast can be seen from the cross shore temperature transect. The water level has dropped by approximately 9 cm at the coast. Upwelling continued until 9 February.

On 10 February 2002, 12:00 (Figure 5-29(b)), during the subsequent wind relaxation event, the wind speed has dropped and the surface waters close to the coast have warmed to between 19°C and 20°C. Overall, the current speeds have dropped significantly. The water level at the coast is 5 cm below MSL. A small region of poleward flow is visible north of the profile line (it does not reach the profile line). In the south of the Bay, cyclonic motion can be seen. No development of a nearshore poleward flow was seen for the rest of the modelling period for this study.

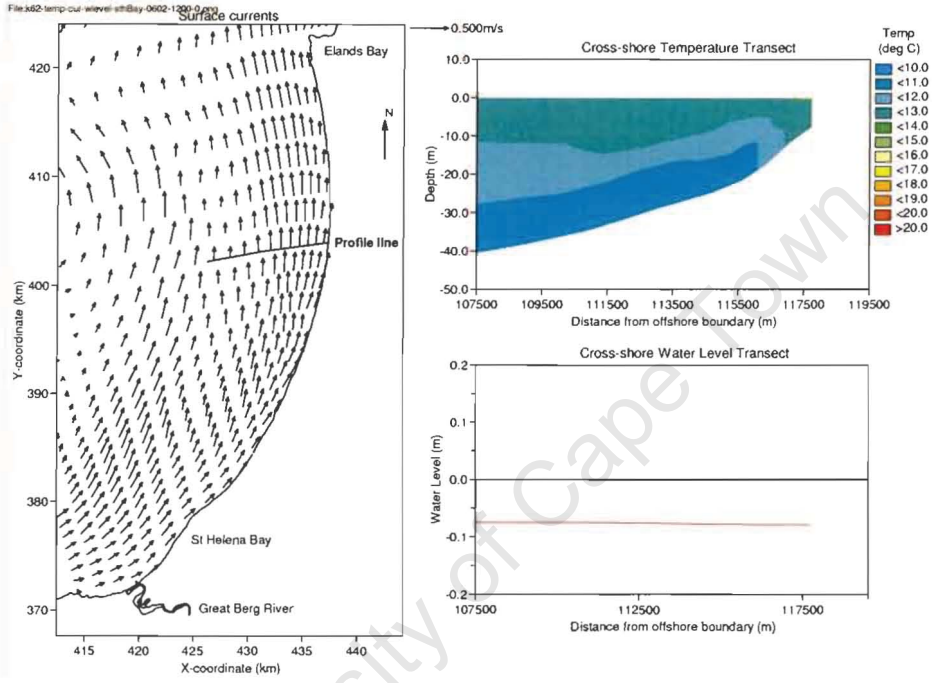

Figure 5-29(a) St Helena Bay model (smoothed St Helena Bay weather station winds) – Eastern part of St Helena Bay: Surface currents (left), vertical cross-section of temperature (top right) and vertical cross-section of surface slope (bottom right) along a profile line on 6 February 2002, 12:00 (a time of upwelling).

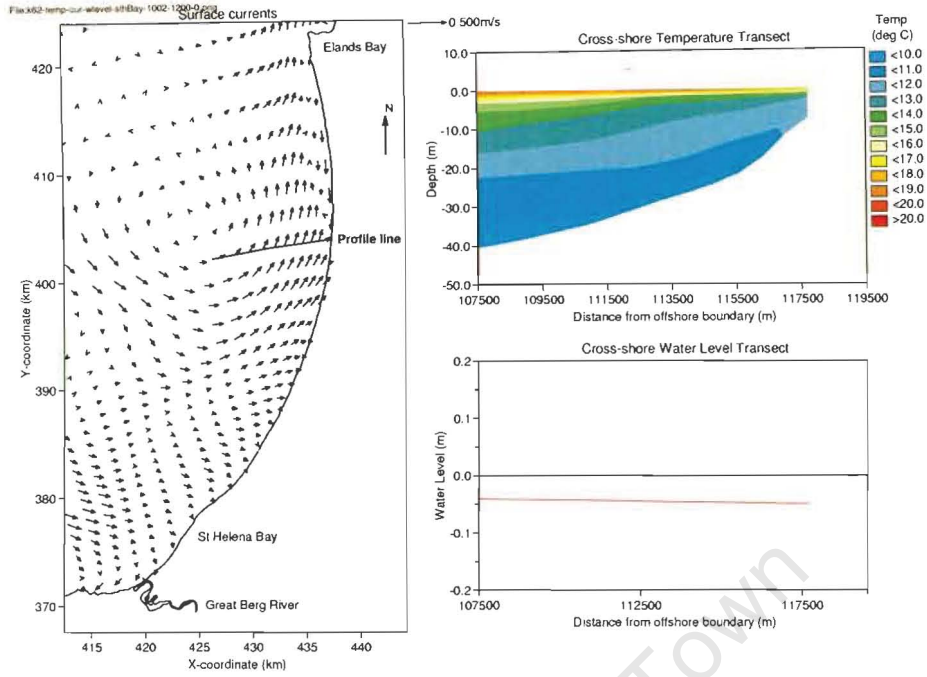

Figure 5-29(b) St Helena Bay model (smoothed St Helena Bay weather station winds) – Eastern part of St Helena Bay: Surface currents (left), vertical cross-section of temperature (top right) and vertical cross-section of surface slope (bottom right) along a profile line on 10 February 2002, 12:00 (a time of wind relaxation).

Figures 5-29(a)-(b) showed that the surface slope has greatly flattened out during each wind relaxation event, although it has not returned to its original zero position. A close up view of the surface slope at the same cross-section as shown in the above figures, from the coast up to approximately 1.7 km offshore, can be seen in Figure 5-30. This figure shows considerably more detail of the surface slopes at the same instances in time as shown in the above sequence of figures. The exact times are indicated on the figure.

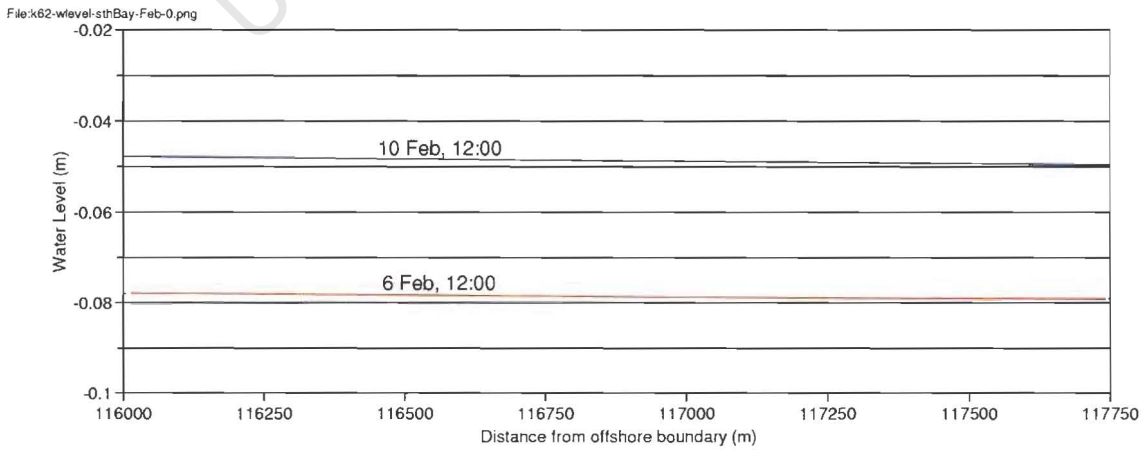

Figure 5-30 St Helena Bay model (smoothed St Helena Bay weather station winds) – Eastern part of St Helena Bay: Comparison between surface slopes (from the coast to 1.7 km offshore) for the February event. The time at which each surface slope is plotted, is indicated on the figure.

At both the above times, no poleward current was visible at the profile line, and the surface slope remained slightly downward sloping towards the coast.

Case 3: Western Part of St Helena Bay

For the western part of St Helena Bay, in the vertical, a comparison of the modelled and measured temperatures at the thermistor chain's location for January 2002 (Figure 2.1) for Case 3 is shown in Figure 5-31(a).

From this figure, it can be seen that the modelled surface waters are between 4°C - 10°C warmer than the measured temperatures. At 10 m and 16 m from the surface, the modelled temperatures seem to be colder than the measured temperatures for most of the simulation time. The modelled temperatures show almost no diurnal variability.

In general, the modelled temperatures in St Helena Bay are too warm when the smoothed St Helena Bay weather station winds are applied. Especially the surface temperatures do not agree well with the measurements.

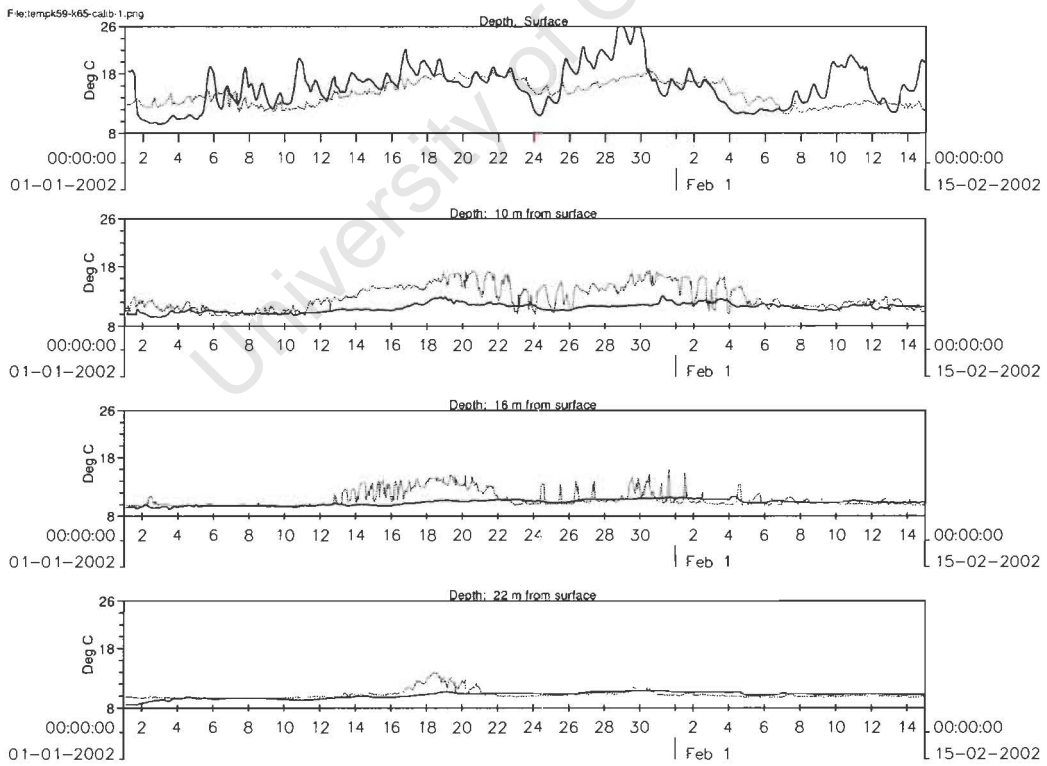

Figure 5-31(a) St Helena Bay model (smoothed St Helena Bay weather station winds): Comparison between measured (dotted) and modelled (solid) temperatures at different depths in the western part of St Helena Bay for January to mid February 2002.

Figure 5-31(b) shows the anomalies for temperature for Case 3 for the period January to mid February 2002. These anomalies were calculated by applying the following formula:

$$\text{Anomaly} = (\text{Measurement} - \text{Model})/(\text{Measurement}) \times 100.$$

At the surface, the figure shows anomalies ranging between 20% and -40% for most of the simulation period. At 10 m and 16 m from the surface, the figure shows highly variable anomalies, mostly ranging between 0% and 20% during the simulation period. At the bottom, the figure shows an anomaly that ranges between -10% and 10% for most of the simulation period.

Overall, Figure 5-31(b) indicates that there is a relatively good correlation between measured and modelled temperatures in all the layers of the water column, although it is not as well correlated as was seen in Case 1.

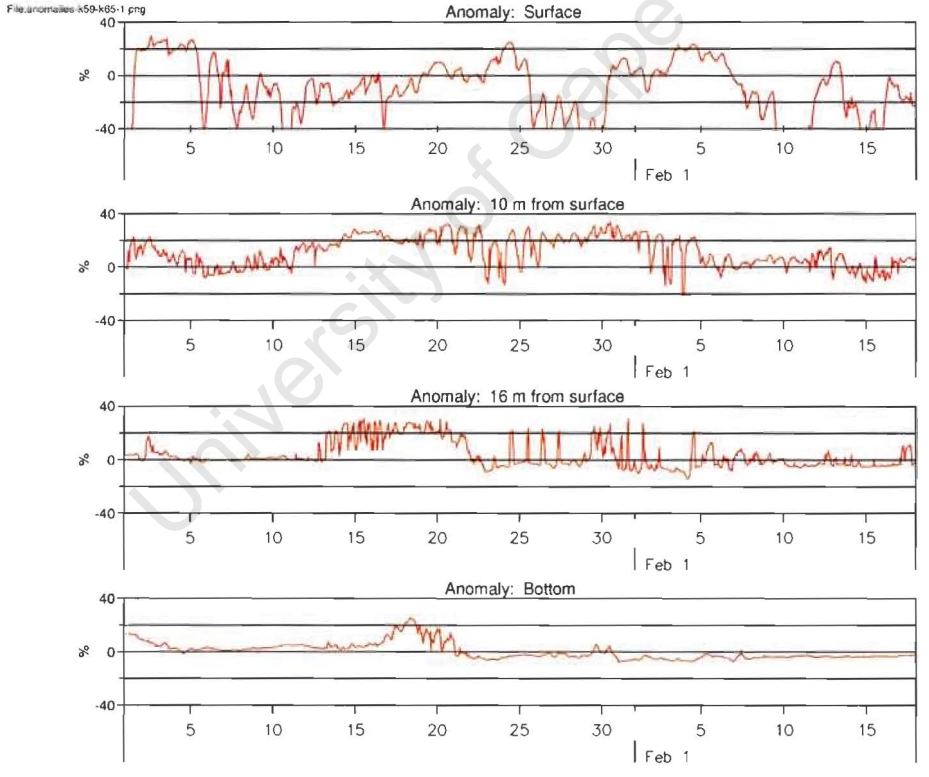

Figure 5-31(b) St Helena Bay model (smoothed St Helena Bay weather station winds): Anomalies for temperature for the period January to mid February 2002, at different depths. Here a positive anomaly indicates that the measured temperature was higher than the modelled temperature.

6. DISCUSSION

The objective of this thesis was to investigate the origin and dynamics of the nearshore, episodic poleward current as observed in the Southern Benguela. Thus far, the drivers and dynamics of this poleward current have not been clearly understood nor thoroughly investigated due to the complexity of the scales and processes. However, the importance of this current in transporting harmful algae from the north into St Helena Bay (Pitcher *et al*, 1998) and its role in habitat hypoxia (Monteiro *et al*, 2004) has emphasized the need to move from a conceptual model to a more quantitative numerical model that would reveal the underlying dynamics.

This thesis focussed on two key questions:

- What is the nature of the narrow coastal poleward flow?
- What processes govern its characteristics?

These questions were mainly explored using the Delft3D-FLOW numerical model forced by both idealised wind stress and a more realistic simulation. Before the numerical modelling experiments were undertaken, a suitable model (without stratification) was used to demonstrate by means of an analytical approach that the processes in the model were behaving in an appropriate way. This served as a validation of the input to the Reference Model.

Reference Model

- **What is the nature of the narrow coastal poleward flow?**

During an upwelling favourable wind, the development of alongshore geostrophic currents are evident in the Reference Model (see the results from Numerical Experiment 1, Chapter 4.2.1). The basic mechanism behind the formation of these geostrophic currents is as follows (Open University, 1989): An upwelling favourable (equatorward) wind gives rise to the offshore movement of surface waters. The drop in sea level at the coast sets up a cross shore horizontal pressure gradient, with a horizontal pressure gradient force acting in the direction of the coast. This horizontal pressure gradient force is balanced by the offshore Coriolis force in a steady state. An equilibrium situation is attained in the water column, which causes the water to flow equatorward (along the coast).

For a steady wind a steady state is reached when the balance of Coriolis and pressure gradient forces has been achieved. In such a state, the currents are uniformly equatorward and alongshore and do not change over time. During this steady state it is still possible an onshore flow of cold water in the sub-

thermocline, while an offshore flow of warm water occurs at the surface.

An important result from the Reference Model studies (see the results in Chapter 4) was that the *formation of a poleward current was always associated with a wind relaxation event.* This is in agreement with the observations and conceptual model of Pitcher & Boyd (1996), Pitcher *et* al (1998) and Probyn *et al* (2000).

When the wind forcing stopped during a wind relaxation event, the remaining cross shore forces no longer balanced the alongshore flow. The flow again became non-steady. Close to the coast, a barotropic adjustment took place in the cross shore surface slope. During this adjustment process, the nearshore surface slope flattened out and reversed, becoming upward sloping towards the coast. Such an adjustment in the surface slope always coincided with a subtle opposite adjustment in the subsurface isotherms. This weak baroclinic adjustment was apparent with upward sloping isotherms that flattened out or even reversed direction and became slightly downward sloping towards the coast (Figure 4-8 in Chapter 4.2.1 shows an example hereof).

A characteristic of a geostrophic adjustment is that it is often a local phenomenon instead of taking place over the whole domain. This is what was observed in the Reference Model experiments (Chapter 4). The above adjustment towards geostrophy was most apparent in the formation of a nearshore poleward current, driven by the horizontal pressure gradient force that was set up during this adjustment. A close up view of the surface slope from three studies undertaken in Numerical Experiment 2 was shown in Figure 4-15. Immediately apparent was that, for all three studies, the cross shore sea surface slope gradually changed from downward sloping to upward sloping towards the coast during wind relaxation. This spatial scale of change coincided with the width of the poleward current in each case. *It thus appeared that the upward sloping surface, which led to a cross shore horizontal pressure gradient force acting in an offshore direction, was the driving force of the poleward current, and that it could therefore be viewed as being 'driven from the surface'.*

It is clear that the presence of a poleward current is the result of a new balance of forces. The model results reflect the geostrophic adjustment process during relaxation of the wind forcing, and the consequent formation of the poleward current. This new balance of forces is evident in the steady state being reached by the poleward current (see the results from the Numerical Experiments in Chapter 4) as well as the steady state reached by the surface slope (see Figure 4-10 in Chapter 4.2.1).

- **What processes govern the poleward flow characteristics?**

One of the most important aims of the Reference Model was to determine what processes govern the characteristics of the nearshore poleward surface current. Several Numerical Experiments were undertaken, of which a summary was shown in Table 4-1. The influence of three processes on the formation of the nearshore poleward current were investigated in some detail namely, stratification, bottom topography and wind variability.

Stratification

When no stratification was present in the model (Numerical Experiment 1 in Chapter 4.2.1), no poleward flow developed during the wind relaxation period. All the currents reduced to almost zero when the wind stopped, but it never turned poleward. When stratification was present, however (Numerical Experiment 1 in Chapter 4.2.1), the development of a nearshore poleward current was noted during the wind relaxation phase (Figure 4-7). From the results obtained from Numerical Experiment 1 it was clear that *the presence of stratification is indeed essential in order for a poleward current to develop during wind relaxation.* This indicates that the vertical temperature field (and by implication the vertical density stratification) is important in the development of the poleward current.

This is a very significant result, as the nature of the poleward flow has previously been identified as being barotropic ('driven from the surface'). This indicates that there exists a relationship between the barotropic response and the density field, and that they have a combined role in leading to the formation of the poleward surface current. The reason stratification is important, probably relates to the nature of the poleward flow described previously. During the wind event, the balance of forces that was achieved when stratification was absent differed from the balance of forces that was achieved when stratification was present. During the absence of stratification, the surface slope simply adjusted and became horizontal when the wind forcing was removed, thus achieving a new balance. When stratification was present, however, the surface slope adjusted in conjunction with the temperature field, and the resulting new balance of forces contained a cross shore horizontal pressure gradient force acting in an offshore direction, leading to the formation of a poleward surface current. The exact nature of the relationship between the surface slope adjustment and the adjustment of the temperature field is unknown at present.

Bottom topography

In order to investigate whether the inner shelf slope (thus the bottom topography) had any influence on the formation and characteristics of a nearshore poleward current, Numerical Experiment 2 was

undertaken (Chapter 4.2.2). Three different inner shelf slopes were applied during this experiment (Figures 3-2(a) and (b)). It should be noted that the variation in the inner shelf slope was achieved by fixing the bottom topography at the offshore edge of the inner shelf, and then pivoting the inner shelf around that point, keeping the inner shelf width constant. By doing this, the minimum (bottom) depth at the coast changed with each slope (the minimum depth became shallower the steeper the slope was, and vice versa). This is recognized as a potential problem, because a change in minimum depth in a model could possibly change the dynamics at the coast. Another option was to fix the depth at the coast and then to pivot the inner shelf slope around that point. This would have led to a fixed minimum depth at the coast, but a variation in the width of the inner shelf, which in turn also could have had an influence on the dynamics. The different methods for achieving a variation in the bottom topography are a complex matter and a separate study will have to be conducted to test the influence of each method. Such a study, however, fell beyond the scope of this thesis.

During the wind event, when a steady state was reached, there was a distinct difference between the three studies concerning the level of cold water intrusion close to the coast. *The position of the temperature front was closer inshore the flatter the inner shelf slope was.* The flatter the slope, the more cold water moved in very close to the coast, reaching the surface and leading to a vertically mixed water column (see Figures 4-13(a), (b) and (c)). When the inner shelf slope is steep, cold water must push up the slope towards the coast, working against gravity. On the other hand, when the inner shelf slope is flat, cold water can easily push in towards the coast and then push upwards to replace the surface water divergence. Because the nearshore water column (vertically) is much deeper when the inner shelf slope is flat, there is more 'space' for upwelled water to move in and push up towards the surface, without pushing the temperature front too far offshore. However, when the inner shelf slope is steep, the nearshore water column is much shallower and any upwelled water will push the temperature front further offshore.

When studying the appearance of this current more closely during the subsequent wind relaxation event (Figures 4-14(a), (b) and (c)), it was clear from each study that the poleward current *did not form over the whole inner shelf region, but that it always formed inshore of the temperature front.* It was also clear that *the poleward current was narrower the flatter the inner shelf slope was.* Important to note, however, is that although the position of the nearshore poleward current was always in the region inshore of the front, its width did not necessarily extend over this whole region, but sometimes only over a part of it, right against the coast. This coincided with the region where the subsurface isotherms have reversed direction and have thus become downward sloping during wind relaxation (even though the slope was very subtle at times). Thus, the width of the poleward current was not solely determined by the width of the region where the water column has re-stratified, but by the region where the

isotherms have reversed (in other words, where the isotherms have become downward sloping towards the coast). As mentioned before, this reversal in isotherm slope happened in conjunction with an opposite adjustment in the surface slope, and therefore it can also be said that *the width of the poleward current is determined by the region where the geostrophic and baroclinic adjustment (due to the removal of the wind forcing) gives rise to a reversal in the surface slope as well as a (opposite) reversal in the isotherm slope.* This reversal in surface slope was indicated in Figure 4-15, which indicated (together with Figures 4-14(a), (b) and (c)) that the width of the poleward current agreed exactly with the width of the reversed (upward sloping) surface.

Furthermore, from Figure 4-12 it was evident that *the flatter the inner shelf slope was, the longer it took for the poleward current to start to develop and it also took slightly longer for the current to reach a steady state.* A possible reason for this observation could be that the inshore water column is colder and has a higher level of mixing (as mentioned before) the flatter the inner shelf slope is. This means that the isotherms will take longer to relax (or to become horizontal), in other words, it would take longer for the water column to re-stratify. In turn, the surface slope will also take longer to adjust, which leads to the poleward surface current taking longer to develop.

Also, for each study it could be seen from Figure 4-15 that the surface jet offshore of the poleward current was associated with the region where surface slope remained downward (and where the subsurface isotherms were upward sloping) towards the coast. The equatorward surface jet reduced in speed during wind relaxation, due to the fact that the subsurface isotherms, as well as the surface slope became flatter, and the horizontal pressure gradient force therefore reduced. The turning point from a downward (towards the coast) to an upward (towards the coast) surface slope appeared closer to the coast the flatter the inner shelf slope was. This was in agreement with the previous observation that the surface jet moved closer towards the coast the flatter the slope was. The same driving force was thus involved during the formation of the equatorward surface jet, but only in the opposite direction.

The area of very weak currents, at times observed in the region between the nearshore poleward surface current and the offshore surface jet, can be associated with relatively horizontal subsurface isotherms and a horizontal surface slope. In this situation, no horizontal pressure gradient force is present and there is no driving force that could cause a current.

It should also be noted that the steady state speed of the poleward current was faster (although at times only marginally) the flatter the inner shelf slope was. This agrees with the fact that the upward sloping surface was slightly steeper the flatter the inner shelf slope was. It follows that *the gradient of the upward sloping surface slope close to the coast determines the strength of the poleward current.* A

higher surface gradient leads to a stronger horizontal pressure gradient force (a barotropic feature), which in turn leads to a stronger poleward current.

Multiple Wind Events

Once more applying the Reference Model, Numerical Experiment 3 (Chapter 4.2.3) was undertaken to determine what happens to the poleward current when multiple wind events are simulated. As expected, each upwelling favourable wind event caused a drop in water level at the coast, as well as the intrusion of cold bottom water into the nearshore environment and upwards towards the surface. Keeping in mind that this study started with the isotherms being horizontal (flat), the first wind event had a significant effect on the adjustment of the isotherms, with the change being less dramatic during the subsequent wind events. Each successive wind event strengthened the upwelling (compare Figures 4-16(a), (b) and (c)) as the warm water was pushed further and further offshore.

During wind relaxation, the upwelled cold bottom waters remained fairly close inshore and did not relax all the way back to its original location in the deeper offshore waters. This is due to upwelling needing a much shorter time to develop than is needed to re-stratify the water column following an upwelling event. Upwelling is actively forced by the wind stress, whereas the relaxation of upwelling only takes place under internal gravitational forces.

From the above observations it was noted that a so-called "spin up wind event" might be necessary when studies are undertaken with the more complex St Helena Bay model. An upwelling favourable wind that blows for a few days at the beginning of each study will ensure the initial intrusion of the cold bottom waters into the inshore region. This will set up a suitable initial condition to ensure that the temperature in the study represents the natural conditions as closely as possible. It was decided to indeed include a spin up period in the St Helena Bay model, as will be discussed later.

It is important to note that, in previous numerical experiments where only one wind event was applied, the poleward current reached a steady state during relaxation following the wind event, indicating that a new balance of forces has been reached. The downward sloping subsurface isotherms and the upward surface slope reached a constant state. When multiple wind events were applied, the poleward current disappeared as soon as the next wind event started. It is concluded that, in the model, *an external force (like another wind event) is necessary to make the poleward current disappear once it has formed.* The appearance of another wind event upsets the balance of forces, which was achieved during the previous wind relaxation (as another force is added).

Some more interesting observations were made when comparing the behaviour of the nearshore surface currents with offshore surface currents, as well as offshore bottom currents. For this purpose, time series of current speed were investigated at three different locations (representing typical current behaviour) for Numerical Experiment 1 (Chapter 4.2.1). The time series were shown in Figure 4-11.

From this figure it was clear that, when the wind stopped, the reduction in current speeds occurred most rapidly at the nearshore location (the shallower region). As discussed before (and once again clear from this figure), this current eventually turned poleward. In the region of the surface jet, the currents started to reduce (gradually) once the wind relaxation event started, reaching a steady state after a few days, but it never turned poleward. The behaviour of the bottom currents, below the surface jet, should also be noted. The time series indicated that the region of the surface jet was eventually associated with a net poleward undercurrent. This undercurrent appeared a few days after the nearshore poleward current appeared. The same behaviour was noted for the other Numerical Experiments.

St Helena Bay numerical model

The setting up of the more complex St Helena Bay numerical model required several observational data sets for initialising the simulation. The wind forcing is pivotal in the development of upwelling events in the St Helena Bay region. Persistent southwesterly winds are upwelling favourable, while a reversal of the wind direction and lower wind speeds lead to relaxation conditions. Regarding the wind data, observations were available from two locations, namely the St Helena Bay weather station at Cape St Martin, as well as the Lamberts Bay – Nortier wind station at Lamberts Bay (the positions of the wind stations were indicated in Figure 2-1). Figure 2-3(a) gave a representation of the wind time series measured at the St Helena Bay weather station during the months of January to mid February 2002 (the simulation period).

It would have been ideal to apply realistic spatially-varying winds in the model, and this possibility must be investigated in future. It is known (Jury, 1984) that the winds in the St Helena Bay area are indeed spatially varying. In order to apply such winds in the model, good quality high resolution wind data is important. Wind data obtained from QuickScat is inadequate to observe the small scale horizontal variation, because of the large pixel size (25 km squares), as well as the location of the data. This data will not be reliable enough to apply as spatially varying winds in the model. There is thus a need for better wind data, and the solution would be to use output from an atmospheric model, such as MM5 (Mesoscale Model 5) at a fine scale (e.g. 2 – 5 km).

Due to the lack of spatially-varying wind data, three studies had to be undertaken with the St Helena Bay model for the purpose of this thesis. Table 5-1 gave a summary of these studies.

Other than the wind data, accurate boundary conditions are important for the model simulations. A detailed account of the boundary conditions with regards to water level specifications was given in Chapters 3.1.1 and 3.2.1 (the same method was followed for the Reference Model and the St Helena Bay model). Concerning the temperature specifications at the boundary, data measured at Hondeklip Bay (Monteiro, 1997) was applied at the St Helena Bay model boundaries, due to a lack of any better data at the time this model was set up. Very few good quality boundary conditions are obtainable from data sources, and the model requires measurements from specific areas at specific time scales, than do not exist.

A limitation of the Delft3D numerical model is the limited flexibility that the user has when specifying boundary conditions. The numerical model only allows for non-dynamic (or static) temperature profiles at the boundary. This leads to the problem of having growing discrepancies between the temperature specified at the boundaries and the temperature inside the model domain as time passes during a model run, because the inside of the model domain is allowed to change under the forcing conditions. This might set up artificial behaviour in the currents close to the boundaries. For this reason, the model domain is usually chosen to be large enough to keep the model boundaries as far away of the area of interest as possible. Keeping the model boundaries removed from the area of interest is also advantageous with regards to the southern boundary, which is usually ill-posed by nature (as seen during the Reference Model experiments). There are, however, also limitations to the size of the model domain (for numerical stability reasons) and at times it is not entirely possible to remove the boundary far enough away from the area of interest. The possible problems that could arise at the model boundaries were minimized during this thesis by the development of a Fortran programme that allowed a "zero gradient" across the model boundaries (see Chapters 3.1.1 and 3.2.1). This was done for the Reference Model as well as the St Helena Bay model.

Concerning the development of the nearshore poleward current in the region of St Helena Bay, Chapter 5 illustrated the horizontal current fields during the above-mentioned upwelling-relaxation phases, as well as vertical cross-sections of the temperature and the surface slopes. The development of this current was studied along the West Coast, from north of Lamberts Bay, into the eastern parts of St Helena Bay.

In agreement with the literature study (Pitcher & Boyd, 1996; Pitcher *et* al, 1998; Probyn *et al*, 2000) the poleward current in the case of the St Helena Bay model also developed during a phase of

relaxation, following an upwelling favourable wind event. It always occurred in quite a narrow band (varying between 0.5 km and 4 km wide), close to the coast. During a wind relaxation event, this current was usually visible all along the West Coast, from north of Lamberts Bay down into St Helena Bay, not only in isolated parts along the coast. The current usually strengthened and widened as the wind relaxation event continued, and disappeared as soon as the next upwelling favourable wind event started.

The development of the poleward current in the St Helena Bay region seemed to be based on similar basic mechanisms as was identified during the Reference Model experiments, but it did not always agree completely with the Reference Model findings. In the Reference Model it was found that, during a wind event, the surface was downward sloping towards the coast. During wind relaxation, the dynamical adjustment led to the surface reversing and becoming upward sloping towards the coast in the nearshore zone. The width of the poleward current agreed with the width of the upward sloping part of the surface (see Figures 4-14(a), (b) and (c) as well as Figure 4-15). Below this upward sloping surface, the temperature isotherms were downward sloping towards the coast to compensate for the adjustment in the surface slope.

In the case of the St Helena Bay model, however, this was not always the case. There were times, during an upwelling event, when the surface slope close to the coast was relatively flat and even slightly upward sloping (instead of downward sloping, as was expected). In agreement with the results from the Reference Model, the surface was usually upward sloping close to the coast during the time when the poleward current was visible, and the width of the poleward current did more or less agree with the width of the upward sloping part of the surface. The slope of the subsurface temperature isotherms, however, was not always downward sloping in this region, as was expected. At times, the temperature isotherms were upward sloping towards the coast while a poleward current was visible. It thus appeared that there could be additional factor(s) that are important during the formation of the poleward current in the St Helena Bay region. A detailed study of these additional factor(s), however, fell beyond the scope of this thesis.

The above discrepancies could probably be attributed to the higher level of complexity of the St Helena Bay model (the irregular coastline, the presence of a cape, and an alongshore variation in bottom topography). These added complexities, as well as the little flexibility provided by Delft3D-FLOW regarding a diagnostic study, made it very difficult to study this poleward current closely.

The presence of strong inertial circulations in this area also complicated the study of the temperature isotherms throughout the water column, as well as the surface slope. Near-diurnal oscillations in the

trajectory time series obtained from observations by Holden (1985) support the presence of these inertial motions. As was illustrated in Figures 5-1(a) and (b), these inertial movements caused the isotherms to move closer/further offshore at regular intervals, and it also caused the water level to rise and drop slightly while these inertial movements took place.

In the western part of St Helena Bay, a thermistor chain was deployed in 25 m of water (Figure 2-1 indicated its position), which provided a time series of temperature at 2 m depth intervals. This time series was used to compare model output with observational data, and it thus served as model validation data. In the vertical (on a seasonal scale), it is important that the model represents the overall behaviour in the vertical temperature structure (i.e. stratification and mixing processes) sufficiently well over the simulation period. The warming and cooling of the water as upwelling-relaxation events take place must be evident, as well as mixing processes and cold bottom water entrainment.

When the measured St Helena Bay weather station winds were applied, it was noted that the model represented the 6-8 day event scale variations in temperature remarkably well (Figure 5-11(a)). The stratification and mixing as strong wind events (and subsequent relaxation of the wind) took place were also reproduced well. The most noticeable discrepancy between the measured and modelled temperature time series is that there were instances when the modelled temperatures were often colder than the measured temperatures. This discrepancy between the measured and modelled values can most probably be attributed to the fact that constant wind speed and direction is applied throughout the model domain for the purpose of this simulation; spatially-varying winds are thus not used. As a result, the model does not take account of the wind shadow that exists in the St Helena Bay area due to the presence of Cape Columbine. This overestimates the wind being applied in the St Helena Bay area, leading to stronger entrainment of cold water into the surface layer, and thus lowers temperatures in the model results. The model also did not reproduce the diurnal variability in the temperature in the surface layer as clearly as it appears in the measurements. A possible reason for this could be that the modelled temperatures are average values per model layer, and not values at a specific point in depth. The anomalies in Figure 5-11(b) show that the model data is already simulating at least 80% of the system correctly. Addressing the wind data and the boundary conditions should lead to a significant improvement in anomalies between measured and modelled data.

A reduction of 30 % in the St Helena Bay weather station measured wind speed led to warmer modelled temperatures throughout the water column (Figure 5-21(a)). Other than that, the modelled temperatures showed a similar observed structure when the measured St Helena Bay weather station winds were applied. The anomalies in Figure 5-21(b) showed that the model data for this study was

simulating approximately 60% of the system correctly. The greatest discrepancy between the measured and modelled temperatures occurred at the surface.

When the diurnal variation in the wind was removed by smoothing the wind data, this led to lower winds speeds (all the peaks were removed), as well as a significant dampening in the inertial oscillations. From Figure 5-31(a) it was evident that the modelled temperatures were higher than the measured temperatures in the surface layer, and lower in the deeper layers. In this study, the overall wind speeds were lower, leading to weaker entrainment of cold water into the surface layer, and thus warmer temperatures in the model results. There was also significantly less diurnal variability (the temperature time series appeared smoother) in the modelled temperatures when compared to the study where the measured St Helena Bay weather station winds were applied. This is probably due to the absence of inertial period variability. The anomalies in Figure 5-31(b) showed that the model data was simulating approximately 60% of the system correctly throughout the water column for most of the period.

In summary, as expected, when the measured St Helena Bay weather stations winds were applied directly in the model, the best correlation between measured and modelled temperatures was obtained (an average agreement of 80 %, see Figure 5-11(b)). This is due to the wind station being close to the position of the thermistor chain, and thus behaviour of the temperature in the region (the western part of St Helena Bay) is most strongly influenced by those winds.

Overall, the St Helena Bay numerical model results reflected the main circulation characteristics of the system over the upwelling cycles (event scales) and the seasonal scale. Some of the event scale features well simulated were:

- The development of the narrow inshore poleward flow during the relaxation phase of the upwelling cycle;
- Upwelling at Cape Columbine;
- The barotropic jet on the seaward side of the plume;
- The variability of stratification as a result of the interactive effects of buoyancy forcing by upwelling, wind driven entrainment and mixing and solar heat flux;
- Inertial circulation.

In all three of the studies there was evidence of cyclonic motion in the southern parts of St Helena Bay during relaxation events. This is a feature that has been modelled in St Helena Bay (Penven *et al*, 2000).

From this study it was realized that the dynamical characteristics of the circulation and stratification of St Helena Bay are very complex and that a detailed study of the formation of the poleward surface current in this region will require more intensive investigation. The lack of spatially varying wind data was a problem in the St Helena Bay numerical model. The application of a uniform wind over the whole model domain led to Cape Columbine not acting properly as a cape, because the wind shadow that normally results from the presence of a cape, did not form. It is therefore very difficult to investigate the exact influence that the presence of a cape has on the formation of a nearshore poleward surface current. Thus, in order to undertake a more detailed and thorough investigation in the St Helena Bay region, it would be valuable to obtain high resolution boundary condition and wind data. Especially the wind data is very important when the development of the poleward surface current is studied. Good quality, high resolution data will be needed before a model can be set up applying spatially varying winds. It will be necessary to resolve the behaviour and influence of Cape Columbine accurately, in order to understand how important this Cape is during the formation of the poleward surface current.

The main findings from this study indicated that cross shore horizontal pressure gradients acting in an offshore direction are the main driving forces of a narrow poleward current in the Southern Benguela. This finding is in contrast to the modelling results of Gan & Allen (2002a and 2002b), who showed that nearshore poleward currents are forced by alongshore pressure gradients which is set up by the interaction of the wind-forced flow with the alongshore variations in shelf topography. The modelling study conducted by Wang (1997) also concluded that a poleward current seems to be forced by an alongshore poleward pressure gradient force which resulted from unbalanced forces when the wind forcing is removed. All the studies agree, however, that wind relaxation and the resulting unbalanced forces (due to the removal of the wind forcing) results in the formation of a narrow poleward current.

It is unfortunate that Delft3D-FLOW does not allow the user to do a proper diagnostic study of the modelling results. As part of this study it would have been ideal to examine the momentum balances in order to attain a complete dynamical understanding of the formation of the narrow poleward current. Without the capability to do such a diagnostic study, however, it is not possible to explain exactly what the driving forces behind the poleward current are.

It is concluded that good progress was made during this thesis in understanding certain elements of the mechanism behind the formation of the poleward surface current, as seen in the St Helena Bay region in the Southern Benguela. However, a complete understanding of the development of this poleward current has not been achieved yet. It is a very complex region and additional investigations will be required to complete the understanding. These future investigations should provide additional insights into the formation of this interesting, distinctive current.

7. REFERENCES

AMERICAN PETROLEUM INSTITUTE (1991) Recommended practise for planning, designing and constructing fixed offshore platforms. API Recommended Practise. ZA (RPZA) 19th edition. Washington DC: 159.

BAILEY, G.W. and CHAPMAN, P. (1985) The nutrient status of the St Helena Bay region in February 1979. South African Ocean Colour and Upwelling Experiment. Shannon, L.V. (Ed.). Cape Town; Sea Fisheries Research Institute: 125 - 145.

BAKUN, A. (1993) The California Current, Benguela Current, and Southwestern Atlantic Shelf Ecosystems: a comparative approach to identifying factors regulating biomass yields. In: *Large Marine Ecosystems – Stress, Mitigation, and Sustainability.* K. Sherman, L.M. Alexander and B. Gold (Eds.) American Association for the Advancement of Science: 199 – 224.

CSIR (2002) Aluminium Pechiney Coega EIA: Spesialist study on discharges to the Marine Environment. CSIR Report ENV-S-C 2002-061, Stellenbosch, South Africa.

CSIR (2003a) Modelling of fin fish farm impacts in Klein Baai: Hydrodynamic model as a first phase of a project to develop a predictive management capability. CSIR Report ENV-S-C 2003-143, Stellenbosch, South Africa.

CSIR (2003b) EIA for the Expansion of the Container Terminal Stacking Area at the Port of Cape Town: Spesialist study on physical impacts of dredging. CSIR Report ENV-S-C 2003-083, Stellenbosch, South Africa.

CSIR (2005) Environmental Fatal Flaws Assessment: Preliminary Assessment of a Proposed CCGT Power Plant Purge Water Discharge into Saldanha Bay. CSIR Report ENV-S-C-2005-067, Stellenbosch, South Africa.

GAN, J. and ALLEN, J.S. (2002a) A modeling study of shelf circulation off northern California in the region of the Coastal Ocean Dynamics Experiment: Response to relaxation of upwelling winds. *J. Geophys. Res.* **107**(C9): 3123.

GAN, J. and ALLEN, J.S. (2002b) A modeling study of shelf circulation off northern California in the region of the Coastal Ocean Dynamics Experiment, 2, Simulations and comparisons with observations. *J. Geophys. Res.* **107**(C11): 3184.

GILL, A.E. (1977) Coastally trapped waves in the atmosphere. *Q. J. R. Meteorol. Soc.* **103**: 431-440. Academic Press. International geophysics Series **30**.

GILL, A.E. (1982) Atmosphere-Ocean dynamics. Academic Press. International geophysics Series **30**.

HART, T.J. and CURRIE, R.I. (1960) The Benguela Current. Discovery Rep. **31**: 123-298.

HOLDEN, C.J. (1985) Currents in St Helena Bay inferred from radio-tracked drifters. *South African Ocean Colour and Upwelling Experiment.* Shannon, L.V. (Ed.). Cape Town; Sea Fisheries Research Institute: 97-109.

HUTCHINGS, L. (1992) Fish harvesting in a variable, productive environment. *S. Afr. J. mar. Sci.* **12**: 297 - 318.

HUTCHINGS, L., BARANGE, M., BLOOMER, S.F., BOYD, A.J., CRAWFORD, R.J.M., HUGGETT, J.A., KERSTAN, M., KORRÛBEL, J.L., DE OLIVEIRA, J.A.A., PAINTING, S.J., RICHARDSON, A.J., SHANNON, L.J., SCHÜLEIN, F.H., VAN DER LINGEN, C.D. and VERHEYE, H.M. (1998) Multiple factors affecting South African anchovy recruitment in the spawning, transport and nursery areas. In: *Benguela Dynamics.* Pillar, S.C., Moloney, C.L., Payne, A.I.L. and Shillington, F.A. (Eds.) *S. Afr. J. mar. Sci.* **19**: 211-225.

JURY, M.R. (1984) Wind Shear and Differential Upwelling along the SW Tip of Africa. PhD Thesis, University of Cape Town.

JURY, M.R. (1985) Mesoscale Variations in Summer Winds over the Cape Columbine-St Helena Bay Region, South Africa. *S. Afr. J. mar. Sci.* **3**: 77 - 88.

LAMBERTH, R. and NELSON, G. (1987) Field and Analytical Drogue Studies applicable to the St Helena Bay area off South Africa's West Coast. *S. Afr. J. mar. Sci.* **5**: 163 – 169.

LANE, A. (1989) The heat balance of the North Sea. Proudman Oceanographic laboratory, Report no **8**.

LESSER, G.R., ROELVINK, J.A., VAN KESTER, J.A.T.M. AND STELLING, G.S. (2004) Development and validation of a three-dimensional morphological model. *Coastal Engineering* **51**: 883 – 915.

LUGER, S. and STELLING, G. (2000) Delft3D Utility Programme TILT.

LUTJEHARMS, J.R.E. and STOCKTON, P.L. (1987) Kinematics of the upwelling front off southern Africa. In: *The Benguela and Comparable Ecosystems*. Payne, A.I.L., Gulland, J.A. and Brink, K.A. (eds). S. Afr. J. Mar. Sci. **5**: 51-62.

MONTEIRO, P.M.S. (1997) The Oceanography, the Biogeochemistry and Fluxes of Carbon Dioxide in the Benguela Upwelling System. PhD Thesis, University of Cape Town, South Africa.

MONTEIRO, P.M.S., VAN DER PLAS, A.K., BAILEY, G.W. and FIDEL, Q. (2004) Low oxygen variability in the Benguela ecosystem: A review and new understanding. CSIR Report ENV-S-C 2004-075, Stellenbosch, South Africa.

MURAKAMI, M., OONISISHI, Y. and KUNISHI, H. (1985) A numerical simulation of the distribution of water temperature and salinity in the Seto Inland Sea, Journal of the Oceanographical Society of Japan **41**: 221-224.

NELSON, G. and HUTCHINGS, L. (1983) The Benguela Upwelling Area. *Prog. Oceanog.* **12**: 333-356.

NELSON, G. and HUTCHINGS, L. (1987) Passive transportation of pelagic system components in the southern Benguela area. *S. Afr. J. mar. Sci.* **5**: 223 - 234.

NICHOLSON, J., BROKER, I., ROLEVINK, J.A., PRICE, D., TANGUY, J.M. and MORENO, L. (1997) Intercomparison of coastal area morphodynamic models. *Coastal Eng* **31**: 97-123.

OCTAVIA, K.A.H., JIRKA, G.H. and HARLEMAN, D.R.F. (1977) Vertical heat Transport Mechanisms in Lakes and Reservoirs. Massachusetts Institute of Technology, Report no **227**.

OPEN UNIVERSITY (1989) Ocean Circulation. Open University Series. Oxford, England; New York: Pergamon Press. Chapter 3: 40-58.

PENVEN, P. (2000) A numerical study of the Southern Benguela circulation with an application to fish recruitment. PhD Thesis, University of Brest, France.

PENVEN, P., ROY, C., COLIN de VERDIÈRE, A., and LARGIER, J. (2000) Simulation of a coastal jet retention process using a barotropic model. *Oceanologica Acta* Vol. **23**, no 5.

PENVEN, P., ROY, C., BRUNDRIT, G.B., COLIN de VERDIÈRE, A., FRÉON, P., JOHNSON, A.S., LUTJEHARMS, J.R.E. AND SHILLINGTON, F.A. (2001) A regional hydrodynamic model of upwelling in the Southern Benguela. *S A J Sci.* **97**: 104-107.

PETERSON, R.G., and STRAMMA, L. (2000) Upper-level circulation in the South Atlantic Ocean. Prog. Oceanogr. **26**: 1-73.

PITCHER, G.C. and BOYD, A.J. (1996) Across-shelf and alongshore dinoflagellate distributions and the mechanisms of red tide formation within the southern Benguela upwelling system. In: Yasumoto T, Oshima Y, Fukuyo Y (eds) Harmful and toxic algal blooms. Intergovernmental Oceanographic Commission of UNESCO, Paris: 243-246.

PITCHER, G.C., BOYD, A.F., HORSTMAN, D.A. and MITCHELL-INNES, B.A. (1998) Subsurface dinoflagellate populations, frontal blooms and the formation of red tide in the southern Benguela upwelling system. *Marine Ecology Progress Series* **172**: 253-264.

PROBYN, T.A., PITCHER, G.C., MONTEIRO, P.M.S., BOYD, A.J. and NELSON, G. (2000) Physical processes contributing to Harmful Algal Blooms in Saldanha Bay, South Africa. *S. Afr. J. mar. Sci.* **22**: 285-297.

REASON, C.J.C., ALLAN, R.J., LINDESAY, J.A. and ANSELL, T.J. (1990) ENSO and climatic signals across the Indian ocean Basin in the global context: Part 1, Interannual composite patterns. *Int. J. Climatol.* **20**: 1285-1327.

REASON, C.J.C. and JURY, M.R. (1990) On the generation and propagation of the southern African coastal low. Q. J. R. Meteorol. Soc. **116**: 1133-1152.

RISIEN, C.M., REASON, C.J.C., SHILLINGTON, F.A. and CHELTON, D.B. (2004) Variability in satellite winds over the Benguela upwelling system during 1999-2000. *J. Geophys. Res.* **109**: C03010.

ROY, C., WEEKS, S., ROUALT, M., NELSON, G., BARLOW, R. and VAN DER LINGEN, C. (2001) Extreme oceanographic events recorded in the southern Benguela during the 1999-2000 summer season. S. Afr. J. of Sci. **97**: 465-471.

SHANNON, L.V. (1985) The Benguela Ecosystem part I. Evolution of the Benguela, physical features and processes. *Oceanogr. Mar. Biol. Ann. Rev.* **23**: 105 – 182.

SHANNON, L.V. and NELSON, G. (1996) The Benguela: large scale features and processes and system variability. In *The South Atlantic: Present and Past Circulation*, G. Wefer, W.H. Berger, F. Seidler and D.J. Webb (Eds.) Springer-Verlag, Berlin, Heidelberg: 163 – 210.

SHILLINGTON, F.A. (1998) The Benguela Upwelling System off Southwestern Africa, Coastal Segment (16,E). In *The Sea*, Volume 11, Robinson, A.R. and Brink, K. H., eds. John Wiley & Sons, Inc.: 583 – 604.

SIMPSON, J.H., HYDER, P., and RIPPETH, T.P. (2002) Forced Oscillations near the Critical Latitude for Diurnal-Inertial Resonance. *J. Phys. Oceanog.* **32**: 177 – 187.

SMITH, S.D. and BLANKE, E.G. (1975) Variation of the sea surface drag coefficient with wind speed. Quart. J. R. Met. Society **101**: 665-673.

SWEERS, H.E. (1976) A monogram to estimate the heat exchange coefficient at the air-water interface as a function of windspeed and temperature; a critical survey of some literature. J. of Hydrology **30**.

WANG, DONG-PING (1997) Effects of small-scale wind on coastal upwelling with application to Point Conception. *J. Geophys. Res.* **102**(C7): 15 555 – 15 566.

WL|DELFT HYDRAULICS (2003) Delft3D-FLOW User Manual Version 3.10. WL|Delft Hydraulics, Delft, The Netherlands.

APPENDIX A

DESCRIPTION OF DELFT3D-FLOW HEAT FLUX MODELS

9.8 Heat flux models

The heat radiation emitted by the sun reaches the earth in the form of electromagnetic waves with wavelengths in the range of 0.15 to 4 µm. In the atmosphere the radiation undergoes scattering, reflection and absorption by air, cloud, dust and particles. On average neither the atmosphere nor the earth accumulates heat, which implies that the absorbed heat is emitted back again. The wavelengths of these emitted radiations are longer (between 4 and 50 µm) due to the lower prevailing temperature in the atmosphere and on Earth. Schematically the radiation process, along with the heat flux mechanisms at the water surface, is shown in Figure 9-9.

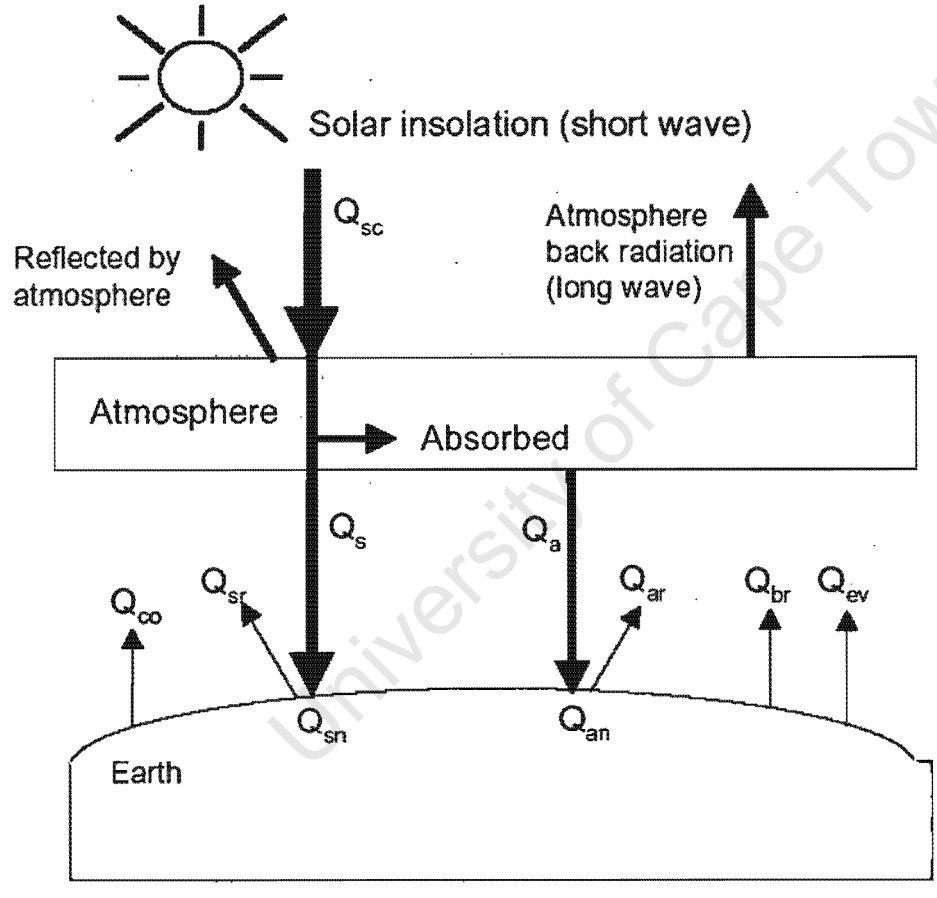

Figure 9-9 Overview of the heat exchange mechanisms at the surface

Legend: Q_s solar radiation (short wave radiation) in [J/m^{2}s]

Q_{sr} reflected solar radiation in [J/m^{2}s]

Q_a atmospheric radiation (long wave radiation) in [J/m^{2}s]

Q_{ar} reflected atmospheric radiation in [J/m^{2}s]

Q_{br} back radiation (long wave radiation) in [J/m^{2}s]

Q_{ev} heat loss due to evaporation (sensible) in [J/m^{2}s]

Q_{co} heat loss due to convection (latent) in [J/m^{2}s]

In Delft3D-FLOW the heat exchange at the free surface is modelled by taking into account the separate effects of solar (short wave) and atmospheric (long wave) radiation, and heat loss due to back radiation, evaporation and convection. In literature there is a great variability of empirical formulations to calculate these heat fluxes across the sea surface. Most formulations differ in the dependency of the exchange on the meteorological parameters such as wind speed, cloudiness and humidity. Some formulations were calibrated for coastal seas others for lakes.

In Delft3D-FLOW five heat flux models have been implemented:

1. *Heat flux model 1*
   The incoming (short wave) solar radiation for a clear sky is prescribed. The net atmospheric (long wave) radiation and the heat losses due to evaporation, back radiation and convection are computed by the model.

2. *Heat flux model 2*
   The combined net (short wave) solar and net (long wave) atmospheric radiation is prescribed. The terms related to heat losses due to evaporation, back radiation and convection are computed by the model.

3. *Excess temperature model*
   The heat exchange flux at the air - water interface is computed; only the background temperature is required.

4. *Murakami heat flux model*
   The net (short wave) solar radiation is prescribed. The effective back radiation and the heat losses due to evaporation and convection are computed by the model. The incoming radiation is absorbed as a function of depth. The evaporative heat flux is calibrated for Japanese waters.

5. *Proctor or Ocean heat flux model*
   The fraction of the sky covered by clouds is prescribed (in %). The effective back radiation and the heat losses due to evaporation and convection are computed by the model. This model formulation typically applies for large water bodies.

For the physical background of the heat exchange at the air-water interface and the definitions, we refer to (Octavia et al., 1977) for model 1 and 2, to (Sweers, 1976) for model 3, to (Murakami et al., 1985) for model 4 and to (Gill, 1982) and (Lane, 1989) for model 5.

With the exception of model 3 the excess temperature model, the heat fluxes through the water surface by incoming radiation, back radiation, evaporation and convection are computed separately. Evaporation and convection depend on the air temperature, the water temperature near the free surface, relative humidity, and wind speed. The excess temperature

model computes the heat fluxes through the water surface in such a way that the temperature of the surface layer relaxates to the natural background temperature specified by you. The heat transfer coefficient mainly depends on the water temperature and the wind speed.

9.8.1 Heat balance

The total heat flux through the free surface reads:

$$Q_{tot} = Q_{sn} + Q_{an} - Q_{br} - Q_{ev} - Q_{co}, \tag{9.182}$$

with:

Q_{sn}	net incident solar radiation (short wave)
Q_{an}	net incident atmospheric radiation (long wave)
Q_{br}	back radiation (long wave)
Q_{ev}	evaporative heat flux (latent heat)
Q_{co}	convective heat flux (sensible heat).

The subscript n refers to a net contribution. Each of the heat fluxes in Eq. (9.182) will be discussed in detail.

The change in temperature in the top layer T_s (in °C) is given by:

$$\frac{\partial T_s}{\partial t} = \frac{Q_{tot}}{\rho_w c_p \Delta z_s}, \tag{9.183}$$

where Q_{tot} (in J/m^{2}s) is the total heat flux through the air-water surface, c_p (3930 J/kgK) is the specific heat capacity of sea water, ρ_w is the specific density of water (in kg/m^3) and Δz_s (in m) is the thickness of the top layer. In Delft3D-FLOW, the heat exchange at the bed is assumed to be zero. This may lead to over-prediction of the water temperature in shallow areas. Also the effect of precipitation on the water temperature is not taken into account.

Remarks:

- The temperature T is by default expressed in °C. However, in some formulas the absolute temperature $\overline{T}$ in K is used. They are related by:
  $\overline{T} = T + 273.15$.
- In Eq. (9.183) the total incoming heat flux is assumed to be absorbed in the top layer. This may result in an unrealistically high surface temperature when the top layer is thin. This can be prevented by absorbing the incoming radiation as a function of depth. Currently, this is only implemented in heat flux model 4.
- The input parameters for the heat flux models are model dependent. For example, the input for the solar radiation has to be specified (measured data) as incoming (short-wave) solar radiation for a clear sky (Q_{sc}) for heat flux model 1, as combined net solar radiation

and net atmospheric radiation (sum of Q_{sn} and Q_{an}) for heat flux model 2, as net solar radiation for heat flux model 4, or is computed by the heat flux model itself (heat flux models 3 and 5).

9.8.2 Solar radiation

The short-wave radiation emitted by the sun that reaches the earth surface under a clear sky condition can be evaluated by means of:

- Direct measurements.
- Applying Stefan-Boltsmann's law for radiation from a black-body:

$$Q = \sigma \bar{T}^4 \tag{9.184}$$

with σ = Stefan-Boltsmann's constant = 5.67 10^{-8} [J/m^{2}s K^4] and $\bar{T}$ the (absolute) temperature [K].

- Empirical formulae.

In the heat flux models 1, 2 and 4 the solar radiation has to be specified by you. In the excess temperature model (model 3) the solar radiation does not play an explicit role, but is part of the background temperature. In the heat flux model 5 the solar radiation is computed by the program and is dependent on the geographical position at the earth and the local time.
Not all of the radiation is absorbed at the water surface. A part (approximately 50%) is transmitted to deeper water. Short waves can penetrate over a distance of 3 to 30 meters, depending on the clarity of the water, while the relatively longer waves are absorbed at the surface. Therefore, it is convenient to separate the incoming solar insolation into two portions: the longer wave portion, βQ_{sn}, which is absorbed at the surface and the remainder part, $(1-\beta)Q_{sn}$, which is absorbed in deeper water. The absorption of heat in the water column is an exponential function of the distance from the water surface:

$$Q_{sn}(z) = (1-\beta)Q_{sn}\frac{e^{-\gamma z}}{1-e^{-\gamma H_{Secchi}}}, \tag{9.185}$$

with:

β part of Q_{sn} absorbed at the water surface which is a function of the wavelength. The default value of beta in Delft3D-FLOW is 0.06.

γ extinction coefficient (measured) in m^{-1}, also related to the so-called Secchi-depth $\gamma = \dfrac{1.7}{H_{Secchi}}$

z distance to the water surface in meters.

Remark:

- The exponential decay function, Eq. (9.185) has only been implemented in the heat flux models 4 and 5. In the other heat flux models the incoming radiation is expected to be absorbed in the top layer.

In heat flux model 5 the flux is computed dependent on the geographical position and the local time. The incoming energy flux at the water surface depends on the angle (declination) between the incoming radiation and the Earth's surface. This declination depends on the geographical position on the Earth and the local time. The Earth axis is not perpendicular to the line connecting the Sun with Earth. This tilting (angle δ) varies with the time of the year and it leads to a seasonal variation of the radiation flux. At June 21, the declination is maximal, 23.5 degrees. Of course, by the rotation of the Earth the solar radiation also varies during the day. Near twelve o'clock local time, the sun elevation above the horizon is maximal. For an overview of the angles used to determine the solar elevation angle γ, see Figure 9-10.

The temporal and latitude-dependent solar elevation angle γ is estimated by:

$$\sin(\gamma) = \sin(\delta)\sin\left(\frac{\pi\phi}{180}\right) - \cos(\delta)\cos\left(\frac{\pi\phi}{180}\right)\cos(\omega_1 t) \tag{9.186}$$

with:

$$\delta = \frac{23.5\pi}{180}\cos(\omega_0 t - 2.95), \tag{9.187}$$

where ω_0 is the frequency of the annual variation and ω_1 the frequency of the diurnal variation; ϕ is the latitude.

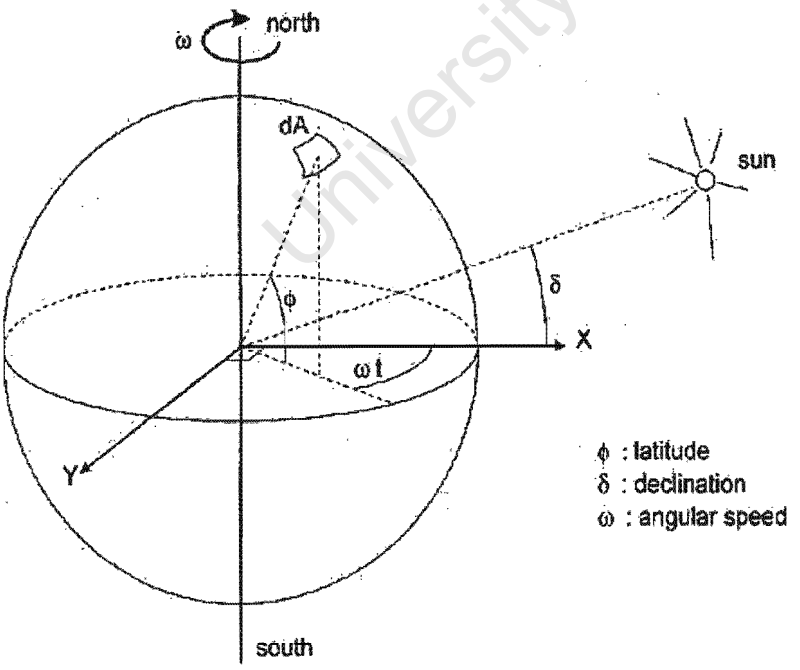

Figure 9-10 Co-ordinate system position Sun

The incoming short-wave solar radiation through a clear sky at ground level Q_{sc} is about 0.76 of the flux incident at the top of the atmosphere (Gill, 1982):

$$Q_{sc} = \begin{cases} 0.76\, S \sin(\gamma), & \sin(\gamma) \geq 0, \\ 0.0, & \sin(\gamma) < 0. \end{cases} \tag{9.188}$$

The solar constant S is 1368 [J/m^{2}s]. This is the average energy flux at the mean radius of the Earth.

A part of the radiation that reaches the water surface is reflected. The fraction reflected or scattered (surface albedo) is dependent on latitude and season. Cloud cover will reduce the magnitude of the radiation flux that reaches the sea surface. The cloudiness is expressed by a cloud cover fraction F_c, the fraction of the sky covered by clouds. The correction factor for cloud cover is an empirical formula. The absorption of solar radiation is calculated (Gill, 1982) as the product of the net downward flux of short wave-radiation in cloudless conditions and factors correcting for reflection and cloud cover:

$$Q_{sn} = Q_s - Q_{sr} = (1-\alpha) Q_{sc} f(F_c), \tag{9.189}$$

with:

Q_{sn} net heat radiation (flux) from the Sun
Q_{sc} radiation (flux) for clear sky condition
α albedo (reflection) coefficient
F_c fraction of sky covered by clouds (user input)
$f(F_c)$ function of F_c

The cloud function $f(F_c)$ and the albedo coefficient α used in Delft3D-FLOW are given in Table 9-1.

Heat flux model	albedo (α)	$f(F_c)$
1	0.06	$1.0 - 0.65 F_c^2$
4	0.09	-
5	0.06	$1.0 - 0.4 F_c - 0.38 F_c^2$

Table 9-1 Albedo coefficient and cloud function

9.8.3 Atmospheric radiation (long wave radiation)

Atmospheric radiation is primarily due to emission of absorbed solar radiation by water vapour, carbon dioxide and ozone in the atmosphere. The emission spectrum of the atmosphere is highly irregular. The amount of atmospheric radiation that reaches the earth is determined by applying the Stefan-Boltsmann's law that includes the emissivity coefficient of the atmosphere ε. Taking into account the effect of reflection by the surface and reflection and absorption by clouds, the relation for the net atmospheric radiation Q_{an} reads (Octavia et al., 1977):

$$Q_{an} = (1-r)\varepsilon\sigma\overline{T}_a^4 g(F_c), \tag{9.190}$$

where $\overline{T}_a$ is the air temperature (in K) and the reflection coefficient $r = 0.03$. The emissivity factor of the atmosphere ε may depend both on vapour pressure and air temperature. The emissivity of the atmosphere varies between 0.7 for clear sky and low temperature and 1.0. The presence of clouds increases the atmospheric radiation. This is expressed in the cloud function $g(F_c)$.

In heat flux model 1 a simple linear formula for the net atmospheric radiation is used (Octavia et al., 1977):

$$Q_{an} = (218.0 + 6.3T_a)g(F_c), \tag{9.191}$$

with T_a the air temperature (in °C). The cloud function $g(F_c)$ in Eqs. (9.190) and (9.191) is given by:

$$g(F_c) = 1.0 + 0.17F_c^2. \tag{9.192}$$

The linearisation of Eq. (9.190) is carried out around $T_a = 15^oC$.

Remarks:

- In heat flux model 1 the atmospheric radiation is computed.
- In heat flux model 2 the atmospheric radiation is part of the (measured) net solar radiation flux specified by you.
- In heat flux models 4 and 5 the atmospheric radiation is part of the total long-wave radiation flux, the so-called effective back radiation, see Section 9.8.5.
- The fraction of the sky covered by clouds F_c is fixed for the whole simulation period in the heat flux models 1 and 4. F_c is not used in heat flux models 2 and 3 and can be prescribed as a function of time in heat flux model 5.

9.8.4 Back radiation (long wave radiation)

Water radiates as a near black body, so the heat radiated back by the water can be described by the Stefan-Boltsmann's law of radiation, corrected by an emissivity factor ε of water (Sweers, 1976), (Octavia et al., 1977) and the reflection coefficient for the air-water interface $r = 0.03$:

$$Q_{br} = (1-r)\varepsilon\sigma\overline{T}_s^4, \tag{9.193}$$

with $\overline{T}_s$ the (absolute) water surface temperature in K.

For heat flux models 1 and 2 Eq. (9.193) has been linearised around $T_a = 15^oC$:

$$Q_{br} = 303.0 + 5.2 T_s . \tag{9.194}$$

Remark:

- In heat flux models 1 and 2 the back radiation from the water surface is computed explicitly. In heat flux models 4 and 5 the back radiation is part of the total long-wave radiation flux, the so-called effective back radiation, see Section 9.8.5. In heat model 3 the back radiation is part of the heat exchange coefficient (Sweers, 1976).

9.8.5 Effective back radiation

In heat flux models 4 and 5 the total net long wave radiation flux is computed. This is called the effective back radiation:

$$Q_{eb} = Q_{br} - Q_{an} . \tag{9.195}$$

The atmospheric radiation depends on the vapour pressure e_a, see Section 9.8.6, the air temperature T_a and the cloud cover F_c. The back radiation depends on the surface temperature T_s.

In heat flux model 4 the effective back radiation is computed using Berliands formula:

$$Q_{eb} = \varepsilon \sigma \overline{T}_a^4 \left(0.39 - 0.058\sqrt{e_a}\right)\left(1.0 - 0.65 F_c^2\right) + 4\varepsilon\sigma \overline{T}_a^3 \left(\overline{T}_s - \overline{T}_a\right), \tag{9.196}$$

with the actual vapour pressure e_a given by Eq. (9.202).

In heat flux model 5 the effective back radiation Q_{eb} is computed following:

$$Q_{eb} = \varepsilon \sigma \overline{T}_s^4 \left(0.39 - 0.05\sqrt{e_a}\right)\left(1.0 - 0.6 F_c^2\right), \tag{9.197}$$

with the actual vapour pressure e_a given by Eq. (9.202).

9.8.6 Evaporative heat flux

Evaporation is an exchange process that takes place at the interface between water and air and depends on the conditions both in the water near the surface and the air above it. The evaporation depends on meteorological factors (wind-driven convection) and vapour pressures.

In the heat flux models 1, 2 and 4 the evaporative heat flux Q_{ev} is given by:

$$Q_{ev} = L_V \rho_w E , \tag{9.198}$$

with L_v the latent heat of vaporisation in J/kg:

$$L_v = 2.5\ 10^6 - 2.3\ 10^3 T_s. \tag{9.199}$$

The evaporation rate E defined as the volume of water evaporated per unit area per unit time is computed using the following Dalton's law of mass transfer:

$$E = f(U_{10})(e_s - e_a), \tag{9.200}$$

with the actual vapour pressure e_a and the saturated vapour pressure e_s, given by the following relations:

$$e_s = 23.38 e^{18.1 - \frac{53303.3}{T_a}}, \tag{9.201}$$

$$e_a = r_{hum} e_s. \tag{9.202}$$

The relative humidity r_{hum} is specified as a function of time in all heat flux models but the excess temperature model (model 3).

Remarks:

- The evaporation rate E computed from a heat flux model can be added as a source term to the right hand side of the continuity equation Eq. (9.4). The keyword required is Maseva = #Y#.
- By default E is computed from the heat flux model formulation selected, but E can also be prescribed as a function of time. In the latter case this user-defined evaporation overrules the computed evaporation both in the heat flux model and in the continuity equation; see Appendix B.5 on how to prescribe a time dependent evaporation.

For models 1, 2 and 3 the wind speed function $f(U_{10})$ following (Sweers, 1976) is used:

$$f(U_{10}) = (3.5 + 2.0 U_{10}) \left(\frac{5.0\ 10^6}{S_{area}} \right)^{0.05}, \tag{9.203}$$

where S_{area} is the exposed water surface in m^2, defined in the input and fixed for the whole simulation. The coefficients calibrated by Sweers were based on the wind speed at 3 meter above the free surface; the coefficients in Eq. (9.203) are based on the wind speed 10 meter above the water level.

In heat flux model 4 the wind speed function following (Murakami et al., 1985) is used:

$$f(U_{10}) = c_e U_{10}, \tag{9.204}$$

with $c_e = 0.0012$ the so-called Dalton number, is calibrated for Japanese waters. (Murakami et al., 1985).

In heat flux model 5 the evaporation rate is computed from the difference in relative humidity, rather than from the difference in vapour pressure. The latent heat flux for heat model 5 reads:

$$Q_{ev} = L_V \rho_a f(U_{10})\{q_s(T_s) - q_a(T_a)\}, \tag{9.205}$$

with q_a and q_s the specific humidity of respectively air and saturated air:

$$q_s(T_s) = \frac{0.62 e_s}{P_{atm} - 0.38 e_s}, \tag{9.206}$$

$$q_a(T_a) = \frac{0.62 e_a}{P_{atm} - 0.38 e_a}. \tag{9.207}$$

The saturated and actual vapour pressures are given by:

$$e_s = 10^{\frac{0.7859 + 0.03477 T_a}{1.0 + 0.00412 T_a}}, \tag{9.208}$$

$$e_a = r_{hum} e_s. \tag{9.209}$$

The relative humidity r_{hum} is specified as a function of time in all heat flux models but the excess temperature model (model 3).

The wind function in Eq. (9.205) is following Eq. (9.204), but the Dalton number c_e in model 5 was calibrated for the North Sea: $c_e = 0.0015$.

9.8.7 Convective heat flux

Assuming that the turbulent exchange of heat at the air-water interface equals the turbulent exchange of mass, the convective heat flux can be related to the evaporative mass flux by the Bowen ratio:

$$Q_{co} = R_b Q_{ev}, \tag{9.210}$$

$$R_b = \gamma \frac{T_s - T_a}{e_s - e_a}, \tag{9.211}$$

with γ the so-called Bowen's constant:

$\gamma = 0.61$ for heat flux models 1 and 2

$\gamma = 0.66$ for heat flux model 4.

The saturated and actual vapour pressures are given by Eqs. (9.201) and (9.202).

In heat flux model 5 the convective heat flux is computed following:

$$Q_{co} = \rho_a c_p g(U_{10})(T_s - T_a), \tag{9.212}$$

with ρ_a the density of air, c_p the specific heat of air and for the wind-speed function $g(U_{10})$ following (Gill, 1982):

$$g(U_{10}) = c_H U_{10}, \tag{9.213}$$

with c_H the so-called Stanton number calibrated for the North Sea: $c_H = 0.00145$.

9.8.8 Overview of heat flux models

Heat flux model 1

For heat flux model 1 the relations used for the computation of the heat balance, Eq. (9.182), are given in Table 9-2.

Table 9-2 Terms of the heat balance used in heat model 1

Quantity	Description	According to
Q_{sc}	short wave solar radiation for clear sky	measured
Q_{sn}	net solar radiation	Eq. (9.189)
Q_{an}	net atmospheric radiation	Eqs. (9.191) and (9.192)
Q_{br}	back radiation	Eq. (9.194)
Q_{ev}	heat loss due to evaporation	Eqs. (9.198) to (9.202)
Q_{co}	heat loss due to convection	Eqs. (9.210) and (9.211)

Heat flux model 2

Heat flux model 2 is based on formulations given by (Octavia et al., 1977). The source of data for the combined net incoming radiation terms $(Q_{sn} + Q_{an})$ must come from direct measurements. The remaining terms (back radiation, evaporation, convection) are computed similarly as for heat flux model option 1, Table 9-3.

Table 9-3 Terms of the heat balance used in heat model 2

Quantity	Description	According to
$Q_{sn} + Q_{an}$	net solar and net atmospheric radiation	measured

Q_{br}	back radiation	Eq. (9.194)
Q_{ev}	heat loss due to evaporation	Eqs. (9.198) to (9.202)
Q_{co}	heat loss due to convection	Eqs. (9.210) and (9.211)

Excess temperature model - model 3

The excess temperature model 3 is based on (Sweers, 1976), the heat exchange flux is represented by a bulk exchange formula:

$$Q_{tot} = -\lambda\left(T_s - T_{back}\right), \tag{9.214}$$

with T_s the water temperature at the free surface and T_{back} the natural background temperature, both in °C.

The heat exchange coefficient λ is a function of the surface temperature T_s and the wind speed U_{10}. It is derived by linearization of the exchange fluxes for back radiation, evaporation and convection. The following relation was derived by (Sweers, 1976):

$$\lambda = 4.48 + 0.049T_s + f\left(U_{10}\right)\left(1.12 + 0.018T_s + 0.00158T_s^2\right). \tag{9.215}$$

For the wind function $f\left(U_{10}\right)$ Eq. (9.203) is applied.

Murakami model - heat flux model 4

The heat flux model 4 was calibrated for the Japanese waters (Murakami et al., 1985). The following relations are used for the computation of the heat terms, Table 9-4:

Table 9-4 Terms of the heat balance used in heat model 4

Quantity	Description	According to
Q_{sn}	net solar radiation	measured
Q_{eb}	effective back radiation	Eq. (9.196)
Q_{ev}	heat loss due to evaporation	Eqs. (9.198) to (9.202)
Q_{co}	heat loss due to convection	Eqs. (9.210) and (9.211)

Ocean heat flux model 5

The heat flux model 5 following (Gill, 1982) and (Lane, 1989) was calibrated for the North Sea and successfully applied for great lakes. The following relations are used for the computation of the heat terms, Table 9-5:

Table 9-5 Terms of the heat balance used in heat model 5

Quantity	Description	According to
Q_{sn}	net solar radiation	Eq. (1.86) and Eq. (9.189)
Q_{eb}	effective back radiation	Eq. (9.197)

Q_{ev}	heat loss due to evaporation	Eqs. (9.205) to (9.208)
Q_{co}	heat loss due to convection	Eqs. (9.212) and (9.213)

The required time dependent input data for each of the heat flux models is summarised in Table 9- 6:

Table 9- 6 Summary of time dependent data of the heat flux models

Quantity	model 1	model 2	Excess temperature	Murakami	Ocean
Q_{sc}	x				
Q_{sn}				x	
$Q_{sn}+Q_{an}$		x			
T_{back}			x		
T_a	x	x		x	x
r_{hum}	x	x		x	x
F_c					x
e_a				x (optional)	

APPENDIX B

DESCRIPTION OF THE BOUNDARY MODULE TILT

Description of the Boundary Module TILT

Background

In hydrodynamic models such as DELFT3D-FLOW, the open boundary conditions may be specified as water levels, currents, discharges or Riemann invariants, and may vary along the boundaries in both time and space. The specification of correct open boundary conditions was identified from the start as one of the most challenging issues for applying the DELFT3D-FLOW model to Southern African conditions, which are characterised by open coastlines, weak tidal currents, strong wind-driven currents, a lack of field data, and a lack of large-scale regional models in which to nest local models. This is in contrast to Europe, where tidal currents are often dominant and the boundary conditions may be specified as tidal levels obtained from well-calibrated regional models.

Objectives

To develop a hydrodynamic boundary module to enable the commonly-encountered hydrodynamic conditions in Southern Africa to be simulated. The conditions include wind-driven current forcing, large-scale ocean circulation, e.g. the Agulhas Current, and a combination of wind and large-scale ocean circulation. The module should support time-varying conditions and the output should be compatible to DELFT3D-FLOW.

Approach

The module assumes a relatively open coastline where the model domain has three open boundaries, i.e. two cross-shore boundaries orientated approximately normal to the coastline and a longshore boundary orientated approximately parallel to the coastline. Of the four possible boundary types, i.e. water levels, currents, discharges or Riemann invariants, water levels have been selected for all three open boundaries. This is because water levels offer the most simple and flexible specification by allowing the hydrodynamic model to determine the details of the two- or three-dimensional flows through the boundaries. The tide can also be added by simple superposition.

The model has 3 different modes of operation:

Option 1 - Current driven by wind only

This option is used when wind effects dominate the currents and no current measurements are available. The module computes the water levels that need to be specified on the boundaries to match the water levels generated inside the model domain due to time-varying winds, taking into account wind-driven currents, Coriolis tilts arising from these currents and wind setup. The inertia

of the water column is taken into account and the water thus accelerates faster in shallower areas than in deep areas. As illustrated in the examples that follow, failure to apply the correct boundary conditions even for a relatively simple case such as this results in large recirculations on the boundaries that will invalidate the model results and could also lead to the model "blowing-up" since an unstable feedback loop develops between the water level error at the boundary, current speed and the resultant Coriolis tilts.

Option 2 - Current driven by wind plus a background ambient current

This option is similar to Option 1, but allows a time-varying background ambient current to be specified in addition to the local wind-driven currents. This option is applied when the currents are dominated by local winds, but a larger-scale ocean circulation is also present. Note that the background current will not be recovered exactly in model since it will be modified by the wind, e.g. a strong wind in the opposite direction will reverse the ambient current, particularly in shallow water. For this option, the total water depth at which the background current applies must be specified.

Option 3 - Current driven by measured current plus wind

This option is applicable when measured timeseries of both currents and winds are available. The module will recover the measured current even if the wind is blowing in the opposite direction. The total depth at which the current was measured needs to the specified, since the measured current will only be recovered at this position. At other depths, the balance between the longshore slope, wind stress and bottom friction will determine the current at any time.

Theory

Assuming that the depth-averaged current is flowing alongshore, the momentum equation is solved in the longshore direction to obtain longshore currents. Thereafter, the momentum equation is solved in the cross-shore direction to obtain the wind setup and coriolis tilt.

The following momentum equation is solved in the longshore (y) direction:

$$\frac{dv}{dt} = -g\frac{dz}{dy} + \frac{\rho_{air} C_d U_y |U_y|}{\rho_{water} h} - \frac{gv|v|}{C_z^2 h} - 0 \qquad \text{.....Equation 1}$$

accelareatoin = -slope + wind stress – bottom friction – Coriolis effect

where:

g	=	acceleration due to gravity
v	=	velocity in longshore direction ($m.s^{-1}$)
t	=	time
z	=	water elevation above still water level (m)
y	=	distance in longshore direction (m)
ρ	=	density ($kg.m^{-3}$)
C_d	=	wind drag coefficient
U_y	=	wind speed in longshore direction ($m.s^{-1}$)
h	=	water depth (m)
C_z	=	Chezy coefficient ($m^{1/2}.s^{-1}$).

The Coriolis term is left out since the velocity in the cross-shore direction is assumed to be small. Equation 1 is first solved to obtain the longshore slope and subsequently to obtain longshore velocities. The slope depends on which of the 3 options are selected:

For Option 1 (current driven by wind only), the longshore slope is zero since the longshore wind stress is balanced by bottom friction, i.e.:

slope = 0.

For Option 2 (current driven by wind plus a background ambient current), the longshore slope is balanced by bottom friction due to the background current and the possible acceleration of the background current at the depth where the current is specified, i.e.:

slope = - acceleration – friction.

For Option 3 (current driven by measured current plus wind) the longshore slope depends on the balance of acceleration (of the measured current), wind and friction at the depth where the current is measured, i.e.:

slope = - acceleration + wind – friction.

These longshore slopes enable the water levels along the offshore boundary to be specified, assuming that the mid-point of the offshore boundary has a zero elevation relative to still water level.

Equation 1 is now solved a second time using slope calculated above in order to obtain the longshore current (v) at each depth point along cross-shore boundaries using a simple explicit scheme.

The next step is to solve the following momentum equation in the cross-shore (x) direction to obtain the slope in the cross-shore direction:

$$0 = -g\frac{dz}{dx} + \frac{\rho_{air} C_d U_x |U_x|}{\rho_{water} h} - 0 - fv \qquad \text{.....Equation 2}$$

(acceleration = -slope + wind stress – bottom friction – Coriolis effect)

where:

g	=	acceleration due to gravity
z	=	water elevation above still water level (m)
x	=	distance in cross-shore direction (m)
ρ	=	density (kg.m^{-3})
C_d	=	wind drag coefficient
U_x	=	wind speed in cross-shore direction (m.s^{-1})
h	=	water depth (m)
f	=	Coriolis parameter
v	=	velocity in longshore direction (m.s^{-1}).

Compared to Equation 1, the acceleration and friction terms are zero because the currents in the cross-shore direction are assumed to be small. The Coriolis term due to the longshore current is now significant. These cross-shore slopes permit the water levels at each depth point along the cross-shore boundaries to be calculated, starting at the offshore end of the boundary and working towards the land.

In order to include tidal effects in addition to wind and large-scale current effects, the tidal levels are simply added to the water levels computed above.

The above theory has been implemented in FORTRAN77, which produces a boundary condition timeseries format file that can be read directly by DELFT3D-FLOW.